UNIVERSITY OF CALIFORNIA SAN DIEGO

Resonance and texture coding in the rat whisker system

A dissertation submitted in partial satisfaction of the
requirements for the degree Doctor of Philosophy

in

Physics

by

Jason Hunter Wolfe

Committee in charge:

Professor Henry Abarbanel, Chair
Professor Daniel Feldman
Professor David Kleinfeld
Professor William Kristan
Professor Herbert Levine

The dissertation of Jason Hunter Wolfe is approved, and it is acceptable in quality and form for publication on microfilm:

_____

_____

_____

_____

_____
Chair

University of California, San Diego

2007

Dedication

This work is dedicated to my mother, Betty, my father, Skip and my two sisters, Lisa and Katie. I would not be the person I am today and this dissertation would not exist if not for their constant support and love.

Table of Contents

List of Figures

Introduction

Chapter 1

Chapter 2

Chapter 3

Chapter 4

Appendix A

Acknowledgements

This dissertation was possible only through the contributions of many people. First and foremost Dan Feldman was my primary advisor throughout this work and his insights have been invaluable. Under his guidance I have just begun to understand what it takes to do good experimental work in neuroscience. Much of the work I did in the Feldman lab was done in collaboration with Shantanu Jadhav. Shantanu has been a terrific friend and person to work with. Experimental science can often be stressful and I have always respected Shantanu's ability to systematically overcome problems and learn from previous experiences. Also in the Feldman lab, Renna Stevens has been a great friend, a constant source of support, and has been a wealth of neuroscience information. We have all benefited tremendously from her presence in the lab. Earlier in my neuroscience career, Tansu Celikel's passion and commitment to science was inspirational and served as a good example as I began my dissertation project. Working in the Feldman lab has been a challenging and stimulating experience and I have enjoyed working with everyone in the lab. Many thanks go to: Kevin Bender, Vanessa Bender, Cara Allen, Sohrab Pahlavan, Patrick Drew, Takeshi Morita, Dave House, Lu Li, and Chris Davenport.

Outside of the lab, Evren Tumer has been one of my closest friends. Not only do I consider him to be a role model in science but his humor and insightfulness have been invaluable over the years. I have also been extremely fortunate be near so many

childhood friends and family during my graduate career. Just to name a few, Patrick Villani, Darin Busby, and Melanie McCutchan are three of my oldest and closest friends and having them close while working on my dissertation has been extremely important over the years.

I also want to thank David Kleinfeld and Dan Hill for their help and patience during our collaboration. Dan Hill performed all surgeries and coherence calculations for the EMG experiments and his advice and experience made the EMG experiments possible.

Chapters 2 and 3 of this dissertation are part of a manuscript in preparation for publication, Wolfe JH, Pahlavan S, Hill D, Kleinfeld D, Feldman DE, untitled. The dissertation author was the primary investigator of the paper.

Vita

Apr 1976	Born, San Diego, California
Sep. 1996 – Jun 2000	Research Assistant, Dr. Zi Qiu, Department of Physics, University of California, Berkeley
Sep. 1999 – Jun 2000	Teaching Assistant, Physics Department, University of California, Berkeley
Jun 1999	B.A., Physics and Economics, University of California, Berkeley
Sep 2001 – Jun 2003	Teaching Assistant, Physics Department, University of California, San Diego
Sep 2002	M.S., Physics, University of California San Diego
Sep 2002 – Jan 2003	Graduate student researcher, Dr. Henry Abarbanel, Physics department, University of California, San Diego
Jan 2003 – Aug 2007	Graduate student researcher, Dr. Daniel Feldman, Department of Neuroscience, University of California, San Diego
Sep 2007	Ph.D., Physics, University of California San Diego

Publications

- J. H. Wolfe, R. K. Kawakami, W. L. Ling, and Z. Q. Qiu, Rodrigo Arias, and D. L. Mills, "Roughness Induced In-Plane Uniaxial Magnetic Anisotropy in Fe/MgO(100)", *J. of Mag. Magn. Mat.* **232**, 36 (2001).
- Hyuk J. Choi, W. L. Ling, A. Scholl, J. H. Wolfe, S. Anders, U. Bovensiepen, F. Toyama, S. Paik, F. Nolting, and Z. Q. Qiu, "Spin reorientation transition in magnetically coupled Fe/Cu/Ni/Cu(001)", *Phys. Rev. B* **66**, 014409 (2002).
- W. L. Ling, Eli Rotenberg, H. J. Choi, J. H. Wolfe, F. Toyama, S. Paik, N. V. Smith, and Z. Q. Qiu, "Double quantum well states in Cu/Co/Cu grown on Co(001)", *Phys. Rev. B* **65**, 113406 (2002).
- Hyuk J. Choi, E. Rotenberg, R. K. Kawakami, U. Bovensiepen, J. H. Wolfe, N. V. Smith, and Z. Q. Qiu, "Effect of interfacial roughness on the phase of quantum well states in Cu/Co(001) and Cu/Ni(001) systems", *Phys. Rev. B* **62**, 6561 (2000).

- Z. D. Zhang, Hyuk. J. Choi, R. K. Kawakami, Enresto Escorcia-Apericio, Martin Bowen, Jason Wolfe, E. Rotenberg, N.V. Smith, and Z. Q. Qiu "Oscillatory coupling between Co films across Cu/Ni30Cu70/Cu(100) double quantum wells", *Phys. Rev. B* **61**, 76 (2000).
- R. K. Kawakami, E. Rotenberg, Ernesto J. Escorcia-Aparicio, Hyuk J. Choi, J. H. Wolfe, N. V. Smith, and Z. Q. Qiu, "Determination of the magnetic coupling in Co/Cu/Co(100) system in terms of the momentum resolved quantum well states", *Phys. Rev. Lett.* **82**, 4098 (1999).
- Ernesto J. Escorcia-Aparicio, J. H. Wolfe, Hyuk J. Choi, W. L. Ling, R. K. Kawakami, and Z. Q. Qiu, "Magnetic phases of thin Fe films grown on stepped Cr(001)", *Phys. Rev. B* **59**, 11892 (1999).
- Ernesto J. Escorcia-Aparicio, Hyuk J. Choi, J. H. Wolfe, W. L. Ling, R. K. Kawakami, and Z. Q. Qiu, "Modification of the Magnetic Properties of Fe/Cr(001) by Controlling the Compensation of the Vicinal Cr(001) Surface", *J. Appl. Phys.* **85**, 4961 (1999).
- R. K. Kawakami, E. Rotenberg, Hyuk J. Choi, Ernesto J. Escorcia-Aparicio, M. O. Bowen, J. H. Wolfe, E. Aronholtz, Z. Zhang, N. V. Smith, and Z. Q. Qiu, "Quantum well states in copper thin films", *Nature* **398**, 132 (1999).

Conference Abstracts and Presentations

- J.H. Wolfe, P.J. Drew, S. Pahlavan, H.D.I. Abarbanel and D.E. Feldman, "Whisker Resonance in the Awake Behaving Animal", Society for Neuroscience, 2006.
- J.H. Wolfe, and D.E. Feldman, "Direct measurement of whisker resonance during active whisking in awake, behaving rats" Barrels Conference, 2006
- J.H. Wolfe, and D.E. Feldman, "Direct measurement of whisker resonance during active whisking in awake, behaving rats" Cosyne Conference, 2007

ABSTRACT OF THE DISSERTATION

Resonance and Texture Coding in the Rat Whisker System

by

Jason Hunter Wolfe

Doctor of Philosophy in Physics

University of California San Diego, 2007

Professor Henry Abarbanel, Chair

The sense of touch provides information about the texture of an object with much better resolution than the other senses. Primates perceive texture by actively moving their fingertips over an object and encoding the resulting spatiotemporal patterns of activation of mechanoreceptors in the skin. Within the primate fingertip many types of mechanoreceptors are densely packed in the skin making it difficult to study the individual components of these complex patterns. Rats' ability to discriminate texture using the whiskers is comparable to humans using the fingertips and due to its discrete array of whiskers on the facial pad the rat whisker system offers considerable advantages for studying texture coding. However, to date, very little is known about how behaving rats actively use their whiskers to extract texture information and how this information is encoded in the nervous system.

Currently there are two main hypotheses on how rats perform texture discrimination using their whiskers. In one hypothesis, whisker motion across a

texture is underdamped, and texture properties drive whisker resonance as the whisker moves across a surface. In this model, the systematic variation in resonance frequency across whiskers enables texture to be encoded by the differential amplitude of vibration across whiskers. In a second, alternative hypothesis, resonance is diminished due to damping and texture information is encoded in the precise motion of each whisker across the surface. Both of these hypotheses are supported by experiments performed in anesthetized animals, however to resolve this debate it is critical to examine whisker dynamics in awake animals to determine 1) to what extent whisker resonance shapes sensory input during active whisker use and 2) how whisker dynamics reflect texture properties when the whiskers are under active muscular control.

Chapter 2 of this dissertation examines whisker vibrations measured in behaving animals trained to whisk in air. We show that, in the absence of any sensory stimulus, high frequency whisker vibrations are presents and that these are filtered by whisker resonance. This suggests that, in the awake behaving animal, resonance can play a role in shaping sensory responses in the whiskers.

Chapter 3 shows that active palpation onto textures can induce whisker resonance. However we argue that the degree to which resonance occurs is not dependent on the spatial properties of the texture and therefore it is unlikely to be critical for texture encoding arguing against the resonance hypothesis. We present an alternative model for texture encoding based on the magnitude of stick-slip events that

were found to occur during texture palpation. We also examine the role that muscles may play in causing these stick-slip events.

Chapter 4 concludes by presenting preliminary results of the neural response to stick-slip events. We show that the spiking probability of a subset of neurons is greatly increased following a texture-induced slip and that the spiking probability increases with slip acceleration, as would be required for the texture encoding hypothesis presented in chapter 3.

Introduction

The sense of touch provides animals with information necessary for survival. The sensation of pain serves as an important warning system, and tactile cues can provide information about an animal's immediate surroundings and can surpass visual cues when distinguishing textural properties (Heller 1989). With some exceptions all the senses require active control of the sensory organ by the observer (e.g. eye movements to scan a room, head movements to increase sensitivity in audition, or sniffing during olfaction). The sense of touch is particularly dependent on the active control of sensory receptors in the skin. Tactile sensation is based on the activation of multiple types of mechanoreceptors, some of which are activated by sustained pressure to the skin, while others are activated by transient vibrations (Johnson 2001; Bensmaia 2006). Active control of skin motion is required to activate these receptors in a meaningful way, such as by scanning a surface with the fingertip to determine its roughness properties. This thesis investigates how active control of a sensory organ can be used to sense and discriminate texture roughness.

In 1925 David Katz proposed *the duplex theory of texture perception* ('The World of Touch' Katz, 1925). In that theory he stated that discrimination of coarse textures depends on a "spatial sense" while discrimination of fine textures depends on

a “vibratory sense.” By this he meant that, when the spatial properties of an object become smaller than the spatial resolution of the receptors in the skin the temporal properties of skin vibration must become important for texture encoding. Supporting Katz’s duplex theory it was shown that humans can sense rough textures (defined as surfaces with feature spacing > 100 μm) by stationary contact between the fingertip and surface. However humans can only sense fine textures (feature spacing < 100 μm) by actively moving their fingertips over the texture (Hollins and Risner, 2000). Fingertip motion translates the inherently spatial properties of a texture into a temporal pattern of vibrations on the fingertip. Fine textures must therefore be represented by the *temporal* patterns of activity in the skin receptors while rough textures are encoded primarily by the *spatial* distribution of activity across different receptors. Neither the relative contributions of spatial versus temporal codes to coarse texture perception nor the exact nature of temporal coding of fine texture properties has been fully explained and remains a subject of debate to this day. (Hollins and Risner 2000; Bensmaia and Hollins 2003; Yoshioka et al 2001; Cascio and Sathian 2001; Johnson 2002). One reason it may be difficult to resolve this issue in the primate is that, as the fingertip scans over a surface, multiple receptors will be simultaneously activated. Due to spatial variations in the surface a spatial pattern of activation will result in the fingertip. Due to motion however, this spatial pattern will change over time resulting in a spatiotemporal activation pattern. The continuous nature of the skin however makes it difficult to isolate the spatial pattern from the temporal pattern, making it difficult to ascertain the relative contributions of each to texture perception.

The rat whisker system offers considerable advantages for studying texture coding. Rats are nocturnal, and must rely on nonvisual cues to navigate their environment. Schiffman et al (1970) showed that information derived from the whiskers can dominate visual cues indicating that rats likely rely on their whiskers when vision is absent. Furthermore, it has been shown that rats can use their whiskers to judge the distance to objects (Hutson and Masterton, 1986) judge the angular position of an object (Mehta et al 2007), and determine the width of a hallway (Krupa et al 2001). In addition rats' ability to perform texture discrimination using the whiskers is comparable to humans using the fingertips (Carvell and Simons, 1990). The set of whiskers on the facial pad of the rat form a distinct, stereotyped array (figure 1.0 A and B). Whiskers are aligned in rows with whisker length decreasing exponentially in the caudal-rostral direction (Brecht et al 1997). The whiskers are therefore an orderly array of discrete sensors which makes it experimentally simple to measure the relative contributions of single whiskers or a subset of whiskers to the encoding of texture. In particular the discrete nature of the whiskers makes the whisker system a good model for understanding the spatial and temporal contributions to the neural code for texture. For example, Carvell and Simons (1995) showed that rats with only one whisker could perform a rough versus smooth discrimination task but were not able to distinguish between two rough textures, suggesting that the spatial distribution of activity across whiskers is important for at least some discrimination tasks.

Primary somatosensory cortex (S1) in the rat is known to be required for texture discrimination (Guic-Robles, 1992). Within the whisker representation of S1, a cortical column principally responds to motion of a single whisker (Armstrong-James, 1975; Simons, 1978). The discrete nature of the whiskers is therefore preserved in S1, making it a relatively straightforward model to study physiologically. The highly modular nature of S1 in rats further makes the rat a good model for understanding how spatial patterns and temporal patterns contribute to texture encoding. While there are significant advantages to using the whisker system as a model for texture discrimination, there is still surprisingly little known about how naturally behaving rats use their whiskers to determine texture properties and what aspects of whisker motion during exploration are behaviorally significant. To date the majority of experiments done in the whisker system have been done in anesthetized animals while delivering controlled mechanical stimuli to the whiskers (Armstrong-James et al 1992). While these experiments have added to our understanding of the circuitry and basic function of the whisker system, substantial data indicate that neural coding of whisker inputs is strongly dependent on the state of the animal (Castro-Alamancos 2004, Fanselow and Nicolelis). Furthermore, during active texture discrimination, the mechanical interaction between the whisker and texture may result in very different whisker vibration patterns than those studied in the anesthetized animal, thus the functional role of the whisker somatosensory cortex in the behaving animal during texture discrimination is largely unknown.

Based on experiments performed in anesthetized animals two competing hypotheses for texture encoding in the behaving animal have emerged. The first hypothesis is based on the observation that whiskers possess intrinsic resonance frequencies which primarily depend on the whisker length (Neimark et al 2003). Because whisker lengths decrease exponentially in the caudal to rostral direction (Brecht et al. 1997) there is a systematic increase in the resonance frequencies of the rostral whiskers compared to the caudal whiskers, creating a map of preferred frequencies on the facial pad that range from ~ 80 Hz to 750 Hz when measured with the whisker tip attached to a piezo (figures I1 C and D). In anesthetized animals it was shown that when a whisker is periodically stimulated at its resonance frequency there is an ~10 fold increase in vibration amplitude which results in a several fold increase in neural response compared to the response at non-resonance frequencies (Andermann et al, 2004). These authors proposed that as a rat sweeps its whiskers across a texture, whisker tips will move across surface microfeatures causing the whiskers to vibrate with a frequency spectrum that is determined by the texture's spatial properties. The resonance hypothesis for texture coding states that when the induced vibration spectrum matches the resonance frequency of a whisker, that whisker will be preferentially excited, and that whisker's principal cortical column will respond more strongly relative to the other cortical columns. By comparing the relative excitation across columns the animal can decode the spatial properties of the texture. In general the shorter whiskers and their corresponding cortical columns would be predicted to respond more strongly to finer textures, while the longer more

caudal whiskers would preferentially respond to coarser textures. The whiskers would thus function analogously to the cochlea in the auditory system, although with much coarser frequency resolution (Moore, 2004).

A second hypothesis, equally well supported by anesthetized experiments, proposes that texture information is encoded not by comparison of vibration amplitude across whiskers, but instead by characteristic patterns of motion of individual whiskers as they move across a texture (Arabzadeh et al, 2005). The underlying assumption of this model is that resonance of the whiskers is sufficiently dampened during natural texture palpation such that the temporal pattern of whisker vibrations directly reflects the spatial properties of the texture rather than the intrinsic resonance properties of the whisker (Mehta and Kleinfeld, 2004). Thus, as the whisker sweeps over a texture the induced vibrations would directly reflect the spatial properties of the texture which would be encoded by the spiking patterns along the neural pathway. In a set of experiments in anesthetized rats the facial nerve innervating the whisker muscles was electrically stimulated to artificially protract the whisker across textured surfaces. The recorded whisker motion was then precisely played back to the whisker and the neural response to repeated playback of the same motion was recorded. Results showed that, during the electrically stimulated whisker motion different textures induced distinct reproducible temporal patterns of whisker motion. When this motion was played back to the whiskers neurons in S1 responded with precisely timed pattern of spikes that also reflected the surface properties (Arabzadeh et al). This result led to the second hypothesis that texture information is contained in the temporal pattern of spikes that

result from texture palpation. Interpretation of this result is made difficult however by Carvell and Simons (1990) who showed that whisking behavior is variable upon repeated presentation of a textured surface, casting doubt on whether, during active texture exploration, whiskers will have the exact same dynamics upon repeated exploration of an object. Whether a precise temporal code for texture is plausible is therefore unclear.

The neural encoding strategies required by the two hypotheses described above are very different. In the resonance hypothesis, depicted in figure I2 A, neural comparison of signals must take place across whiskers in the spatial dimension, because texture information is contained in the spatial distribution of excitation, while the temporal dynamics of neural responses are largely unimportant. In the second hypothesis (figure I2 B) the temporal dynamics of neural responses are crucial and thus the neurons must be able to precisely encode timing of whisker vibrations, however the necessity to integrate across whiskers is unclear.

To resolve this debate it is critical to examine whisker dynamics in awake animals to determine, 1) to what extent whisker resonance shapes sensory input during active whisker use and 2) how whisker dynamics reflect texture properties when the whiskers are under active muscular control. This thesis attempts to address these issues by precisely measuring whisker motion while animals actively whisk in air and onto textured surfaces. We examined the effects of whisker resonance during active texture palpation and asked whether the resonance hypothesis is a plausible coding mechanism during active whisker use. We then examined an alternative coding

scheme and compared it to the two hypotheses outlined above. Finally we present preliminary neural recordings in S1 which may bear on texture encoding.

The results of this work are divided into four chapters. Chapter one explains three main parts of the biological system particularly relevant to the current study: the musculature of the whisker follicle which is responsible for whisker movement, the neural pathway that relays information from the whisker to primary somatosensory cortex and an elastic beam model of the whisker. Following past work, we consider the intact whisker to be a thin elastic beam and the trimmed whisker to be a truncated beam (Neimark et al 2003; Conway 1964, Georgian 1965). Both of these models are presented here.

Chapter two presents experimental results measuring whisker motion in air during natural, active whisking. In this chapter we show that, even in air, whiskers vibrate at high frequencies (> 30 Hz). These vibrations are robustly filtered by the resonant properties of the whiskers, demonstrating that whisker resonance is prominent in awake, behaving animals. We show that artificial stimulation of the facial muscles causes whisker resonance similar to that observed in the awake, behaving animal.

Chapter three reports results of measuring natural whisker motion onto sandpaper textures. Results showed that during active whisking onto textures whisker resonance does occur. However this resonance appears to be due to transient ringing induced by sharp stick-slip motion on the texture, and does not appear to encode texture properties. Thus our results do not support the resonance hypothesis for

texture discrimination. As an alternative to the resonance hypothesis we show that the magnitude of stick-slip events correlates with texture roughness, suggesting that texture may be encoded in the rate and amplitude of stick-slip events. We present a simplified physical model which may explain this dependence of stick-slip magnitude on texture roughness. Also in this chapter we examine how the timing of stick-slip events depends on muscle activity during active whisking[1].

Finally, in chapter four, we show preliminary results of chronic recordings performed in primary somatosensory cortex (S1)[2]. These results show that slip events during active texture palpation are precisely encoded by spiking of S1 neurons and that slip acceleration can be encoded by spiking probability. These results bolster the hypothesis that slips are a salient feature of whisker input during texture palpation and may convey texture roughness information.

Taking these results together we propose a model in which whisker sticking and slipping across a texture provides an important cue for texture discrimination. The sensory side of this model posits that the roughness of a texture determines the relative rate of occurrence of large versus small slip events. Larger slip events have higher acceleration and are proposed to evoke higher probability spiking in S1. On the motor side of this model, the timing of the slip events would be influenced by the pattern of muscle activity during active whisking.

---

[1] EMG experiments presented in this chapter were performed in collaboration with Dan Hill and David Kleinfeld

[2] All chronic recording experiments were done with Shantanu Jadhav. SJ was responsible for all spike sorting and surgical procedures.

In this model texture decoding would require neural integration across time because roughness is reflected in the average rate of small versus large stick slip events. Spatial comparison of slip information across whiskers would not be explicitly required, however we predict that discrimination ability would greatly increase by integrating neural responses to stick-slip events across whiskers. This is consistent with the observation that discrimination ability decreases as rats are deprived of whiskers (Carvell and Simons 1995). Whisker resonance does not play a direct role in this model, however our results indicate that resonance is present during texture palpation and therefore could serve to amplify the response to the stick-slip events.

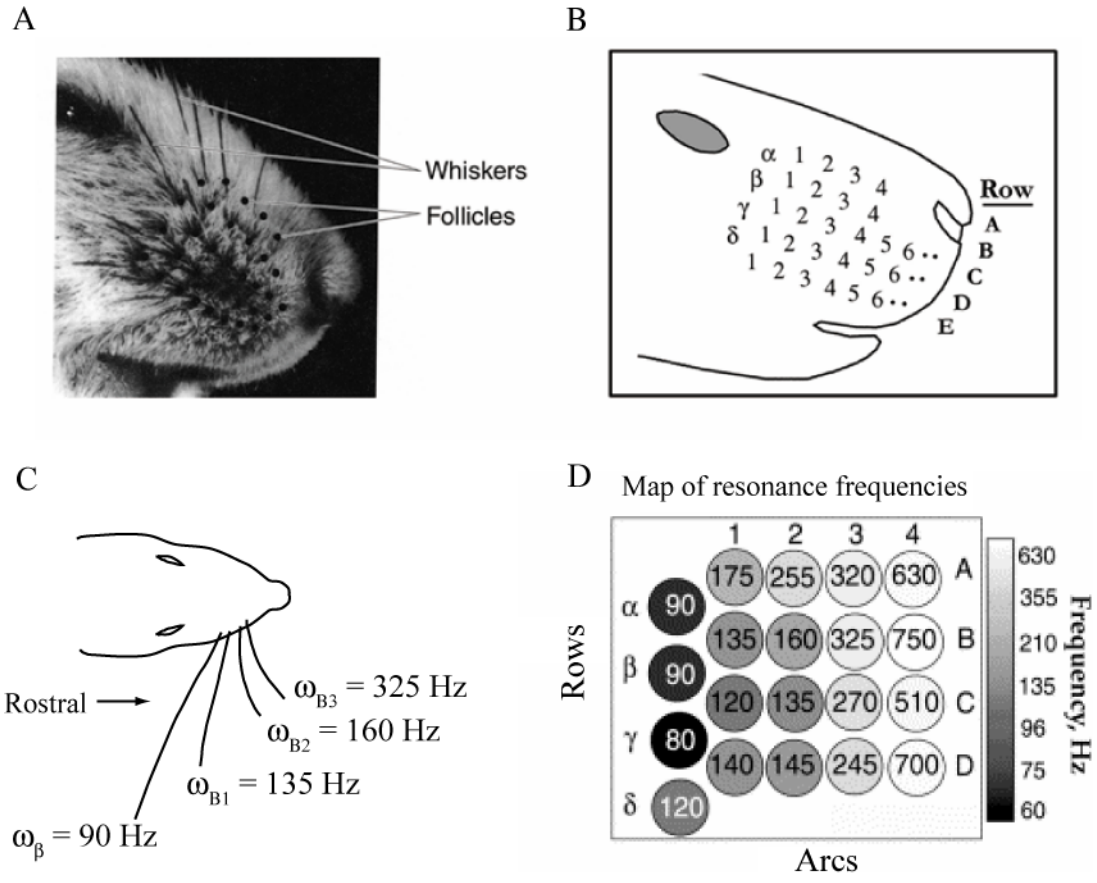

Figure I1. **Schematic representation of the whisker pad and the resonance properties of the whiskers**. A,B) Whiskers are arranged in rows labeled A-E. C) Whisker length decreases exponentially in the caudal-rostral direction. As whisker length decreases, whisker resonance frequency increases. D) Due to the varying whisker length across the facial pad there is a systematic map of resonance freqeuncies.

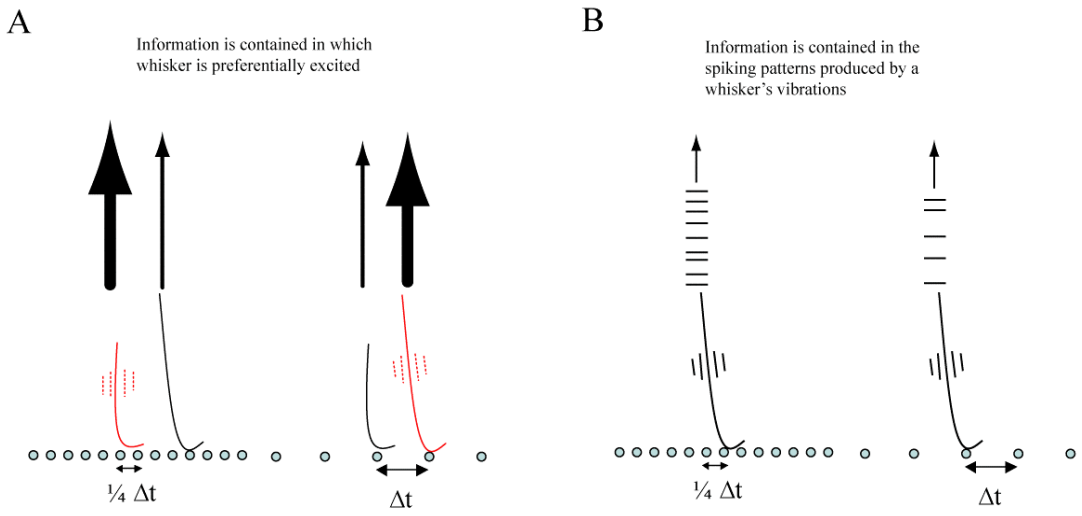

Figure I2. A) **Schematic representation of the resonance hypothesis**. Because finer textures are predicted to induce higher frequency whisker vibrations than coarse textures, finer textures would excite resonance in the shorter whiskers (left), while coarse textures would excite the longer whiskers (right). Texture properties would be encoded by the spatial distribution of excitation along the neural pathway. B) In the direct encoding hypothesis spatial properties of the texture are encoded by the timing of spikes along the neural pathway

I1 References

Andermann ML, Ritt J, Neimark MA, Moore CI. **Neural correlates of vibrissa resonance; band-pass and somatotopic representation of high-frequency stimuli**. Neuron. 2004 May 13;42(3):451-63

Arabzadeh E, Zorzin E, Diamond ME. **Neuronal encoding of texture in the whisker sensory pathway.** PLoS Biol. 2005 Jan;3(1):e17. Epub 2005 Jan 11.

Armstrong-James M. **The functional status and columnar organization of single cells responding to cutaneous stimulation in neonatal rat somatosensory cortex S1** 1975 Apr;246(3):501-38

Armstrong-James M, Fox K, Das-Gupta A. **Flow of excitation within rat barrel cortex on striking a single vibrissa**. J Neurophysiol. 1992 Oct;68(4):1345-58.

Bensmaia SJ, Hollins M**. The vibrations of texture**.Somatosens Mot Res. 2003;20(1):33-43

Brecht M, Preilowski B, Merzenich MM. **Functional Architecture of the mystacial vibrissae**. Behav Brain Res. 1997 Mar;84(1-2):81-97

Carvell GE, Simons DJ. **Biometric analyses of vibrissal tactile discrimination in the rat.** J Neurosci. 1990 Aug;10(8):2638-48

Carvell GE, Simons DJ. **Task- and subject-related differences in sensorimotor behavior during active touch**. Somatosens Mot Res. 1995;12(1):1-9.

Cascio CJ, Sathian K. **Temporal cues contribute to tactile perception of roughness**. J Neurosci. 2001 Jul 15;21(14):5289-96

Castro-Alamancos MA. **Dynamics of sensory thalamocortical synaptic networks during information processing states**. Prog Neurobiol. 2004 Nov;74(4):213-47. Review.

Conway HD, Becker ECH, Dubil JF. **Vibration frequencies of tapered bars and circular plates**. J App Mech 1964 June 329-331

David Katz. **The World of Touch.** New Jersey : Lawrence Erlbaum Associates, Inc. 1989 (Originally published 1925)

Georgian JC. **Vibration frequencies of tapered bars and circular plates.** J App Mech 1965 March 234-235

Guic-Robles E, Valdivieso C, Guajardo G. **Vibrissal roughness discrimination is barrelcortex-dependent**. Behav Brain Res. 1992 Jun 8;48(2):145-52.

Guic-Robles E, Jenkins WM, Bravo H. **Vibrissal roughness discrimination is barrelcortex-dependent**. Behav Brain Res. 1992 Jun 8;48(2):145-52

Heller MA**. Picture and pattern perception in the sighted and the blind: the advantage of the late blind**. Perception. 1989;18(3):379-89

Hollins M, Risner SR. **Evidence for the duplex theory of tactile perception**. Percept Psychophys. 2000 May; 62(4):695-705

Hutson KA, Masterton RB. **The sensory contribution of a single vibrissa's cortical barrel**. J Neurophysiol. 1986 Oct;56(4):1196-223.

Johnson KO. **Neural basis of haptic perception**. (2002) In H. Pashler and S. Yantis (Eds.) *Stevens handbook of experimental psychology* (3rd ed), vol. 1: *Sensation and Perception* (pp 537-583) New York: Wiley

Krupa DJ, Matell MS, Brisben AJ, Oliveira LM, Nicolelis MA. **Behavioral properties of the trigeminal somatosensory system in rats performing whisker-dependent tactile discriminations**. J Neurosci. 2001 Aug 1;21(15):5752-63

Mehta SB, Kleinfeld D. **Frisking the whiskers: patterned sensory input in the rat vibrissa system.** Neuron. 2004 Jan 22;41(2):181-4. Review

Mehta SB, Whitmer D, Figueroa R, Wiliams BA, Kleinfeld D. **Active spatial perception in the vibrissa scanning sensorimotor system**. PLoS Biol. 2007 Jan;5(2):e15

Moore CI. **Frequency-dependent processing in the vibrissa sensory system**. 2004 Jun;91(6):2390-9

Neimark MA, Andermann ML, Hopfield JJ, Moore CI. **Vibrissa resonance as a transduction mechanism for tactile encoding.** J Neurosci. 2003 23(16):6499-6509

Schiffman HR, Lore R, Passafiume J, Neeb R. **Role of vibrissae for depth perception in the rat (Rattus norvegicus).** Anim Behav. 1970 May;18(2):290-2

Simons DJ. **Response properties of vibrissa units in rat SI somatosensory neocortex**.
J Neurophysiol. 1978 May;41(3):798-820

Yoshioka T, Gibb B, Dorsh AK, Hsiao SS, Johnson KO. **Neural coding mechanisms underlying perceived roughness of finely textured surfaces**. J Neurosci. 2001 Sep 1;21(17):6905-1

Chapter 1

The rat whisker system and elastic beam model of the whisker

1.0 Introduction

The goal of this thesis is to understand how awake behaving rats actively use the whiskers to extract texture information from objects and how this information may be represented in the brain. A critical determinant of how whiskers extract texture information is their movement across surfaces. The first part of this chapter therefore presents background information about the musculature responsible for active whisker motion. The second part describes the neural pathway from the whisker follicle to sensory cortex. Because we are testing whether the resonance properties of the whiskers play a role in shaping sensory input it is important to understand how the resonance properties of the whiskers depend on the their geometrical properties. The third section therefore presents a model of the whisker as a thin elastic beam and expands this whisker model to include truncated beams. The truncated beam model is then used in the following chapter to model the trimmed whiskers during whisking in air.

1.1 Musculature of the whisker follicle

The facial muscles responsible for retraction and protraction of the whiskers are divided into the intrinsic and extrinsic muscle classes. (Berg and Kleinfeld 2003, Dorfl 1982, Brecht et al 1997) These muscles are innervated by the facial motor nerve which has its cell bodies in the facial nucleus in the brainstem (figure 2.1). The sensory nerves which project back to the brainstem (labeled 'sn' in figure 2.0A) densely innervate each whisker follicle. The intrinsic muscles form a sling around the whisker follicle within the mystacial pad (labeled 'i' in fig 2.0A). The mechanics of protraction can be seen in figure 2.0B. The intrinsic muscle is attached to the base of the whisker, below the pivot point in the skin. Contraction of the intrinsic muscle pivots the whisker forward in the rostral direction (Berg and Kleinfeld 2003).

The extrinsic muscles lie within the skin and are anchored external to the mystacial pad. Contraction of the extrinsic muscles causes the pivot points where the whiskers leave the skin to move backward in the caudal direction causing retraction of the whiskers (see figure 2.0B). Because contraction of the extrinsic muscles moves the pad as a whole, the extrinsic muscles generally move all whiskers on the pad whereas the intrinsic muscles are able to move individual whiskers.

It was shown that both protraction and retraction are under active muscular control and that normal whisking behavior persists in the absence of sensory

feedback (Berg and Kleinfeld 2003; Fee et al 1997, Ganguly and Kleinfeld 2004). During whisking the electromyogram (EMG) signals of the extrinsic and intrinsic muscles oscillate out of phase with each other (figure 2.0C). The intrinsic muscles are activated during the protraction phase (green) of whisking while the extrinsic muscles are activated during the retraction phase (red). The black traces overlayed on the EMG traces are the EMG signals smoothed over 40 ms. Previous experiments have measured whisker motion in anesthetized animals by electrically stimulating the facial nerve causing protraction of the whisker. While this may be a better approximation of whisker dynamics than passively deflecting the whiskers, the muscle forces responsible for whisking are likely very different than in the case of the animal actively using its whiskers. Any difference in muscular control may affect both the whisker dynamics and the sensory response to whisker deflections (Szwed et al 2003; Szwed et al 2006).

1.2 Lemniscal pathway from whisker to S1

Although the role of S1 in texture discrimination is unknown, it is known that S1 participates in texture encoding because when the whisker representation in S1 is lesioned rats can no longer perform the task (Guic-Robles et al 1992). There are 3 major separate pathways from the whisker follicle to S1 (Yu et al 2006, Pierret et al 2000). The paralemniscal pathway was shown to primarily represent proprioceptive information about whisker position. The extralemniscal pathway was recently

discovered and was shown to respond only to touch signals and conveyed no information about whisker position. The lemniscal pathway conveys both information about whisker contact and proprioceptive information about whisker position (Yu et al 2006). Here we concentrate on the lemniscal pathway because it conveys touch information and its response properties have been well characterized (Castro-Alamancos 2004; Temereanca and Simons 2003; Pinto et al 2000, Brumberg et al 1999).

Each whisker follicle is densely innervated by mechanoreceptors which respond to deflections due to whisker contact (Ebara et al 2002; Rice et al 1986). Sensory information represented by these deflections is transmitted via afferents, whose cell bodies lie in the trigeminal ganglia, to the brainstem where the first synapse is located . Within the lemniscal pathway information then ascends to the ventral posterior medial (VPM) sector of the thalamus where the second synapse is located. From VPM the pathway ascends primarily into layer 4 of primary somatosensory cortex (S1) where the third synapse is located. The general response properties to periodic trains of stimuli of neurons along this pathway are depicted by the left-hand panels of figure 2.1 (Deschenes et al 2003; Chung et al 2002). One very distinct feature of this pathway is that the frequency following ability of individual neurons declines very rapidly between the brainstem and S1. For example neurons in brainstem are able to follow in a one-to-one manner a sinusoidal stimulus at 300 Hz. Neurons in VPM however cannot spike in a one-to-one manner with a 100 Hz stimulus, although the membrane potentials of these cells may follow

at this frequency. In S1 however, neurons cannot follow whisker deflections at 4 Hz. While the caveat must be made that these experiments were performed under anesthesia which is known to affect the response properties of these neurons, poor frequency following ability is a general property of neurons in S1. While single neurons in S1 generally cannot follow high frequency whisker stimulation, it has been shown that the spiking rate increases linearly with the logarithm of the stimulation frequency (Arabzadeh et al 2003, 2004). Subsequently, however, it was shown that a rate code does not suffice to encode texture (Prigg et al 2004l). Therefore it is likely that texture information is encoded by something other than just the frequency of whisker deflections as it passes over bumps in a texture.

1.3 Thin beam and truncated beam models of the whisker

In all sensory systems the physical properties of the sensor determine how an animal encodes information about its environment. It was previously shown by Andermann et al that, due to the physical properties of the whiskers, each had a unique resonance frequency. Based on this they proposed that each whisker could act as bandpass filter so that if all the whiskers were stimulated, the spectral properties of that stimulus could be encoded by the relative excitation across whiskers. In order to understand the role of whisker resonance during sensory processing we analyzed whisker motion in animals trained to whisk both in air and onto textured surfaces. In order to determine the degree to which whisker resonance

shapes sensory input we modeled the whiskers as thin conical beams (Kirchoff 1882 ;Weaver and Timoshenko 1990; Neimark et al 2003) and used this to predict the resonance frequencies of each whisker. The predicted results from the model were then compared to whisking power spectra measured in the awake behaving animal.

By equating the shearing and bending moments of a cross section of a thin conical beam it can be shown that the angular resonance frequency of a thin beam fixed at the base and free to oscillate at the tip is:

$$f_i = t_i \frac{a}{l^2}\sqrt{\frac{E}{4\mu}} \qquad \text{with} \qquad t_i = 4.4, 10.6, 19.2... \qquad \text{(Eq. 1)}$$

The derivation of this result is presented in appendix A.

Where (see figure 2.3B):

a = radius at the base
μ = linear mass density
E = Young's modulus
l = length of the whisker
t_i = multiplicative factor representing the vibration mode (i = 0 for fundamental resonance frequency)

The method used to calculate the resonance frequencies and harmonics was to measure the fundamental resonance frequency (corresponding to $t_0 = 4.4$, shown in figure 2.3B) and calculate the first and second harmonics (corresponding to $t_1 = 10.6$ and $t_2 = 19.2$) based on the calculated ratios of $f_1 / f_0 = 2.4$ and $f_2 / f_0 = 4.4$ as shown by the dashed lines in figure 2.3 C. In chapter two of this thesis we show how whisker trimming alters the spectral properties of whisker vibrations in air. By modeling the trimmed whisker as a truncated beam we show that whisker resonance

can account for this change. When a thin conical beam is truncated however the result for the resonance frequencies must be modified. The truncation of the beam has a twofold effect. First the truncation causes an obvious shortening of the beam and this decrease in the length must increase the beam's resonance frequency. Second, the truncated beam no longer comes to a point at the end. Instead the tip now has finite area and a nonzero radius. As a result of this change in geometry, the constants t_i in equation 1 change. Conway et al (1964) numerically computed the modified t_i constants based on the difference in lengths between the intact conical beam and the truncated beam for a given base diameter and slope of the cone (fig 2.3E). In that work these constants were calculated for four different ratios of l_1/l_2, where l_1 is the natural length of the thin conical beam and l_2 is the change in length (see figure 2.3B). Here we make use of that work by interpolating between those numerically calculated values in order to approximate the t_i constants for an arbitrary truncated length. Figure 2.3B shows the previously calculated constants (open circles) and the solid line is an exponential fit used to interpolate between these values. Looking at equation 1 it can be seen that:

$$\frac{t_1}{t_0} = \frac{f_1}{f_0}, \quad \text{and} \quad \frac{t_2}{t_0} = \frac{f_2}{f_0}$$

So that the theoretical first and second harmonics of the resonance frequency can be calculated by knowing the t_i multiplication constants for the first and second harmonics. As can be seen in figure 2.3C the ratio of the first and second harmonics to the fundamental resonance frequency increase as the beam becomes more

truncated. For example, at $l_1/l_2 = 3$ the ratio of the first harmonic to the fundamental resonance frequency is 3.8 (see figure 2.3E) whereas at $l_1/l_2 = 9$ this ratio is 2.6. As l_1/l_2 goes to infinity (or l_2 goes to zero which is the untruncated length) this ratio approaches the ratio derived for the intact conical beam which is 2.4.

In the following chapter data will be presented showing the change in the spectra of whisker vibrations as the whiskers are trimmed. In order to compare the change in power spectra to the change in the whisker's resonance frequency and harmonics we measure the fundamental resonance frequency of the whisker by delivering a sharp impulse and watching the ringing decaying whisker oscillations. The harmonics are calculated by measuring the truncated whisker lengths and using the ratios calculated above to predict the truncated harmonic frequencies. In the next chapter we show that the change in power spectra as the whiskers are trimmed nicely match both the change in the resonance frequencies and the change in harmonics as predicted by the truncated beam model. A much worse match between the spectra and resonance frequencies is obtained if we do not use the truncated beam model.

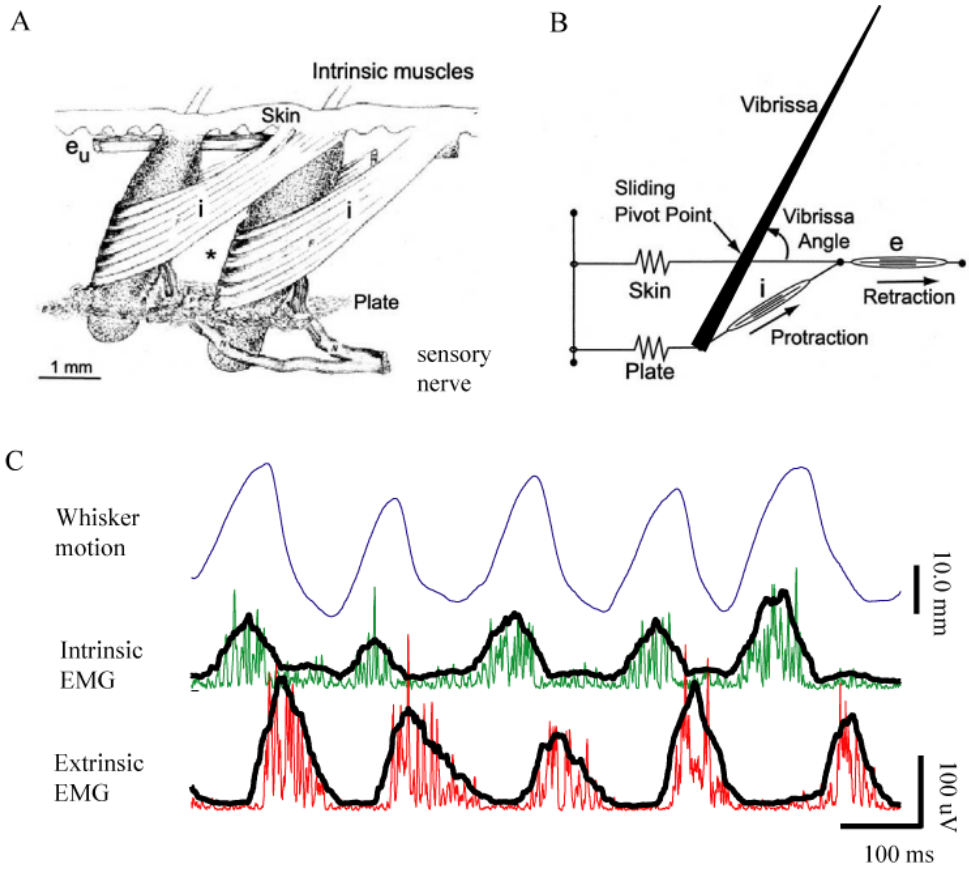

Figure 1.0. **Muscle forces resopnsible for whisking motion**. A) Musculature of the whisker follicle (Dorfl 1982, adapted from Berg and Kleinfeld 2003). The intrinsic muscles ('i') form a sling around the whisker follicle. B) Mechanical diagram showing forces of muscles on the whisker follicle. Contraction of the intrinsic ('i') muscle causes the whisker to pivot forward. Contraction of the extrinsic muscles ('e') moves the pivot point in the skin backward causing whisker retraction. C) Example EMG trace showing the relative phase relationship between activation of the intrinsic (green) and extrinsic (red) muscles. Intrinsic muscles are active during whisker protraction. Extrinsic muscles are active during retraction.

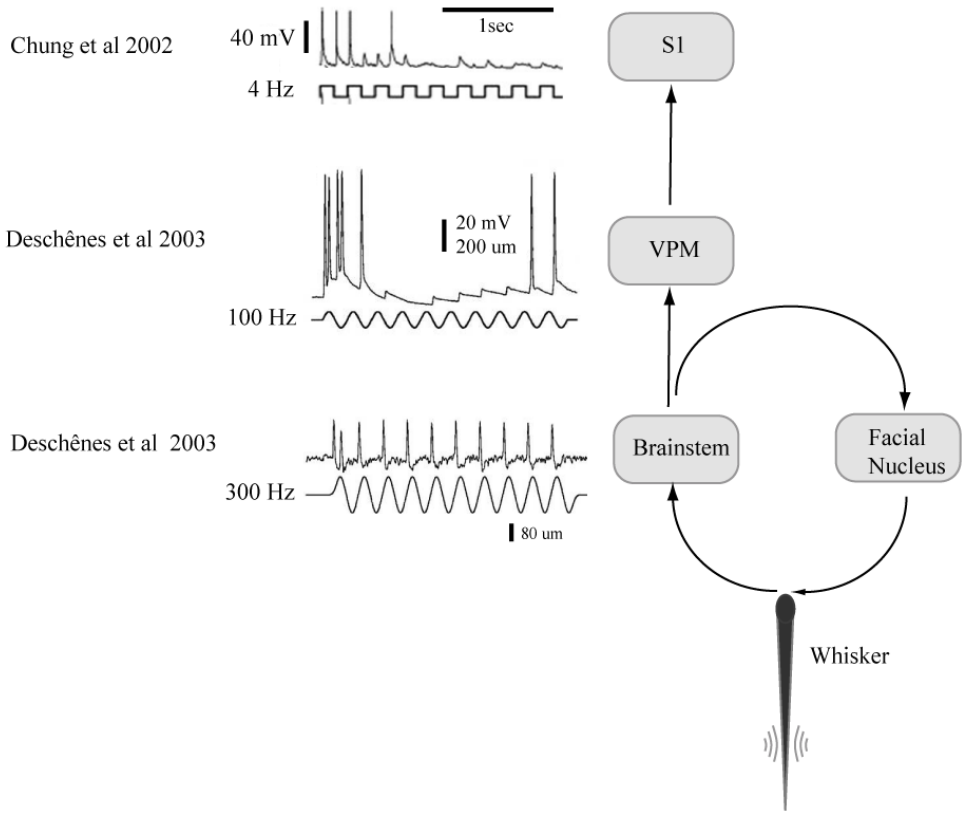

Figure 1.1. **Neural pathway from whisker to S1**. Diagram of the descending pathway from the facial nucleus to the whisker and the ascending pathway from the whisker to primary somatosensory cortex (S1). The facial nucleus contains the motorneurons responsible for controlling the intrinsic and extrinsic muscle groups. Traces on the left show the frequency response of neurons measured intracellulary from the brainstem, thalmus, and cortex. At the brainstem, neurons can follow very high frequency stimulation, whereas neurons in S1 rapidly adapt to trains of stimuli even at 4Hz.

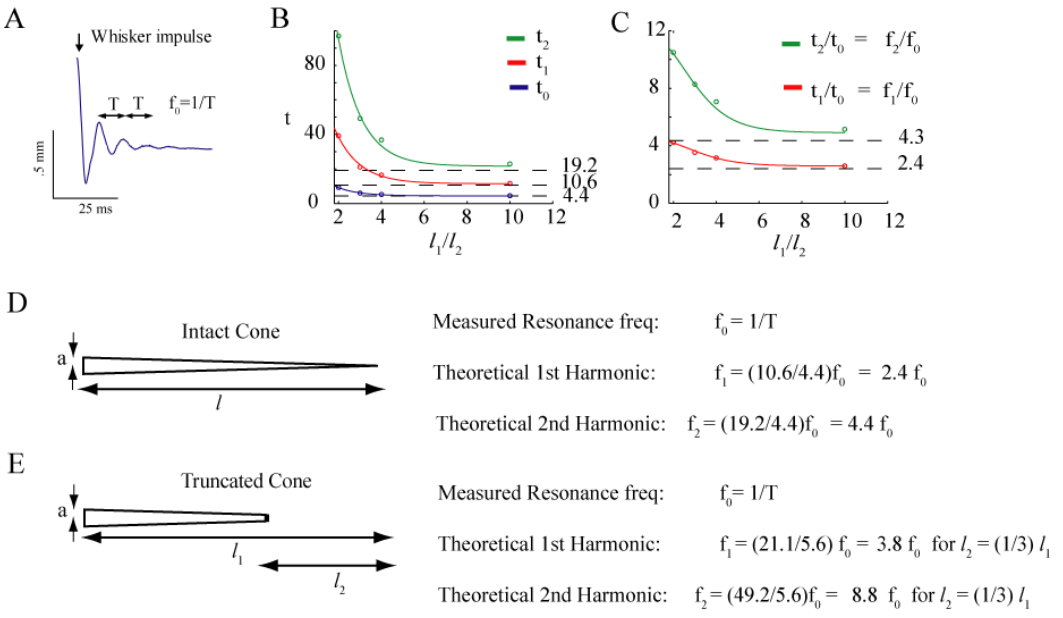

Figure 1.2. **Elastic beam model of the whisker**. A) Example measurement of the fundamental resonance frequency by delivering a sharp impulse and measuring the decaying oscillations. B) The multiplicative constants ti increase as the conical beam becomes more truncated. This corresponds to l2 getting bigger (see 2.3E) C) Numerically calculated values of the ratios of t1/t0 and t2/t0. From equation 1 it can be seen that these ratios are equal to f1/f0 and f2/f0. As the conical beam (whisker) becomes more truncated the harmonics of the resonance frequency increase at a faster rate than the resonance frequency. D) Diagram of intact cone. For intact cones the first and second harmonic frequencies are 2.4 and 4.4 times the resonance frequency. E) Diagram of truncated cone. As the whisker is trimmed l2 increases. An example calculation for l2 = 1/3l1 is given. This example corresponds to l1/l2 = 3. From 2.3C it can be seen that the first harmonic is then 3.8 f0 and the econd harmonic is 8.8 f0

1.4 References

Arabzadeh E, Petersen RS, Diamond ME. **Encoding of whisker vibration by rat barrel cortex neurons: implications for texture discrimination**. J Neurosci. 2003 Oct 8;23(27):9146-54

Arabzadeh E, Panzeri S, Diamond ME**. Whisker vibration information carried by rat barrel cortex neurons.** J Neurosci. 2004 Jun 30;24(26):6011-20.

Berg RW, Kleinfeld D. **Rhythmic whisking by rat: retraction as well as protraction of the vibrissae is under active muscular control**. J Neurophysiol. 2003 Jan;89(1):104-17

Brecht M, Preilowski B, and Merzenich MM. **Functional architecture of the mystacial vibrissae**. Behav Brain Res 84: 81-97, 1997

Brumberg JC, Pinto DJ, Simons DJ. **Cortical columnar processing in the rat whisker-to-barrel system**. J Neurophysiol. 1999 Oct;82(4):1808-17.

Castro-Alamancos MA. **Dynamics of sensory thalamocortical synaptic networks during information processing states**. Prog Neurobiol. 2004 Nov;74(4):213-47. Review.

Chung S, Li X, Nelson SB**. Short-term depression at thalamocortical synapses contributes to rapid adaptation of cortical sensory responses in vivo**. Neuron. 2002 Apr 25;34(3):437-46

Conway HD, Becker ECH, Dubil JF. **Vibration frequencies of tapered bars and circular plates**. J App Mech 1964 June 329-3

Deschenes M, Timofeeva E, Lavallee P. **The relay of high-frequency sensory signals in the Whisker-to-barreloid pathway.** J Neurosci. 2003 Jul 30;23(17):6778-87

Dorfl J. **The musculature of the mystacial vibrissae of the white mouse**. *J Anat* 135: 147-154, 1982

F.L. Rice, A. Mance and B.L. Munger, **A comparative light microscopic analysis of the sensory innervation of the mystacial pad. I. Innervation of vibrissal follicle-sinus complexes**, J. Comp. Neurol. **252** (1986), pp. 154–174

Fee MS, Mitra PP, Kleinfeld D. **Central versus peripheral determinants of patterned spike activity in rat vibrissa cortex during whisking**.J Neurophysiol. 1997 Aug;78(2):1144-9.

Ganguly K, Kleinfeld D. **Goal-directed whisking increases phase-locking between vibrissa movement and electrical activity in primary sensory cortex in rat**. Proc Natl Acad Sci U S A. 2004 Aug 17;101(33):12348-53. Epub 2004 Aug 5.

Guic-Robles E, Valdivieso C, Guajardo G. **Vibrissal roughness discrimination is barrelcortex-dependent**. Behav Brain Res. 1992 Jun 8;48(2):145-52.

Kirchoff GR. **Gesammelte Abhandlungen**, Leipzig 1882

Neimark MA, Andermann ML, Hopfield JJ, Moore CI. **Vibrissa resonance as a transduction mechanism for tactile encoding.** J Neurosci. 2003 23(16):6499-6509

Pierret T, Lavallee P, Deschenes M. **Parallel streams for the relay of vibrissal information through thalamic barreloids**. J Neurosci. 2000 Oct 1;20(19):7455-62.

Pinto DJ, Brumberg JC, Simons DJ. **Circuit dynamics and coding strategies in rodent somatosensory cortex**. J Neurophysiol. 2000 Mar;83(3):1158-66

Prigg T, Goldreich D, Carvell GE, Simons DJ. **Texture discrimination and unit recordings in the rat whisker/barrel system**. Physiol Behav. 2002 Dec;77(4-5):671-5

S. Ebara, K. Kumamoto, T. Matsuura, J.E. Mazurkiewicz and F.L. Rice, **Similarities and differences in the innervation of mystacial vibrissal follicle-sinus complexes in the rat and cat: A confocal microscopic study**, J. Comp. Neurol. **449** (2002), pp. 103–119

Szwed M, Bagdasarian K, Ahissar E. **Encoding of vibrissal active touch**.Neuron. 2003 Oct 30;40(3):621-30

Szwed M, Bagdasarian K Blumenfeld B, Barak O, Derdikman D, Ahissar E. **Responses of trigeminal ganglion neurons to the radial distance of contact during active vibrissal touch**. J Neurophysiol. 2006 Feb;95(2):791-802. Epub 2005 Oct 5.

Temereanca S, Simons DJ. **Local field potentials and the encoding of whisker deflections by population firing synchrony in thalamic barreloids**. J Neurophysiol. 2003 Apr;89(4):2137-45.

Weaver SP, Timoshenko DH. **Vibration Problems in Engineering.** New York : Wiley 1990

Yu C, Derdikman D, Haidarlu S, Ahissar E. **Parallel thalamic pathways for whisking and touch signals in the rat**. PLoS Biol. 2006 May;4(5):e124. Epub 2006 Apr 18

Chapter 2

Whisking in air

2.0 Introduction

As a first step toward understanding the role of whisker vibrations and resonance in sensory processing, we measured active whisker motion in air. This was done for two reasons: first, understanding the vibrations that occur in air will allow us to see the baseline state of whisker input, from which texture-driven input must be differentiated. Second, naturally occurring whisker vibrations in air provide an important opportunity to understand the properties and prevalence of whisker resonance during natural whisking behavior. The degree of damping in the whisker system is crucial to the viability of the resonance hypothesis (Kleinfeld et al 2006, Hartmann et al 2003, Neimark et al 2003). If vibrations in air are not filtered by whisker resonance then there must be a large amount of energy lost to damping which would make resonance an unlikely mechanism for texture encoding. If vibrations in air are filtered by whisker resonance, then the whisker must be underdamped making resonance more likely to play a role in texture discrimination and also making it a possible mechanism for other sensory tasks. Previously it was reported that when a rat actively swept its whisker past a bar, following deflection past the bar whiskers underwent approximately one oscillation at the resonant frequency (Hartmann et al 2003). This suggested that whisker resonance was highly damped, however the

authors suggested that resonance may play a role in facilitating the detection of edges by the whiskers. The same study also reported that no resonance was observed during active whisking in air. We found however that there are high frequency whisker vibrations in air and that these are filtered by whisker resonance. This suggests that whisker resonance is prevalent in the behaving animal and may play a more active role in shaping sensory input than previously thought. This also makes whisker resonance a plausible mechanism for both texture encoding and other sensory tasks (Moore et al 2004). In Sections 2.4 and 2.5 we then make the argument that the observed vibrations in air must be due to high frequency muscle activity acting on the whisker follicle.

2.1 Whiskers exhibit coherent high frequency vibrations in air

In order to measure whisker motion and resonance in the behaving animal, five adult Long-Evans rats (2 male, 3 female) were trained to hold their nose in a nosepoke and whisk for water reward. While in the nosepoke a laser line (60 mm long, 2mm wide) was projected along the right side of the animal approximately 10 mm from the whisker pad (figure 2.0A). This laser projected through a slit in the floor onto a linear CCD array (4 kHz frame rate) positioned under the training cage. The shadows created by the whiskers resulted in voltage offsets in the CCD image (figure 2.0C) and these shadows were tracked over time to produce whisker position as a function of time (figure 2.0D) with a spatial resolution of ~ 5 μm. In order to confidently identify whiskers in the CCD image up to four whiskers within a single row were left intact on

the right side of the face while all other whiskers were trimmed at the base. Four phototransistors sitting in the floor of the cage underneath the whiskers registered whisker motion. The signals from the phototransistors were used to train the rat to whisk while in the nosepoke. Before water was delivered to the drinkport a set number of pulses had to be generated by whisker motion over the phototransistors to insure the rat was whisking while in the nosepoke. For each trial a 1.5 second block of data was collected and rats typically performed 50-100 trials per day. Details of this training procedure are given in the methods section at the end of the chapter.

Whisker measurements included periods of 6 - 8 Hz whisking, periods when the whiskers were held relatively still, and periods of erratic motion that could not be categorized as either whisking or still. Examples of these three types of whisker motion are shown in figure 2.1A. Figure 2.1B shows high pass filtered segments of the three types of whisker motion (low, high cutoffs were 30 Hz and 1 kHz). During all types of motion there were small amplitude, high frequency vibrations superimposed on the lower frequency motion.

We performed two control experiments to determine the source of these vibrations. First, we attached an isolated whisker to an electric motor, which moved sinusoidally at 8 Hz to mimic normal whisking (Fig 2.1 C). No significant vibrations above 8 Hz were observed (see bottom trace), indicating that the vibrations in the whisker motion of the awake animal are neither due to interactions between the whisker and the air nor are they due to external vibrations in the recording apparatus. Second, we simultaneously measured the head and whisker motion in two rats by

attaching a horizontal bar to a post fixed to the head. The bar cast a shadow on the CCD array which was offset from the shadows cast by the whiskers. The spectral coherence between the head and D1 whisker motion (Fig 2.1D) shows a peak at about 8 Hz but on average only 13% coherence at frequencies greater than 10 Hz, indicating that head motion is not the source of higher frequency vibration. Interestingly the spectral coherence is much greater between whiskers than between the whisker and the head. This indicates that there is a common driving force across whiskers, which is separate from the head, or external vibrations. Figure 2.1E shows the average coherence between whiskers and between a subset of whiskers and the head for one rat. Whisker vibrations are highly coherent across arcs, although the coherence magnitude falls off slightly as the distance between whiskers increases. We therefore see that, even in the absence of a texture, there are high frequency vibrations superimposed on the low frequency whisking motion and that these vibrations are highly coherent across whiskers.

2.2 High frequency vibrations are filtered by whisker resonance

To test whether whisker resonance shapes whisker vibrations in air we measured the spectral content of whisker vibrations as the whiskers were shortened. Decreasing the length of the whisker causes the resonance frequency to increase (see chapter 1). If whisker vibrations are being selectively filtered depending on the

resonance frequencies of the whiskers then we expect to see the spectral content of the whisker vibrations shift as the resonant frequencies shift.

The resonant properties of the whiskers depend primarily on the whisker length, which varies systematically across the facial pad. Figure 2.2A shows the effect of delivering a sharp impulse to Delta (52.0 mm) and D3 (24.8 mm), and measuring the resultant decaying oscillations. The decaying oscillations occur at the resonant frequencies, which in this example were 36.7 Hz (Delta) and 112.0 Hz (D3). Figure 2.2B shows the power spectra of D1 and D3 measured simultaneously in the same animal during natural whisking in air (on average 70 +/- 20 trials were used for computing each power spectrum shown here). The open circles were the resonant frequencies of each whisker measured with the impulse method. The asterisks were the theoretical first harmonics which are predicted to be (10.6/4.4) x FRF for a conical beam. Figure 2.2C shows the second derivative of the logarithm of the power spectra in B. Points at which the second derivative is a minimum were used to find where the power spectra have negative concavity, indicating a peak at that frequency. As can be seen in B and C, minima in the second derivative aligned nicely with the measured FRF's and the calculated harmonics. Figure 2.2D shows the FRFs measured with the impulse method plotted against the first point of minimum concavity in the power spectra. These points fall around the 45 degree line indicating that FRFs could be calculated solely from the shape of the whisking power spectra. Similarly, figure 2.2E shows the first harmonic calculated from the measured FRF plotted against the second point of minimum concavity in the power spectrum. Again, these points lie along the

45 degree line, indicating that the first harmonic of the FRF can also be predicted from the shape of the power spectra. We tested whether the ratio of the frequencies at which the first and second peaks in the power spectra occured follows the predicted ratio of 10.6/4.4 = 2.41. Figure 2.2F shows the measured ratios for the eight whiskers. The average ratio of 2.35 +- .14 is shown as the dotted line and the solid line is the theoretical ratio. Figure 2.3 shows the cumulative result of all FRFs measured with the impulse method and the FRFs found by looking at the first peak in the power spectra. The FRF falls off faster than $1/l$, as expected from the theoretical relationship of FRF ~ r/l^2, where r is the radius at the base and l is the whisker length. This relationship is explained in more detail in chapter 1 and is derived in appendix A.

In order to verify that the whiskers' resonance properties were filtering the HF vibrations in air, we looked at the change in power spectra as the whisker lengths were altered. If the peaks in the power spectra were due to resonance filtering then we expected the peaks to shift as the resonance frequencies changed due to changing length.

Figure 2.4 shows the result of the trimming experiment in two animals. On each day the D2 and D1 whiskers were trimmed ~2mm in rat 1 and δ and D1 were trimmed in rat 2. D3 and δ were left untrimmed in rat 1 to serve as a control. All other whiskers on the pads of both rats were trimmed at the base. At each length the FRFs were measured with the impulse method (white open circles) and the first and second harmonics were calculated from the measured FRFs (white asterisks, diamonds respectively). Here, because the whiskers were being trimmed we modeled them as

truncated conical beams and use the results of Conway et al (1964) as described in chapter 1. For truncated beams the ratio of FRF to the first and second harmonics no longer stays constant, instead the ratio increases as the whisker is trimmed.

In figure 2.4, a clear relationship can be seen between the increase in the resonance frequencies and harmonics and the shift in the power spectra for the trimmed whiskers. By comparison, the untrimmed whiskers, D3 and Delta, did not have a shift in their power spectra. The effect of the harmonics can be clearly seen in the D1 and δ power spectra. The D1 spectra for the two rats show bands of amplification which followed the increase in the first harmonics of the resonance frequencies. The δ power spectrum in rat 2 has bands of amplification which follow both the increase in the first and second harmonics. The resonant properties of the whiskers therefore prominently shape the magnitude of whisker vibrations even in air.

We also looked at the opposite case of what happens to the resonance filtering as a whisker naturally grows. As the length increases due to re-growth the resonance frequency will decrease so we expected to see the power spectra shift to lower frequencies. This case is shown in figure 2.5. In one rat we show that, as the D2 whisker re-grows from 19.8 mm to 32.0 mm the peak in the power spectrum at ~100 Hz before re-growth is filtered out after re-growth and a small peak occurs at ~ 60 Hz. Again we compare this to the D3 whisker which remained approximately constant length over the 14 days of re-growth. In comparison to the re-growing whisker, the D3 whisker power spectrum remains unchanged.

2.3 High frequency vibrations are phase-shifted across whisker due to resonance

A general property of a driven, resonating system is that the phase between the driving force and the system response will depend on the difference between the resonance frequency of the system and the driving frequency. For driving frequencies just below the resonance frequency the response of the system will have a positive pi/2 phase shift relative to the driving phase, and for driving frequencies just above the resonance frequency the system will respond with a negative pi/2 phase shift. Figure 2.6 shows the response of a model resonating system with a resonance frequency of 100 Hz. The left and middle traces show the system response when it is being driven just below the resonance frequency (80 Hz) and just above the resonance frequency (120 Hz). At 80 Hz the system response (blue trace) is positively phase shifted with respect to the driving force. When the driving frequency is 120 Hz however the response is negatively phase shifted with respect to the drive. The graph on the right of figure 2.6 shows the theoretical dependence of the phase on frequency for this system. The area of transition between plus and minus pi/2 is centered at the resonance frequency (100 Hz). The sharpness of this transition is determined by the amount of damping in the system.

While we do not have a direct measurement of the forces driving the whiskers, we can look at the relative phase between whiskers. Because the whisker vibrations appear to be coherent in different whiskers we expect that the driving forces across

whiskers must be phase-locked to each other. If multiple whiskers have the same driving force then we expect the relative phase between whiskers to be well-defined. If whisker resonance is filtering the driven vibrations then we predict that the relative phase between vibrations in different whiskers will change as a result of changing the resonance frequency.

We tested this prediction in one rat trained to hold its nose in the nosepoke and whisk. While in the nosepoke we measured whisker motion of the D1, D2, D3, and δ whiskers using the linear CCD array as described above and in the methods section. Over the course of 11 days we trimmed the whiskers ~ 2mm/day and measured the whisker motion on each day. This data was the same as the data shown for rat 1 in section 2.2. The coherence between each combination of the four whiskers was calculated for each day and we looked at how the phase relationships changed as the resonance frequencies increased. From the model explained above we expected the relative phases between whiskers to go through sharp transitions at frequencies near the resonance frequencies and that this region of transition would shift as we changed the resonance frequencies.

Figure 2.7 left shows an example of the phase relationship between vibrations in D1 and D3 whiskers as a function of frequency. There was a distinct phase shift of ~ $\pi/2$ for frequencies below the D3 fundamental resonance frequency (red circle) and a shift of ~ $-\pi/2$ above the D3 resonance frequency. For frequencies much above the resonance frequencies there was no phase shift as would be expected if this is a resonance effect.

The sharpness of this peak also suggests that the whiskers are relatively underdamped.

To verify that the observed phase shifts were due to the resonant properties of the whiskers we looked at the phase change as a result of changing the resonant frequencies. In contrast to the untrimmed whiskers (fig 2.7 middle), the frequency region where D1 vibrations lead D2 vibrations (red band) followed the change in resonant frequencies as these two whiskers were trimmed (fig 2.7 right). The relative lag between peaks in the whisker vibrations caused by the resonant properties can be as much as 3-4 ms (fig. 2.7 right). The phase dependence on the resonance frequency is further evidence that resonance shapes whisker responses when whiskers move in air. In addition, the distinct phase relationships across whiskers indicate that the whiskers are being driven by phase-locked forces.

2.4 What drives high frequency vibrations?

Because we previously ruled out head motion and external vibrations as the source of high frequency vibrations we measured the EMG of a subset of the facial muscles to determine if muscle activity drives vibrations in the whiskers. EMG stereotrodes were chronically implanted in the intrinsic and extrinsic muscles of 5 animals (1 nosepoke and 4 head-fixed). Whisker data from the nosepoke animal was collected in the same manner as described in the introduction to this chapter. EMG data from the nosepoke animal was recorded continuously throughout the recording session. Trigger pulses used to begin whisker data acquisition were recorded in order

to synchronize the EMG data with the whisker data. In order to simultaneously collect whisker and EMG data from the head-fixed rats, they were placed in approximately the same position as the nosepoke animals with respect to the imaging laser (figure 2.0 B). The whiskers therefore cast shadows onto the CCD array and these were tracked over time. EMG data was collected simultaneously from chronically implanted stereotrodes in either the intrinsic or extrinsic muscles. Whisker data and EMG data was collected in 3 second blocks for the head-fixed rats. Head-fixed animals were sporadically coaxed to whisk in order to have data during both whisking and non-whisking behavior. The high frequency vibrations studied in both the head-fixed and nosepoke animals appeared qualitatively similar.

In order to determine whether the muscles responsible for whisking motion may also drive higher frequency vibrations, we calculated the spectral coherence between the rectified, low-pass filtered (1 kHz cutoff) EMG signal and the whisker motion. We then compared the frequencies at which there was significant coherence magnitude to the resonance frequencies of whiskers in the same arcs. If the frequencies at which the coherence is significant lie within the range of the resonance frequencies then it is likely that contractions of these muscles contribute to driving whisker resonance.

Figure 2.8 A shows an example of the spectral coherence measured between the D1 whisker and an EMG recording from the extrinsic muscles of one rat. The red line is the 95 % confidence interval calculated as in O'Connor et al (2002). The green trace is the coherence after smoothing with a 20 Hz window. The black vertical line

shows the cutoff frequency at which the smoothed coherence drops below the 95% confidence interval. For this example the cutoff frequency was ~ 75 Hz. Figure 2.8 B shows the cutoff frequencies measured in all 5 animals. The results are separated into the coherence between the whiskers and either the intrinsic or extrinsic EMG recordings (figure 8 B, the two leftmost plots). Only EMG recordings that were clearly distinguishable as either extrinsic or intrinsic were included for analysis, resulting in 8 measurements of the cutoff frequencies, which fall between approximately 50 Hz and 200 Hz. For comparison with the resonance frequencies, we separated the cutoff frequencies for the D1 and D2 whiskers. The two rightmost plots in figure 8 B show the cutoff frequencies for the D1 and D2 whiskers separately as well as all arc 1 and arc 2 resonance frequencies measured from this and other experiments. On average the coherence between the whisker vibrations and the EMG recording was significant at frequencies that span the resonance frequencies of these whiskers, indicating that muscle contractions can contribute to higher frequency whisker vibrations. Figures 8 C-E show the average coherence for the 5 intrinsic and 3 extrinsic EMG recordings. On average the coherence between the whiskers and the extrinsic EMG dropped below significance at ~ 70 Hz while the intrinsic EMG had a coherence cutoff of ~ 100 Hz. While the magnitude of the coherence was significant it was relatively small indicating that the specific muscles we recorded from were not the only cause of whisker vibrations. One explanation for the low coherence values may be that there were many other forces driving the whiskers during active whisker

use, resulting in a low average coherence magnitude between the whisker vibrations and the subset of muscles we measured.

In anesthetized animals it was observed that, although the whiskers did not make large amplitude movements, there was still electrical activity measured on the EMG electrodes. We therefore tested whether the EMG/Whisker coherence was higher in the anesthetized animal when there is less background activity and therefore fewer other forces acting on the whiskers. The upper left trace of figure 2.9 shows the coherence measured while the animal was relatively deeply anesthetized (i.e. little to no toe pinch reflex). Under anesthesia, there were pronounced coherence peaks centered at 56.6 Hz and 163.1 Hz. We then allowed the animal to come out of anesthesia slightly while we continued recording whisker motion and EMG activity. As can be seen in figure 2.9, as the anesthesia began to wear off, the magnitude of the coherence peaks decreased. As the anesthesia wears off there is also an increase in general EMG activity suggesting that in the awake animal there is much more background activity which causes the average coherence between a single EMG recording and the whisker motion to be lower. The lower right trace in figure 2.9 shows the average coherence measured in the awake, behaving animal measured on a separate day. Although the magnitude of the coherence was significant in the awake animal up to ~ 100 Hz, it was small, indicating that other forces must also be responsible for driving whisker vibrations.

The effects of anesthesia on the coherence are shown more directly in figure 2.10. The top traces show the whisker acceleration measured in the deeply

anesthetized, lightly anesthetized and awake animal. The bottom panels are the temporally aligned intrinsic EMG recordings. The black dots in the upper traces show where the peaks in the EMG occur relative to the whisker oscillations. Under deep anesthesia the phase locking between EMG peaks and whisker oscillations is good, however when the animal is lightly anesthetized and just beginning to whisk that phase-locking disappears which is also generally true for the awake animal. We also saw that the amplitude of oscillations greatly increases between the anesthetized and awake animal suggesting that, in the awake animal there are additional muscle forces responsible for driving the whiskers which may account for the lack of general coherence across all whisker motion in the awake animals. We therefore find that, while muscle forces can drive coherent high frequency oscillations in the whiskers, in general the coherence between high frequency muscle activity is low which is likely due to an increase in activity that we are not measuring.

2.5 Resonance filtering during controlled muscle stimulation

One drawback to the previous experiments is that there can be multiple muscle forces acting simultaneously on the whiskers and we only record the EMG activity in a subset of these. Furthermore, the whiskers were being driven with a wide range of frequencies. In order to look more closely at resonance filtering of muscle-induced vibrations we stimulated the facial nerve with burst of 5 V pulses at a single frequency (110 Hz) to induce artificial protraction of the whisker. Each burst contained 5 pulses

and the bursts were separated by 100 ms. Following the protraction due to the stimulation, the whiskers passively retracted, generating 10 Hz artificial whisking. By trimming the whisker, we were able to look more directly at the interaction between the single driving frequency and the resonance frequency. Figure 2.11A shows the effect of trimming the D1 whisker on filtering during facial nerve stimulation. Whisker motion is shown for three whisker lengths (20.6, 16.1, 12.6 mm) and resonance frequencies (82.6, 120.5, 172.4 Hz). As can be seen in the middle trace, there was a large amplification of the driving force when the D1 resonance frequency (120.5 Hz) came closest to the drive frequency (110 Hz). Figure 2.11B (top) shows the change in power spectra in the same experiment for all whisker lengths. From 2.11B it can be seen that the middle trace in 2.11A corresponds to the point of intersection between the resonance frequency and the driving frequency. By comparison, the D2 whisker was left untrimmed and the power spectra did not change over the course of the experiment. Figure 2.11B (bottom) shows the results of a similar experiment in a second animal. Again, the power spectra of whisker vibrations shift to higher frequencies in the trimmed whiskers while the spectra stay constant in the untrimmed whisker. In this example the interaction between driving force and whisker resonant properties is nicely seen in the D3 power spectra. The first harmonic of the D3 resonance frequency overlaps with the first harmonic of the drive frequency. This results in a clear band of amplification at 220 Hz. This shows that whisker vibrations during active motion can reflect muscle activity and we clearly see that the whisker resonant properties affect the filtering of these vibrations.

2.6 Discussion

Whisker resonance is hypothesized to be important for texture coding (Neimark et al 2003, Andermann et al 2004). As a whisker passes over a texture it is hypothesized that the spatial properties of the texture will induce a unique set of frequencies in the whiskers and that these vibrations will be differentially filtered across whiskers due to their different resonance frequencies. Whisker resonance has been clearly shown to filter whisker vibrations in the anesthetized animal (Neimark et al 2003). The degree to which resonance can play a role in shaping sensory input however is largely dependent on the amount of damping in the system during active whisker use. Due to constantly changing muscles forces acting on the whisker follicle and potential energy loss due to friction as the whisker pivots in the skin, it is possible that whiskers are in a more highly damped state during active use.

The only observation of whisker resonance in the awake behaving animal was during active palpation of a stationary bar (Hartmann et al 2003). As the whisker deflected past the bar it underwent ~1 oscillation at its resonance frequency before being damped out. In that study it was also claimed that no whisker resonance in air was observed. More work is needed however to understand the role of resonance in shaping sensory input in the behaving animal.

To this end we measured whisker motion in behaving animals during whisking in air. During natural whisker motion in air there were higher frequency vibrations superimposed on the large amplitude 6-10 Hz whisking motion (fig. 2.1). These

vibrations could be seen by eye after high-pass filtering the whisking data and the frequency content of the vibrations were quantified by calculating the power spectra of whisker motion. The frequency content of these vibrations was within the range of the resonance frequencies of the Greek through arc 3 whiskers. By trimming the whiskers and measuring the change in the vibration power spectra we found that they drove resonance in these whiskers (fig. 2.4). This observation is in contradiction to the observation made in the Hartmann et al paper. However in this set of experiments resonance in air is a robust effect that at least implies that whisker vibrations are not overly damped.

We found that the higher frequency vibrations in air were coherent across whiskers (fig. 2.1E). This general coherence can be seen by eye in figure 2.1 B by comparing the filtered whisker vibrations across the different whiskers. We measured the relative phases of whisker vibrations across whiskers and found that the phases displayed abrupt phase transitions between +/- $\pi/2$ (fig. 2.7), a characteristic property of resonating systems. This observation implies two things about whisker motion in air. First, due to the relatively pronounced phase transitions centered at the whiskers' resonance frequencies, it implies that whiskers are not in an overdamped regime and whisker vibrations are robustly filtered by resonance. Second, the distinct phase relationships at high frequencies imply that the whiskers must be driven with a common source and that this driving force must be coherent across whiskers.

This suggests that correlated activity in the facial muscles may drive correlated whisker vibrations which could be important for determining whisker dynamics as the

whiskers are actively swept across a textured surface. We tested whether high frequency muscle contractions can drive whisker vibrations by simultaneously measuring the whisker motion and the EMG activity in the intrinsic and extrinsic muscles. We found that there are high frequency oscillations in the EMG that can be coherent with the high frequency whisker motion. We found that the average coherence between the EMG and whisker motion is significant up to ~ 70 Hz and ~100 Hz for the extrinsic and intrinsic muscles respectively, measured in the D1 and D2 whiskers. Because resonance frequencies of these whiskers span a frequency range of approximately 25 Hz to 65 Hz the extrinsic and intrinsic muscles can drive higher frequency vibrations and whisker resonance. The magnitude of the coherence at the higher frequencies is small however, indicating that the forces reflected by the EMG recordings must only be a subset of the forces driving the whiskers.

We further explored the interaction between muscle contractions and the intrinsic resonance frequencies of the whiskers by artificially stimulating the muscles to cause fictive whisking. During this fictive whisking we found that the stimulation frequencies are present in the large whisker motion and that these are robustly filtered by whisker resonance (fig. 2.11).

On the sensory side, the prevalence of whisker resonance in air makes it plausible that resonance does play a role in shaping sensory information during active whisker use. From the perspective of whisker control, for accurate whisker positioning the animal may want to avoid resonance. This could mean driving the whiskers with a broad frequency band such that no whisker is preferentially excited by

the muscle control. Or the muscle contraction frequencies could be far away from the resonant frequencies of the whiskers. This may be difficult however because, as we showed, the harmonics may be excited also and it could be difficult to avoid all resonance frequencies and harmonics. Resonance may also be avoided by increasing the damping forces acting on the whisker. The idea that the damping in the whisker may be actively modulated by the rat through changes in pressure exerted on the whisker follicle has been previously suggested as a means by which the animal may change the impact of whisker resonance on sensory information (Hartmann et al 2003, Neimark et al 2003). We also suggest that increasing the damping in the whisker may be beneficial for avoiding muscle-induced whisker resonances such as those seen in the artificial whisking experiments above (specifically see the middle trace of figure 2.11A).

In chapter 3 we look at the role of whisker resonance in shaping whisker vibrations during texture palpation and ask whether the spatial properties of the texture determine the degree to which resonance occurs.

2.7 Methods

Whisker measurements in behaving animals whisking in air were performed using two methods. In the first method rats were trained to hold their nose in a nosepoke and whisk for water reward (figure 2.0A). In the second method animals were head-fixed and coaxed to whisk (figure 2.0 B). In total 7 adult Long-Evans rats

were used for whisking in air measurements. Five of these were trained to do the nosepoke behavior and two were head-fixed.

EMG recordings were performed in two head-fixed animals and one nosepoke animal. Additionally artificial whisking experiments were performed in two adult Long-Evans rats that had undergone acute surgery and remained anesthetized throughout the experiments. The details of these methods are described below.

In order to measure high frequency vibrations during active whisker motion, rats were trained to hold their nose in a nose poke and whisk for water reward (Fig 2.0A). While in the nose poke, whiskers blocked a laser line projected along the right side of the animals whisker pad. The laser was focused onto a CCD array which sat below the whiskers. Shadows in the laser produced voltage offsets in the CCD image (figure 2.0C). These shadows were tracked over time to produce whisker motion traces (figure 2.0 D) Phototransistors in the floor of the cage registered whisker motion which was required for water delivery.

2.7.1 Behavioral training apparatus

The behavioral apparatus for measuring whisker motion in the animals trained to nosepoke consisted of two chambers, a reward chamber and a measurement chamber. This training cage was modeled after Krupa et al. The measurement chamber had a nose poke in the center of the front wall (Fig 2.0 A). Inside the nose poke there was an infrared phototransistor/photodiode pair which registered when the

animal was in the nose poke. At the side of the nose poke there was a slit in the floor which allowed the laser beam used for whisker tracking to pass through to the CCD array below the cage. The position of the slit and light were adjustable so that whisker motion could be measured at different locations with respect to the head. Four phototransistors sat in the floor of the cage, parallel to the slit. These were illuminated by a set of five infrared LEDs sitting above the nosepoke. The signal from each phototransistor was converted to a five volt pulse by differentially amplifying and bandpass filtering it using a custom built circuit. These five volt pulses were sent to the training software which kept count of how many pulses were generated during one nosepoke trial. In order to train the rats to whisk, the animals were required to generate a set number of pulses before water was delivered to the drinkport. Water delivery was accompanied by a white noise tone which signified the availability of water. By slowly increasing the whisking requirement we trained the animal to whisk while in the nosepoke.

The reward chamber contained a drink port that was controlled by a solenoid valve (GC valves S511GA16N1AD5). A phototransistor inside the drink port registered the presence of the animal and was used to trigger the valve to open. All of the training and recording procedures were computer controlled using custom written programs in Labview (National Instruments).

2.7.2 Training Procedure

Animals were water deprived 22 hours/day to motivate them to do the training. Animals received water in 50 µl aliquots as reward for doing the task and they received ad-lib water for one hour following the training sessions which took place Monday - Friday. Animals received ad-lib water Friday night through Sunday night.

Training took place in three stages. In stage one, rats were trained to associate a white noise tone (WNT) with water delivery at the drink port. Animals were monitored via an infrared camera sitting above the cage. When an animal was near the drinkport water was delivered to the drink port following a 100 ms long WNT. Initially, after the animal drank the first drop of water in the drinkport, additional water was delivered followed by the WNT in order to reinforce associating the tone with the water. As the animal learned this association the additional water was discontinued. Stage one training was considered complete when the rat anticipated water delivery at the drink port following the WNT and immediately went to the drink port to drink. Stage one training took ~ 4 days.

In stage two, animals were trained to poke their nose in the nose poke to trigger the WNT and water delivery to the drink port. At the beginning of stage 2 the nosepoke was put in the reward chamber and the nosepoke chamber was sealed off. In order to motivate the animals to poke their nose, a small drop of water was delivered to the nose poke at the beginning of stage two. Each time the animal drank the water in the nose poke it triggered the WNT and water delivery at the drink port. Additional water was delivered to the nose poke upon drinking from the drink port. The additional water in the nose poke was gradually removed until the animal triggered the

WNT without the need for water in the nose poke. After water was discontinued at the nosepoke, the nosepoke was moved to the nosepoke chamber where it was left for the rest of the training and measurements. At that point stage two was considered complete. This took ~ 5 days.

In stage three animals were trained to hold their nose in the nose poke while actively moving their whiskers. The WNT was triggered after a set number of pulses had been generated by the whisker motion. The number of pulses required to trigger the WNT and water delivery was slowly increased until the animals held their nose in the nose poke and whisked for ~ 1 second. At this point training was considered complete and animals did between 80 and 150 trials per day. This took ~ 14 days. The day before collecting whisker motion data the animals were lightly anesthetized with isoflourane and all but a subset of the δ, D1, D2, and D3 whiskers were trimmed. While whisking in the nosepoke, data was collected using the CCD array as described below. The CCD array was placed at approximately a 7 degree angle with respect to the nose poke and 10 mm from the whisker pad which was approximately parallel to the face. Breaking the infrared beam in the nosepoke triggered a 1.5 second block of data collection. Only whisking data taken while the animals were in the nosepoke was analyzed.

2.7.3 Head-fixed whisker measurements

In the second method of measuring whisker motion in awake animals we head-fixed the animals by affixing a post to the head and holding this post in a rigid location

during whisker measurements. Prior to attaching the head post animals went through two stages of gentling. In the first stage animals were held in the lap of the experimenter once a day for ~20 minutes per rat. During this time the rat became accustomed to being handled. This stage lasted ~ 1 week. When the animals had become accustomed to being held, rats were then trained to stay in a body sack. Once a day rats were placed in the sack which was cinched around the body so that they appeared comfortable but were unable to escape from the sack. At the beginning of this stage, animals remained in the sack for just a few minutes. As the animals became more accustomed to being in the sack, this time increased. After animals were comfortable being in the sack for ~15 minutes they were placed in a plexiglass tube with an inner diameter of 2 inches (figure 3.0A). This stage of the gentling was considered complete when the animals were able to stay calm in the tube for at least ten minutes. This entire stage took approximately 10 days.

After reaching the end of stage 2, animals underwent a chronic surgery. During this surgery electrodes used to record the electromyogram (EMG) were implanted in the facial pad and a screw was affixed to the skull using dental cement. Details of the surgery are explained in the EMG section below. After animals had recovered from the surgery (3-5 days) all but 2-3 whiskers in either the C or D rows were trimmed at the base. In order to do the trimming animals were lightly anesthetized with isoflourane gas as described below. On the following day animals were placed in the body sack inside the plexiglass tube. A post was attached to the head screw and the post was held rigid (figure 2.11B). The animal was placed parallel

and approximately 10.0 mm from the laser beam which was used for imaging the whiskers. While head-fixed, animals were allowed to move their whiskers freely. At times rats were gently coaxed to whisk by placing an object in front of them. Whisking data was taken in 3.0 second blocks using the linear CCD array as described below.

2.7.4 Whisker position measurement

Whisker position was measured along one dimension using a collimated light beam and linear CCD array (Fairchild imaging CCD 133AEDC, figure 2.12). Whiskers in the path of the beam produced a shadow on the linear array resulting in a voltage offset (fig 2.11 C) which was read out using custom built electronics (UCSD Physics electronics shop). Voltage traces from the array were stored and processed offline to determine the whisker positions. We use a red diode laser as our light source (Thorlabs, wavelength = 670 nm). Light from the laser was focused into a collimated line 60 mm long and 1 mm wide using two cylindrical lenses (Thorlabs) rotated 90 degrees relative to each other (Front and side views, figure 2.12). The first lens (focal length = 10.0 mm) collimated the beam from the laser diode in the direction perpendicular to whisker motion producing a laser line ~ 2 mm in width. The second lens (focal length = 120.0 mm) collimated the light in the direction parallel to whisker motion, producing a beam ~ 60mm long and 2 mm wide. Below the whiskers, light was then focused down onto the CCD array using a third

cylindrical lens which was identical to the second lens. The linear array was sampled at 4 kHz frame rate and consisted of 1060, 13 μm wide elements. Every other element in the array was used for determining whisker location which was calculated by weighting the pixel number by the voltage offset and averaging. Whiskers in the path of the beam produced a shadow which covered 8-10 pixels on the CCD array so the whisker position was a weighted mean over these pixels resulting in a spatial resolution of ~ 5μm. Whisker position was measured at ~ 10 mm from the facial pad and up to four whiskers in a row could be tracked simultaneously without shadows overlapping. All whiskers which were not being measured were trimmed at the whisker base.

2.7.5 Whisker Trimming

In order to unambiguously image the whiskers using the linear CCD array whiskers on the pad had to be trimmed down to a subset of at most four whiskers within a single row. This was to avoid whisker shadows crossing or whiskers leaving the CCD image such that it would be unclear which peak in the CCD image corresponded to which whisker. Trimming took place under light isoflourane (4%) anesthesia delivered through a nose cone. All but the subset of whiskers to be measured were trimmed as close to the skin as possible. Following trimming the whisker lengths were also measured under 4X magnification using calipers. Whisker

trimming was done weekly and generally took place following the measurement sessions.

2.7.6 Resonance Measurement

To measure the resonance frequencies of the whiskers animals were lightly anesthetized with isoflourane (xxx) and placed in the measurement chamber. The whiskers were placed in the laser beam such that the whiskers were in a similar position as they were during the nose poke whisker measurements. The fundamental resonance frequency (f_0) was measured by delivering an impulse to the whisker and measuring the ringing frequency (fig 2.2A). In the anesthetized animal individual whiskers were deflected manually and allowed to oscillate in free air. The resonance frequency was calculated as the inverse of the average time between peaks in the oscillations (Neimark et al 2003). For untrimmed whiskers the first and second harmonics of the resonance frequency were respectively calculated as: $f_1 = (10.6/4.4)\ f_0$ and $f_2 = (19.2/4.4)\ f_0$ respectively. For trimmed whiskers, the ratios of f_1/f_0 and f_2/f_0 are functions of the truncated length. These ratios were calculated by interpolating the results of Conway et al.(1964) See chapter one (figure 1.3) for a more detailed explanation.

2.7.6 Artificial Whisking

In artificial whisking experiments (Brown and Waite, 1974), an incision was made in the side of the snout posterior to the whisker pad of the anesthetized animal (Urethane n mg/kgA). The buccal motor nerve was separated from the underlying muscle and cut to prevent antidromic activation of the motor nerve (Szwed et al., 2003). The lower branch of the buccal nerve was also cut, generating more natural, horizontal whisks than stimulation with this nerve intact. The distal portion facial nerve was isolated in a stimulating cuff with electrodes placed around the nerve (figure 2.13A). Saline was applied to keep the nerve moist. The nerve was stimulated with brief monophasic pulses (50 μsec duration, 3-6V) from a Grass Stimulator (Model S88K). Pulses were generated at either 110 Hz or 160 Hz in bursts lasting 50 ms followed by 50 ms with no stimulation. Whiskers protracted during the bursts and passively retracted during the 50 ms following the bursts, generating 10 Hz artificial whisking (figure 2.13B).

2.7.7 EMG Surgery[*]

All surgeries were performed under ketamine (90 mg per kg rat mass) and xylazine (10 mg per kg rat mass) anesthesia. Injections were made intraperitoneally with supplemental injections of ketamine (20 mg per kg rat mass) given every 2 hours

[*] All EMG surgeries were performed by Dan Hill in the Kleinfeld lab.

as needed. Bupivicaine, a local anesthetic, was administered at the surgical incision to minimize post-operative pain.

Electrodes for muscle implantation were constructed from Teflon-coated tungsten microwire (0.002" diameter, California Fine Wire, Grover Beach, CA). Microwires were stripped of 1 mm of insulation and implanted in pairs. The tips were separated by approximately 1 mm and oriented along the muscle fibers to obtain the maximum signal (Kamen and Caldwell, 1996). Two incisions were made to expose the musculature for implantation of EMG electrodes: (i) a midline incision extending from the back of the skull to the end of the snout; and (ii) a lateral incision just caudal to the mystacial pad extending from the midline to the most ventral vibrissa row. The skin was deflected to reveal the extrinsic muscle m. nasolabialis. The exposed tip of each electrode was pressed into the muscle tissue and secured at its entry point using Nylon sutures (no 6-0 Ethicon, Johnson and Johnson, Piscataway, NJ). It was not practical to directly expose the intrinsic muscles because of their small size within the pad. These muscles were implanted by threading the microwires through a 26-guage needle and shuttling the needle beneath the skin to its target (Berg and Kleinfeld, 2003). Wire tips were bent back at the needle tip to anchor the wires to the surrounding tissue. These wires were sutured in place at the point where they exited the pad. Finally, a pair of reference wires were stripped of 4 mm of insulation and implanted in the dermis at the tip of the snout, beyond the extent of m. transversus nasi. Electrical signals were conditioned, acquired, and processed as previously described (Fee et al., 1997; Ganguly and Kleinfeld, 2004). Positions were verified at

the conclusion of surgery by passing current through the implanted microwires to stimulate the muscles and confirm the site of implantation.

2.7.8 EMG Recordings

EMG and whisker data were collected in 3 second long contiguous blocks. EMG activity from the electrodes was amplified 20 times and impedance buffered on the head using an 8-channel headstage amplifier (Plexon Instruments HST/8o50-G20). The signal from the headstage amplifier was then transmitted via a set of twisted thin gauge wires to a second amplifier and filter (Plexon Instruments PBX2/16sp-G50). The second amplifier bandpass filtered the signal with high/low cutoff frequencies of 300 Hz and 8 KHz and amplified the signal an additional 50 times. This signal was then passed to the data acquisition card (National Instruments PCI 6259) which was sampled at 32 KHz. At the beginning of each 3 sec block of data, a trigger pulse was sent to both the neural data acquisition card and the whisker data card. Both cards began data acquisition at the onset of this pulse to ensure simultaneous recording of the two signals.

Acknowledgement

Parts of chapter 2 are part of a manuscript in preparation for publication, Wolfe JH, Pahlavan S, Hill D, Kleinfeld D, Feldman DE, untitled. The dissertation author was the primary investigator of the paper.

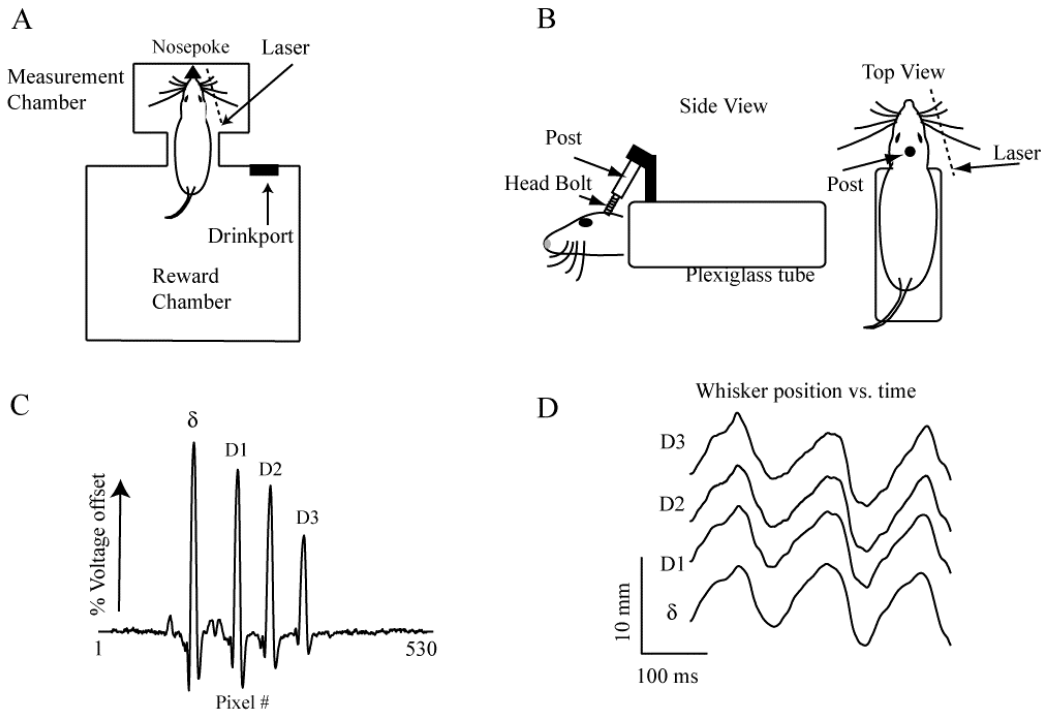

Figure 2.0 **Training and measurement methods**. A) Diagram of nosepoke training. Animals were trained to hold their nose in a nosepoke and whisk for water reward. While in the nosepoke the whiskers were imaged using a linear laser that projected across the whiskers and down onto a linear CCD array. B) Diagram of head-fixed setup and measurements. Animals were held in a plexiglass tube and headfixed. They were then placed in a similar position as the nosepoke animals relative to the laser. C) Shadows from the whiskers cast shadows on the CCD array, resuting in voltage peaks in the CCD output. D) The shadows were tracked over time to measure whisker motion

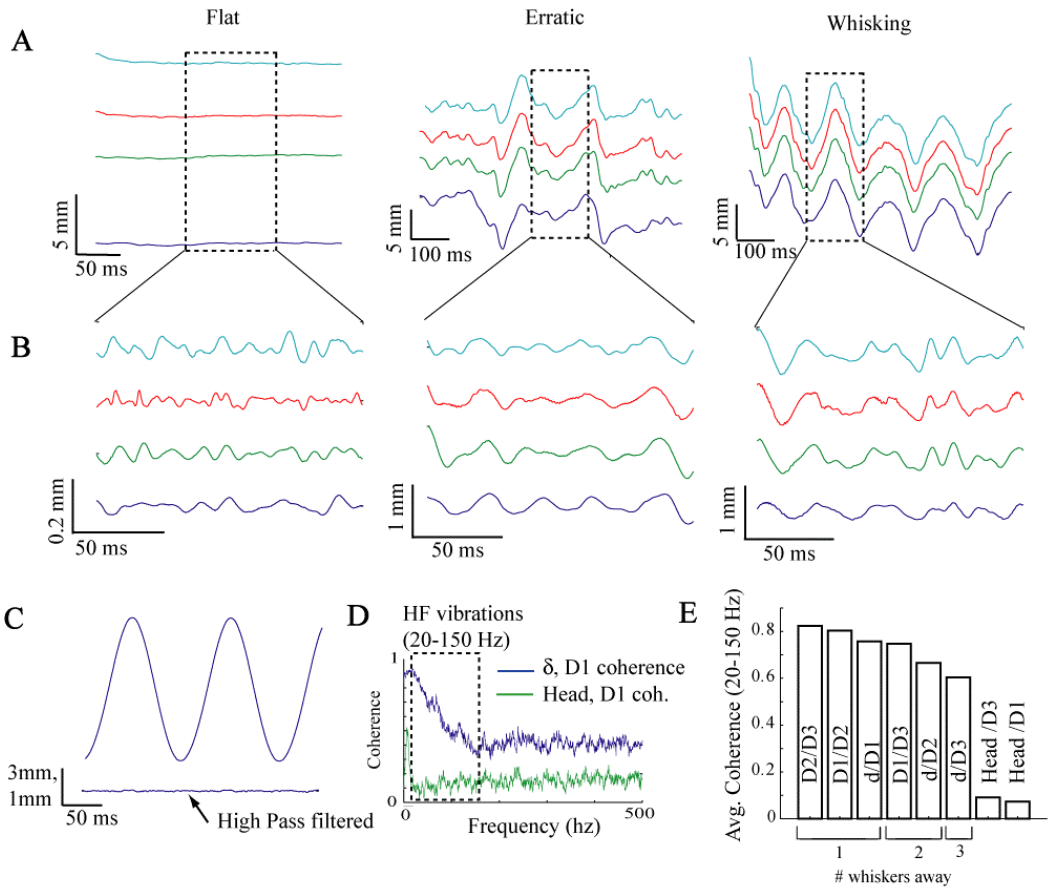

Figure 2.1. **High frequency vibrations are present during natural whisker motion in air**. During all types of whisker motion, higher frequency vibrations are superimposed on the larger amplitude, low frequency motion. A) Whisker motion is classified as either Flat, Erratic or Whisking. B) High pass filtered, expanded view of whisking segments shown in A. High frequency vibrations are superimposed on all types of whisker motion. C) HF vibrations are neither due to vibrations in the training cage, nor are they due to head motion. C) Vibrations are absent in mechanically drivenwhisker. D) Spectral coherence between d and D1 is much higher than the coherence between D1 and the head motion. The driving force for the vibrations must be coming from the facial pad. E)summary of mean coherences across whisker and head motion. (Avg. coherence is the mean coherence between 20 and 100 Hz)

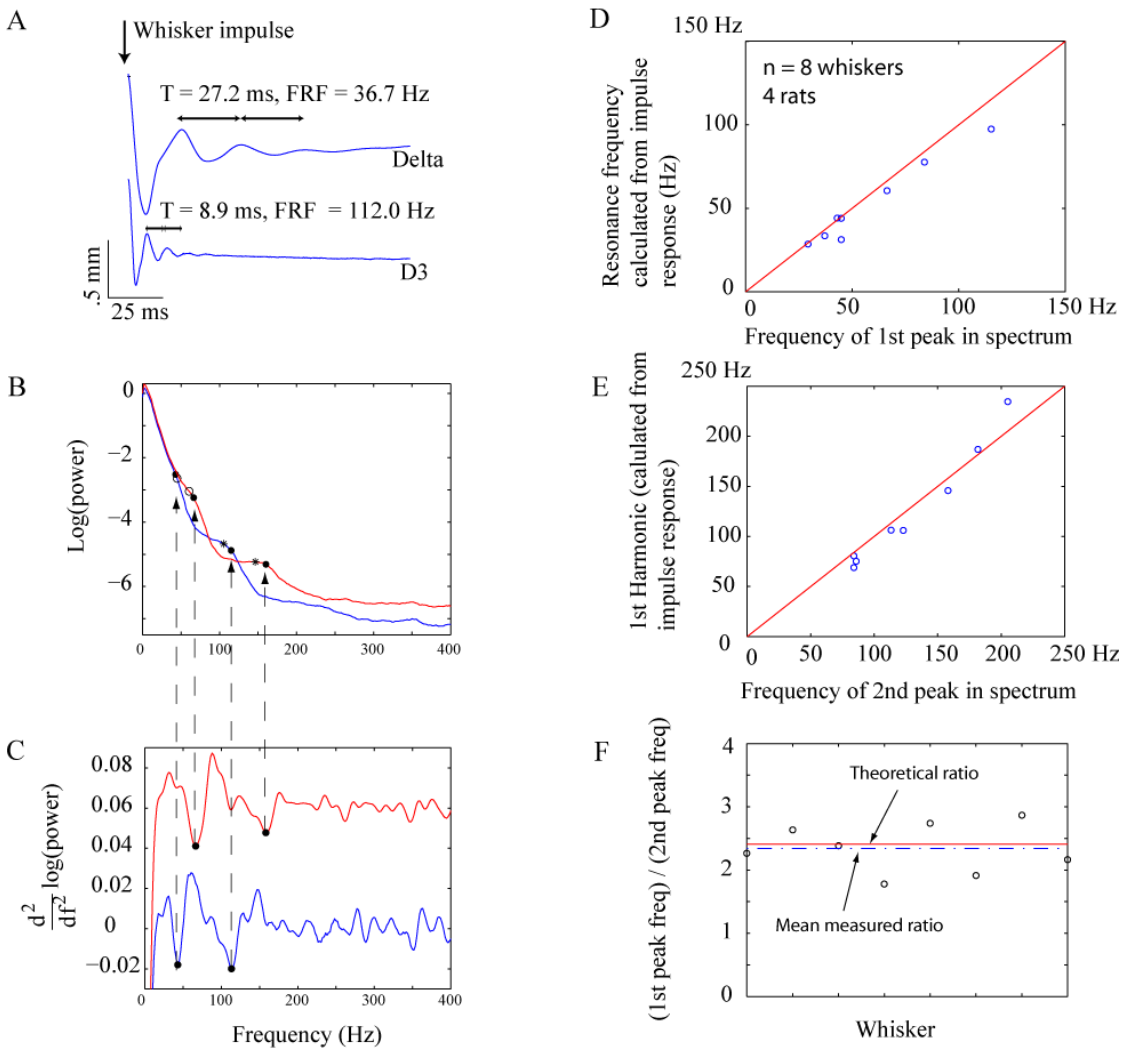

Figure 2.2. **Resonance filters whisker vibrations in air**. Whiskers' resonance frequency was measured using two methods:by measuring the ringing frequency after delivering sharp impulse, and by looking at points of negative concavity in the power spectra. A) Example traces of Delta and D3 whiskers ringing after impulse. B) Power spectra of whisker motion in air. Open circles are the resonance frequencies measured with impulse method and asterisks are the calculated second harmonic frequency. C) Second derivative of D3 and Delta power spectra. Closed circles are the points of maximum negative concavity, also shown in B. D, E) Plots of resonance frequency from impulse method versus the peaks in the power spectra. These points lie along the 450 line indicating that both methods of measuring the resonance frequency and second harmonics give similar answers. F) Open circles, the measured ratio of resonance frequency to second harmonic. The line represents the theoretical value of 2.41.

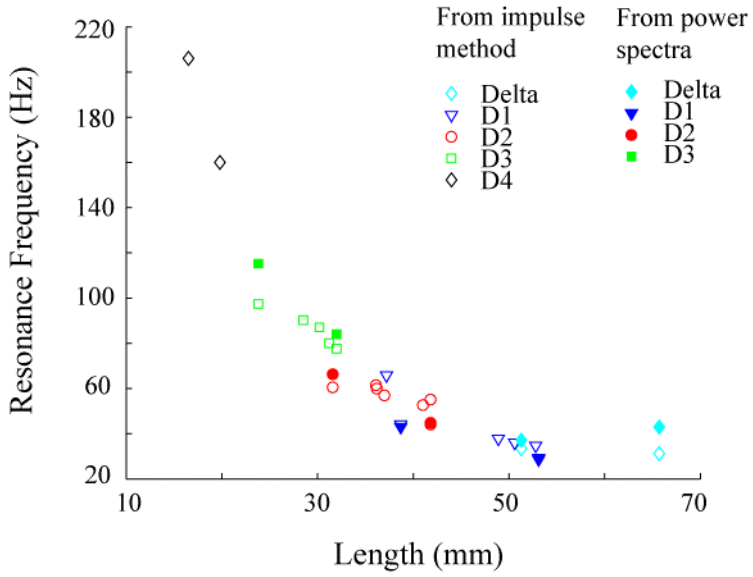

Figure 2.3. **Resonance frequency vs whisker length**. Cumulative results for all measured resonance frequencies and whisker lengths. Open symbols are the resonance frequencies measured by the impulse method. Filled symbols are the resonance frequencies calculated in a subset of whiskers by calculating the frequency at which the first peak in the power spectrum occurs. The data and calculations that are represented by the filled symbols are also shown in figure 3.

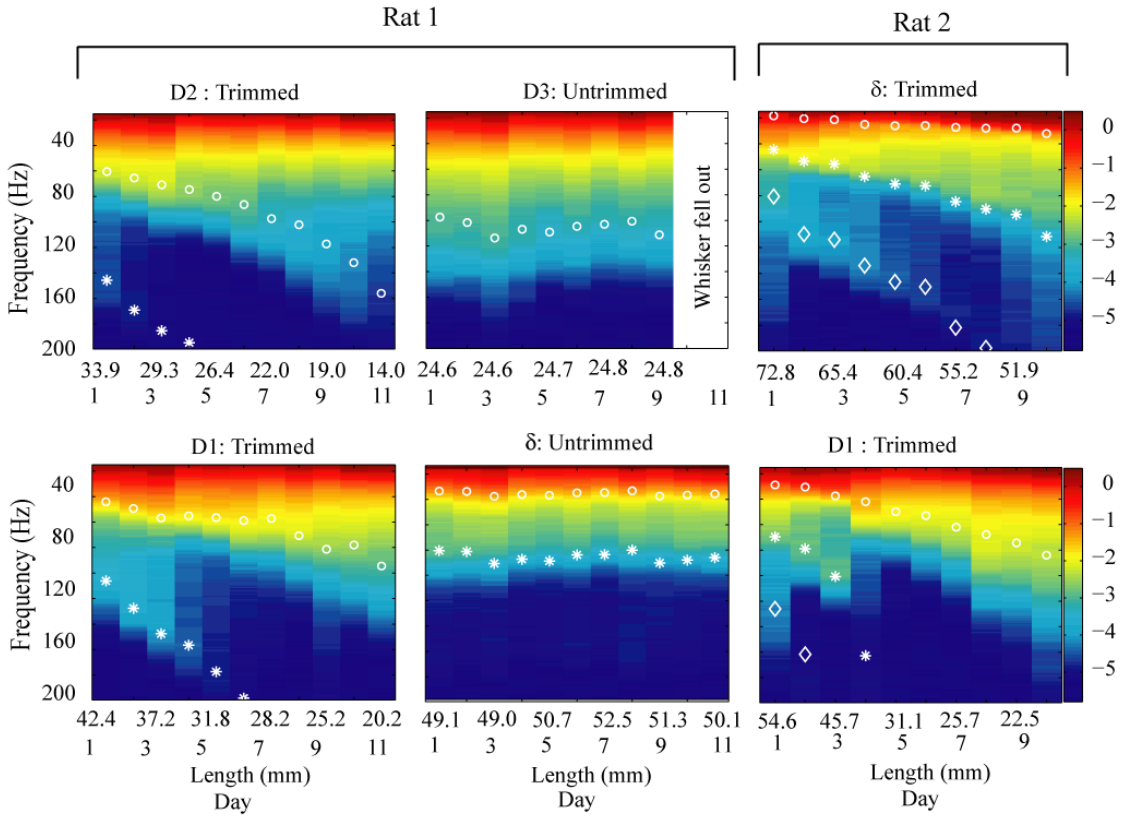

Figure 2.4. **Whisking spectra systematically shift to higher frequencies as the whiskers aretrimmed over consecutive days**. In rat 1 D1 and D2 were trimmed and D1 and d were trimmed in rat 2. D3 and Delta were not trimmed in rat 1 to act as controls. On each day the resonance frequencies were measured (white circles) and the harmonics (white asterisks and diamonds) were calculated based on the truncated cone model of the whisker. In both animals, as the whiskers were trimmed, the power spectra shift to higher frequency values. This shift follows the increase in the resonance frequencies and harmonics, showing that both the fundamental resonance frequency and the harmonics affect filtering of whisker vibrations. In contrast to the trimmed whiskers the untrimmed whiskers' power spectra remain relatively unchanged over the course of 11 days.

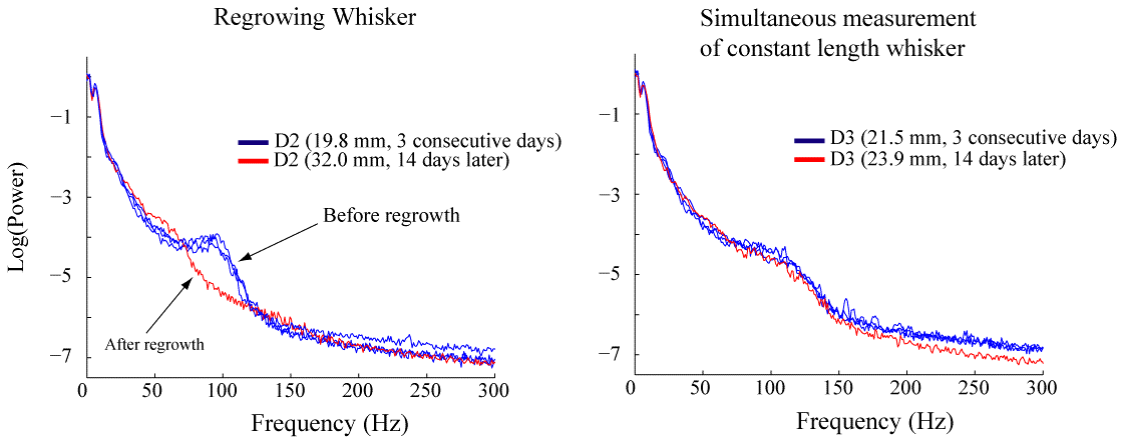

Figure 2.5. **Power spectra of whisker motion in air shift to lower frequencies as the whiskers naturally regrow**. Left, D2 power spectra measured on three consecutive days (blue) compared to the spectrum after 14 days of regrowth. The power spectra clearly shift toward lower frequencies as the resonant frequency decreases due to increasing length. Right, in comparison D3 length stays relatively constant and the power spectrum does not shift.

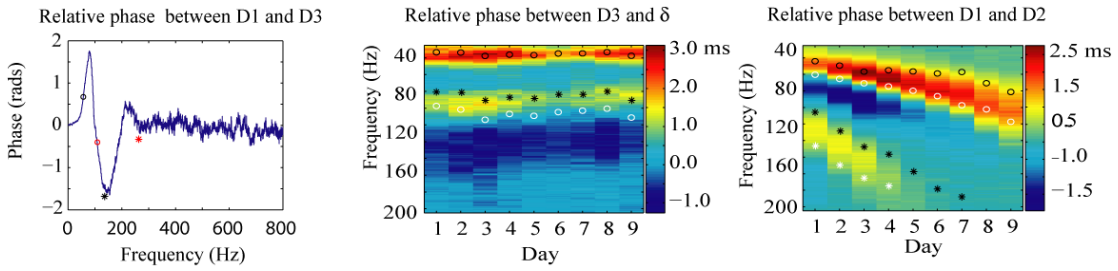

Figure 2.7. **Coherence phases shift during trimming**. Whisking data is taken from rat 1in figure 2.5. Left, example of coherence phase between D1 and D3, Resonant frequencies of D1 (black) and D3 (red) are shown by open circles . Middle, magnitude of the coherence between D3 and d does not change compared to the coherence between D1 and D2 (right). B, the relative phase between the whiskers depends on the resonant frequencies. Middle and right, the relative phase between D1 and D2 changes with the change in the resonant frequencies.

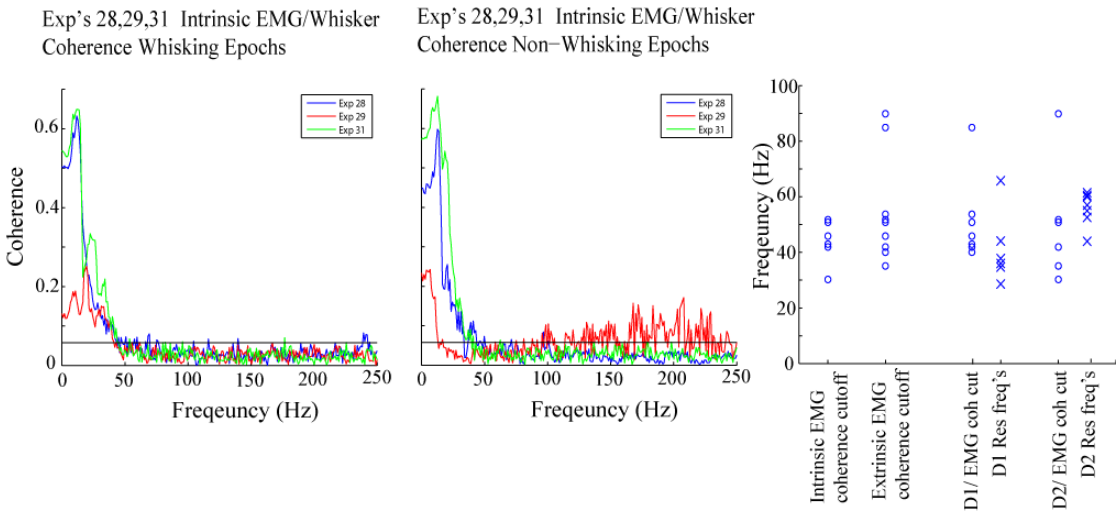

Figure 2.8. **Coherence measurements between whisker vibrations and EMG recordings in the awake animal** A) Coherence between whisker motion and Intrinsic muscles during whisking epochs. Red line denotes the 95 % confidence interval. The green trace is the coherence after smoothing with a 20 Hz box filter. B) Whisker motion/EMG coherence measured during epochs when the whiskers were being held still. C) Two leftmost plots show the cutoff frequencies measured for the extrinsic and intrinsic muscles. The two rightmost plots show the cutoff frequencies separately for the D1 and D2 whiskers (circles). Also shown are D1 and D2 resonance frequencies (these are not necesarily the same whiskers for which the coherence was measured). On average the coherence is significant at frequencies spanning the resonance frequencies of whiskers in arcs 1 through 3.

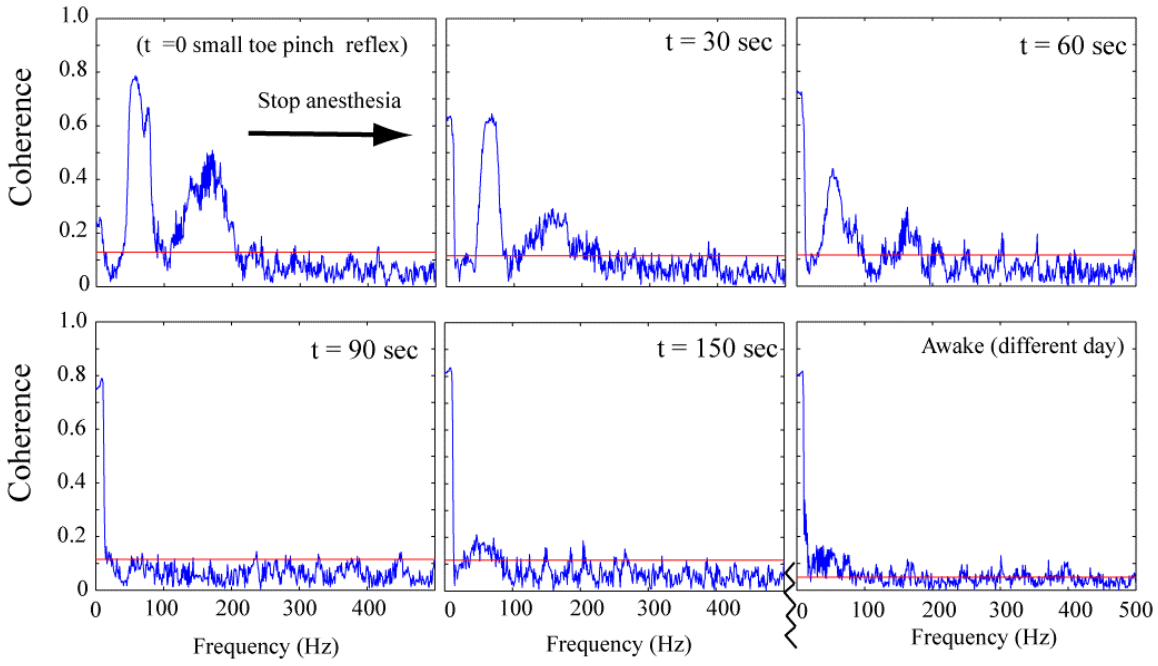

Figure 2.9. **D2 Whisker/Intrinsic EMG coherence under anesthesia.** The lower right panel is the average coherence over 54 trials. In contrast to the anesthetized animal the averagecoherence in the awake animal is not significant at frequencies above the whisking frequencies. The coherence in the awake animal was calculated by averaging the coherence over all types of whisker motion

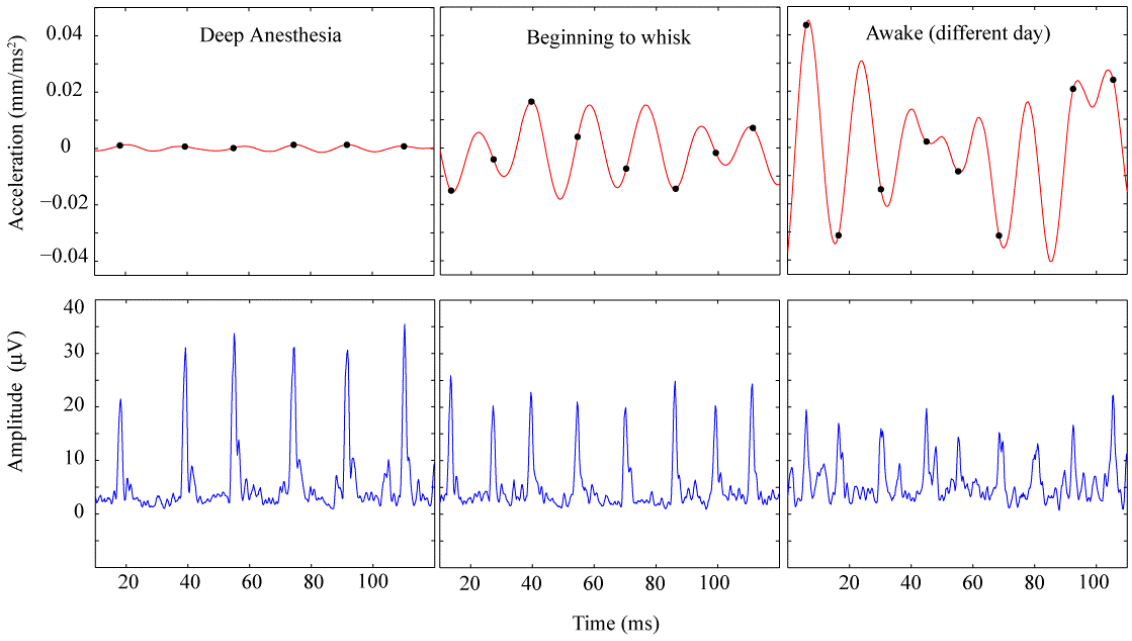

Figure 2.10.**Phase-locking between whisker and EMG can depend on anesthesia**. Whisker motion and intrinsic EMG measured in the animal while deeply anesthetized (left), when it is anesthetized but just beginning to whisk (middle) and in the awake animal measured on a separate day (right). Only when the animal is deeply anesthetized do the EMG peaks phase-lock to the whisker oscillations.

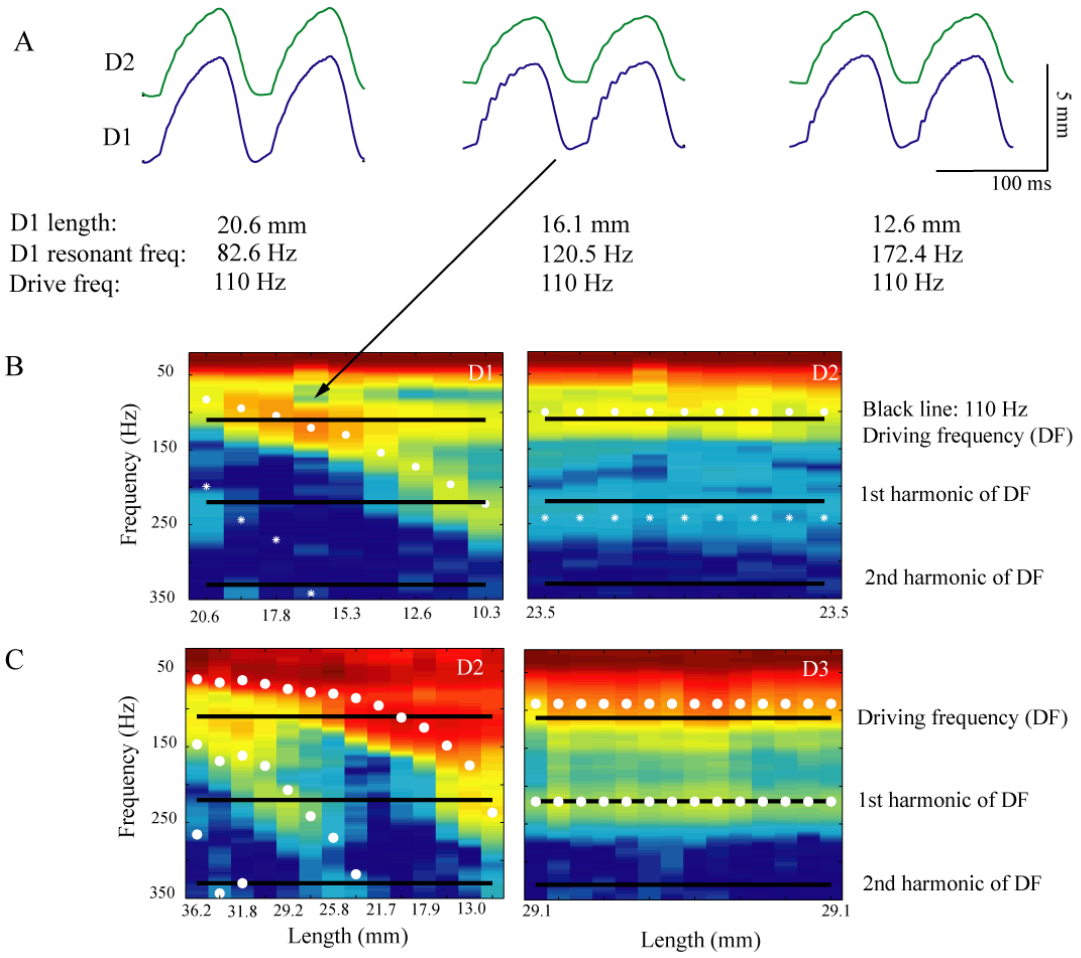

Figure 2.11. **Artificial whisking experiments show that whisker resonance filters muscle-driven vibrations** A) D1 is trimmed while D2 stays constant length (23.5mm) and resonant frequency (100.5 Hz). From left to right the interaction between the D1 whisker's resonant properties and the driving frequency can be directly observed. As D1 is trimmed it amplifies the driving frequency (110 Hz) when its resonant frequency (120.5 Hz) most closely matches the driving frequency. B) top, same data as 2.11A but showing the power spectra at all whisker lengths. Here it can be seen that the driving frequency is amplified as the resonance frequency cross 110 Hz. The black arrow shows the point where the whisker vibrations are maximally amplified (also shown in 2.11A middle). The bottom spectra show a similar experiment in a second animal. The power spectra in the bottom right show a clear band of amplification where the second harmonic matches the driving frequency.

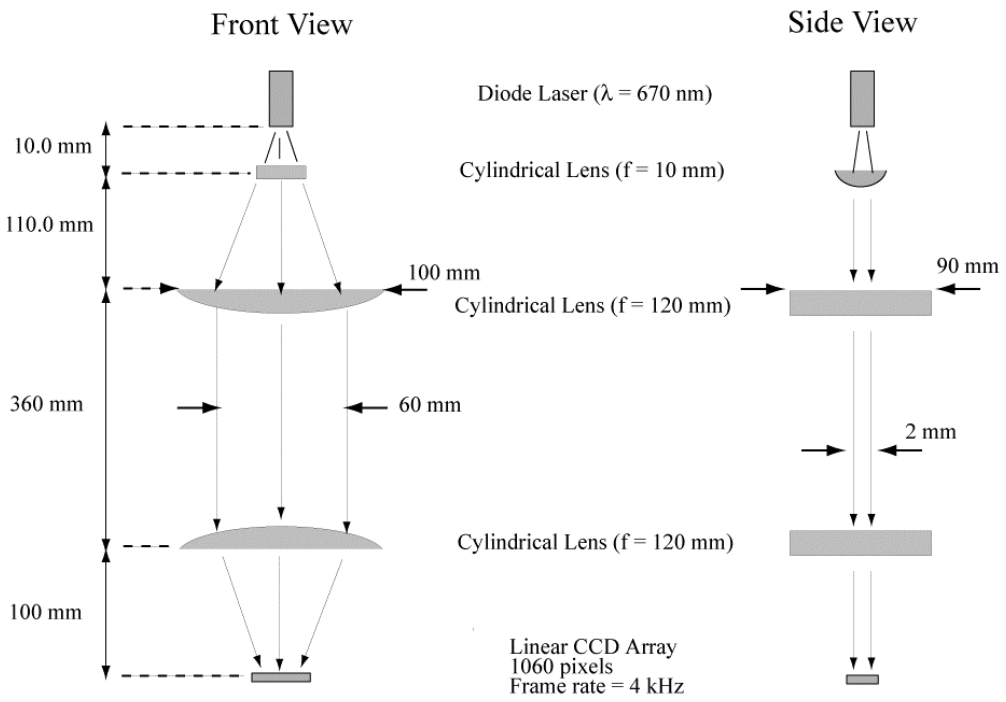

Figure 2.12. **Whisker imaging setup**. The laser diode produces an elliptic beam. This is shaped into a line using two cylindrical lenses. The first lens (focal length = 10 mm) collimates the width of the beam. The second lens (focal length = 120 mm) collimates the beam in the opposite direction and fixes the length of the beam at ~ 60 mm.

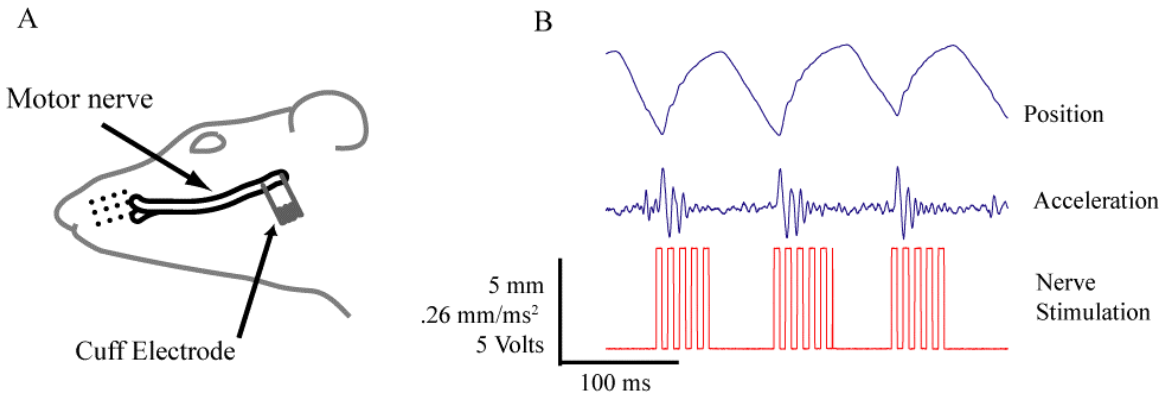

Figure 2.13. **Electrical stimulation of the motor nerve causes contraction of the intrinsic muscles and whisker protraction**. A) A cuff electrode is inserted around the motor nerve and stimulated with 5 Volt pulses at 110 Hz to cause whisker protraction, then whiskers passively retract. B) Example of artificially induced whisking. The electrical stimulation is applied to the nerve for 50 ms during protraction. The stimulation is removed for 50 ms and the whisker passively protracts, inducing 10 Hz whisking. The acceleration trace shows that the stimulation frequency is present in the whisker motion

2.8 References

Andermann ML, Ritt J, Neimark MA, Moore CI. **Neural correlates of vibrissa resonance; band-pass and somatotopic representation of high-frequency stimuli**. Neuron. 2004 May 13;42(3):451-63

Berg RW, Kleinfeld D. **Rhythmic whisking by rat: retraction as well as protraction of the vibrissae is under active muscular control**. J Neurophysiol. 2003 Jan;89(1):104-17

Brown AW, Waite PM. **Responses in the rat thalamus to whisker movements produced by motor nerve stimulation.** J Physiol. 1974 Apr;238(2):387-401.

Conway HD, Becker ECH, Dubil JF. **Vibration frequencies of tapered bars and circular plates**. J App Mech 1964 June 329-331

Fee MS, Mitra PP, Kleinfeld D. **Central versus peripheral determinants of patterned spike activity in rat vibrissa cortex during whisking**.J Neurophysiol. 1997 Aug;78(2):1144-9.

Ganguly K, Kleinfeld D. **Goal-directed whisking increases phase-locking between vibrissa movement and electrical activity in primary sensory cortex in rat**. Proc Natl Acad Sci USA. 2004 Aug 17;101(33):12348-53.

Georgian JC. **Vibration frequencies of tapered bars and circular plates.** J App Mech 1965 March 234-235

Hartmann MJ, Johnson NJ, Towal RB, Assad C**. Mechanical characteristics of rat vibrissae: resonant frequencies and damping in isolated whiskers and in the awake behaving animal.** J. Neurosci. (2003) 23(16):6510-6519

Kamen G, Caldwell GE. **Physiology and interpretation of the electromyogram.** J Clin Neorphysiol. 1996 Sep;13(5):366-84.

Kirchoff GR. **Gesammelte Abhandlungen**, Leipzig 1882

Kleinfeld D, Ahissar E, Diamond ME **Active sensation: Insights from the rodent vibrissa sensorimotor system.** Current Opinions in Neurobiology (2006) 16:435-444

Krupa DJ, Matell MS, Brisben AJ, Oliveira LM, Nicolelis MA. **Behavioral properties of the trigeminal somatosensory system in rats performing whisker-dependent tactile discriminations**. J Neurosci. 2001 Aug 1;21(15):5752-63.

Moore, CI. **Frequency-dependent processing in the vibrissa sensory system. J Neurophysiol**. 2004 Jun;91(6):2390-9. Review.

Neimark MA, Andermann ML, Hopfield JJ, Moore CI. **Vibrissa resonance as a transduction mechanism for tactile encoding.** J Neurosci. 2003 23(16):6499-6509

Szwed M, Bagdasarian K, Ahissar E. **Encoding of vibrissal active touch**.Neuron. 2003 Oct 30;40(3):621-30.

Chapter 3

Whisking onto textures

3.0 Introduction

In chapter 2 we showed that whiskers vibrate at high frequencies in air, well above the 6 – 12 Hz whisking frequencies, and that these vibrations are filtered by the resonance properties of the whiskers. This indicated that energy loss due to viscous forces and friction in the whisker follicle are not sufficient to overly dampen whisker vibrations and resonance. This suggests that resonance filtering by the whiskers may be important for sensory processing. The goal of this chapter is to understand how whisker dynamics may encode texture properties and whether whisker resonance plays a role in this encoding.

The resonance hypothesis for texture discrimination states that, due to each whisker's physical properties whiskers have unique intrinsic resonance frequencies. As multiple whiskers sweep over a texture the range of frequencies excited in the whiskers will depend on the spatial properties of the texture. Whiskers whose resonance frequency lie within this range of texture-induced frequencies will be preferentially excited and the spatial properties of the texture may be decoded by

judging the relative amplitudes of excitation across the multiple whiskers (Neimark et al 2003, Andermann et al 2004). The resonance hypothesis makes two important predictions: 1) Texture-driven vibrations should be filtered by whisker resonance and 2) The degree to which whiskers resonate depends on the spatial properties of the texture such that each whisker will be preferentially excited by specific spatial frequencies.

To evaluate the importance of resonance during texture discrimination we asked two questions. First we asked whether the frequency spectrum of whisker vibrations shifts toward higher frequencies in the shorter whiskers compared to the longer whiskers which must be a prerequisite for the resonance hypothesis. Second, we asked whether power at the resonance frequency varied as the surface roughness varied from smooth to rough, i.e. whether whiskers are preferentially excited by different ranges of spatial frequencies.

Results indicated that the frequency spectra of shorter whiskers are shifted to higher frequencies relative to the longer whiskers, indicating that whisker resonance does play a role in filtering texture-induced vibrations. However we found that the degree to which whiskers resonate does not depend on the spatial properties of the textures. We argue that resonance is not induced due to a matching of the resonance frequencies to the texture-induced frequencies but rather that whisker resonance is induced by sharp stick-slip events that cause ringing in the whisker. The whisker dynamics during ringing are predominately determined by the whisker's intrinsic elastic properties rather than the texture properties and therefore would not be an

encoding mechanism for the spatial properties of a texture. We therefore examined an alternative coding mechanism for texture in the last part of this chapter. Because we found that whiskers prominently stick and slip as they move over textures, we examined whether the magnitude and frequency of stick-slip events depended on texture roughness. We found that there was a shift toward more frequent larger amplitude slip events on rough textures relative to smoother textures and based on this we propose that this could be an important mechanism for texture encoding. We also looked at the role of whisker muscles in driving stick-slip events, and show that slip events were correlated with EMG activity that the slip events were correlated in time across whiskers.

3.1 Vibration spectra during texture palpation depend on whisker length

Whisker motion was measured across a range of 7 sandpaper roughnesses (p150 [roughest], p240, p400, p600, p800, p1200, p1500 [finest]) in 5 rats. 3 rats were trained on the nosepoke task (N1, N2, N3) and 2 rats were head-fixed (H1, H2). Textures were mounted on a stepper motor that was under precise computer control so that up to four textures could be presented to the animal within a single measurement session. For the nosepoke animals textures were rotated through slits in the wall into the measurement chamber while the animal was at the drinkport (figure 3.0A). For the headfixed animals (figure 3.0B) textures were interleaved by briefly moving the animal out of the path of the textures, rotating the textures into place and then moving the animal back into the measurement position. Air trials were presented on separate

days because we found that the positioning of the laser relative to the whisker pad had to be adjusted when no texture was present. Because whisking motion onto sandpapers was more irregular than whisking in air we were restricted to measuring at most two whiskers simultaneously, all other whiskers were trimmed at the base. Because of different whisker lengths, lateral freedom of head movement within the nosepoke (~ 5 mm), and because the surfaces are planar while whisker tips move in an arc it was not possible to place the surface where only the tip would move across the surface. The surfaces were therefore positioned as far from the whisker pad as possible while still ensuring that the whiskers maintained contact with the surface for the majority of a trial. This resulted in ~ 2- 10 mm of the whisker being in contact with the texture. This positioning is consistent with the observed positioning during texture-discrimination in which 'the bowed aspect of the hair shaft, not its tip, was the interface between the textured surface and the animal' (Carvell and Simons 1990).

In the following analysis we combined data from all textures and looked at the change in power spectra across the D1, D2, and D3 whiskers. Figure 3.1A shows an example trace from rat N1of the D3 whisker position (top) and acceleration (bottom) during whisking onto a rough (p150) sandpaper surface. Aligned with figure 3.1A, figure 3.1B shows the time-frequency representation of this whisker motion (calculated using the Wigner-Ville representation, for details see methods). For this example we see that there are at least three transient events that appear to be large acceleration events followed by oscillations at ~ 180 Hz (as seen in the time-frequency representation). The average frequency spectrum for this example is shown at the right

side of the spectrogram in figure 3.1B. In this example we therefore see that there is an average increase in spectral power at ~180 Hz due to this sharp slipping and ringing during whisker protraction. Figure 3.1D shows the trial averaged frequency spectra of this whisker for the five different textures presented to this animal. In order to calculate the average power spectra of texture-induced vibrations we limited the analysis to only include epochs during which the whisker was either protracting or retracting across the texture. Protraction and retraction events were defined as continuous movement in either the backward or forward direction for at least 4 mm in less than 200 ms. On average, for this whisker, on all five textures we found that there was a peak in the frequency spectrum centered at approximately 150 Hz. By comparison, figure 3.1C shows the average power spectra for the D1 whisker from the same trials. The D1 power spectra have there most pronounced peaks centered at approximately 80 Hz.

In order to determine if there was a systematic shift in the spectral content of whisker vibrations across whiskers, we calculated the mean vibration frequency weighted by the power between 50 and 250 Hz. Each open circle in figure 3.2A is the mean vibration frequency for the indicated whisker where no distinction is made as to which texture each circle represents. The closed circles in figure 3.2A are the average mean vibration frequencies over all textures. These results show that there was a shift toward higher frequencies in the shorter whiskers relative to the longer whiskers as would be expected if the whiskers' resonance properties were filtering the induced vibrations.

The peaks observed in the power spectra during whisking onto textures are similar to those peaks observed during whisking in air. However, with a texture present the peaks are shifted to higher frequencies. This is consistent with these peaks being due to whisker resonance. The presence of the texture should have two effects on the whisker resonance frequencies (Kirchoff 1884, Weaver and Timoshenko 1990, Neimark et al 2003, Hartmann et al 2003). First, because a part of the whisker is in contact with the texture, the portion of the whisker free to vibrate is effectively shortened which will increase the resonance frequency and second, the pinning of the whisker on the texture imposes a quasi-fixed boundary condition on the whisker tip which will also increase the resonance frequency. From the observed shift toward higher frequencies in the shorter whiskers we argue that whisker resonance does play a role in shaping whisker vibrations during active texture palpation.

3.2 Spatial properties of textures are uncorrelated with whisker resonance

We next looked at whether the magnitude of whisker resonance changed as the texture roughness was varied. In order for whisker resonance to play a role in texture discrimination as outlined by the resonance hypothesis, a given whisker must be preferentially excited by a subset of textures. We found however that, within the subset of textures measured, no whisker was preferentially excited by a single texture. Figure 3.2B shows the results of one D1 whisker, four D2 whiskers and one D3 whiskers across all textures. Here we inferred the resonance frequency of the whisker

when it was pinned against the texture by calculating the negative peaks in the second derivatives of the power spectra. Only power spectra with well-defined peaks were used in this analysis. This is the same method that was used in the whisking in air section that was shown to correlate well with the directly measured resonance frequencies. After computing the resonance frequencies of these whiskers we then calculated the average power centered at the resonance frequency (+/- 10 Hz) for each texture. Figure 3.2B shows the relative change in this measure as the surfaces vary. In no case did we see a preferential excitement of a whisker on a particular texture. Thus, for the set of textures and the geometric position of the textures in this study, the amplitude of whisker resonance was not dependent on surface roughness as would be required by the resonance hypothesis.

The presence of slipping and ringing events may account for the fact that whiskers do resonate during texture palpation but that the amplitude of resonance is independent of the spatial properties of the texture. The contribution to the power spectra from slip-ring events can be seen directly in 3.1B. The large slip events followed by ringing are the only epochs of whisker motion in this example that contribute to the 180 Hz peak in the average power spectrum shown on the right in figure 3.1B. While the frequency of these ringing events must depend on the whisker resonance frequencies, the actual texture spatial properties are largely unimportant for determining the ringing dynamics. The only necessity being that a sharp event occurs which excites a broad band of frequencies.

3.3 Stick-slip dynamics correlate with texture roughness

In the previous section we showed that, within our experimental design, the degree to which whiskers resonate during texture palpation is not a good coding mechanism for texture properties. We made the argument that although whiskers resonate during texture palpation this resonance is likely driven by the sharp sticks and slips on the texture and does not depend on the surface roughness. We next asked whether the magnitude and frequency of these prominent sticks and slips depends on the surface roughness and whether this could be a useful coding mechanism for texture.

In this analysis we controlled for the different whisking behaviors of the rats by only looking at the p150, p400, p800 and p1200 surfaces which were presented to a subset of 3 rats (N3, H1, H2). In N1 the surfaces were interleaved in blocks of 5 in order to control for changes in whisking behavior. In H1 and H2 the surfaces were interleaved in blocks of twenty because the process of moving the head-fixed animals while changing the textures appeared to be somewhat stressful for the animal. Figure 3.3A shows examples of whisker motion in air (left) on a smooth sandpaper (middle), and a rough sandpaper (right). In these examples the top traces are the whisker position and the bottom traces are the whisker acceleration. The red dots denote small slip events with peak accelerations between .12 mm/ms^2 and .37 mm/ms^2 and the green dots are large acceleration events greater than .37 mm/ms^2. This division between large and small events corresponds to acceleration peaks 6 standard

deviations above zero calculated on the smooth (p1200) surface. This division is rather arbitrary and the following analysis holds true for a wide range of cutoff values between the 'large' and 'small' events. In these examples the number of large slip events is much higher on the rough sandpaper while the number of small events is higher on the smooth sandpaper. Two expanded examples of slips on the smooth and rough sandpapers are shown in figure 3.3B. In the expanded view of the slips it is clear that the slips on the rough sandpaper are sharper than the slips on the smooth sandpaper and therefore have higher acceleration. We then asked whether there is a systematic shift toward higher acceleration slip events as the surface roughness increases. Figure 3.4A shows how the number of slips crossing a set acceleration threshold changes as the threshold value increases for the four sandpapers and during whisking in air. For low threshold values there is either no statistical difference across textures or the rougher sandpapers have fewer slips. At higher threshold values however the four textures become distinguishable based on the number of threshold crossings with the rougher surfaces having more threshold crossings per whisk. The systematic relationship between slip size and surface roughness became more pronounced when we looked at the ratio of the number of small acceleration events to the number of large acceleration events. Figure3.4B shows that, on average across these three animals, the number of large slip events relative to the number of small slip events decreased as the texture became smoother.

The correlation between large slip acceleration and rougher textures is reasonable from a physical standpoint. Figure 3.5 shows a schematic representation of

a cartoon model of whisker dynamics during a slip event. As a whisker is moving across a texture the tip of the whisker experiences a frictional force in the opposite direction of this motion (figure 3.5A). If the whisker stops, it gets stuck because it must overcome the static frictional force which is larger than the frictional force during motion. In order to move again the force on the whisker must increase. However, as this force increase the static frictional force also increases in the opposite direction so that the whisker stays stuck. This is shown as positions 1,2 and 3 in figure 3.5A. At some point the force exerted by the whisker overcomes the maximal frictional force and the whisker begins to slip (position 4). At this point there is an abrupt switch from static friction to kinetic friction which causes the large acceleration during the slip. This large acceleration is depicted in figure 3.5B. In this simplified model, at the beginning of the slip event there is an instantaneous switch to kinetic friction (red trace, figure 3.5B). The force exerted by the whisker however relaxes over time resulting in the large acceleration shown in the bottom panel of 3.5B. If we further assume that the whisker loses contact with the surface during the slip, then the normal force (N) goes to zero and the slip acceleration is directly proportional to the coefficient of static friction. Higher friction would then directly translate to larger acceleration events. While this model very simplistic, it highlights the general dependence of slip events on frictional properties of the texture. Specifically, it can be seen from this model that a stick slip event is dependent on the difference between static and kinetic frictional forces. From a neural coding standpoint it has been shown in anesthetized animals that the cortical response to a sharp deflection increases as the

deflection velocity (or acceleration) increases. We would thus expect that the increased magnitude in slip acceleration would drive spiking in cortex more reliably and could contribute to the neural code for texture.

In this section we concentrated on the dependence of the magnitude of slips on texture roughness. In the model however, the muscle forces are required to induce the whisker to slip. We therefore measured muscle activity during slip events and asked whether the timing of slip events can be affected by the changing muscle activity.

3.4 Muscle correlations with stick-slip motion across texture

In the previous section we showed that the magnitude of stick slip events can depend on the roughness of the surface. We next tested whether the timing of sticking and slipping across a texture correlated with the changing muscle forces which occur during whisking. In order to look at the correlation between slip events and muscle contractions we calculated the slip triggered average EMG. This was done by calculating all intrinsic EMG segments triggered on positive slips during protraction (figure 3.6 left) and all extrinsic EMG segments triggered on negative slips during retraction (figure 3.6 right). We found that for the four muscles studied the average delay between EMG peak and slip was 5.8 +- 1.7 ms with the slip always following the peak in the EMG. Because whisker motion across different whiskers is generally highly synchronous (Towal et al 2006) and the EMG can serve as a reference for whisker motion (Fee et al 1997, Berg and Kleinfeld 2003) we would predict from this

that the timing of slips across whiskers may also be synchronous. Calculation of the cross-correlation between the slip events (figure 3.6) showed that the times of slips occurring in two neighboring whiskers (either C1 and C2 or D1 and D2) are well correlated with each other with zero delay. The blue traces are the calculated cross-correlations. For each rat these have a peak at 0 ms. By adding noise to the occurrence times of the slips however this peak at zero is strongly diminished. The red trace in figure 3.7 shows the result of adding Gaussian noise with a standard deviation of 10 ms to the timing of the slip events in each whisker. The green trace is the cross-correlation after adding Gaussian noise with a 100 ms standard deviation. On average there is a 34% decrease in the peak cross-correlation when the 10 ms standard deviation noise is added and a 63 % reduction with the 100 ms standard deviation noise. The slip events therefore are well correlated in time across neighboring whiskers which may serve to increase the fidelity with which slip events are encoded by neural activity.

3.5 Discussion

Currently there are two main hypotheses on texture discrimination in rats (Neimark et al 2003, Arabzadeh et al 2005, Mehta and Kleinfeld 2004). Underscoring our lack of knowledge of the function of the neural pathway during texture discrimination, these two hypotheses assume very different neural coding strategies. In the resonance hypothesis texture information is encoded in which whiskers are

preferentially excited. The main function of the neural pathway would then be to compare the spatial distribution of neural activity generated by the different whiskers. In this case the temporal dynamics of neural activity would be unimportant and texture information would be converted to a spatial code. In the direct encoding hypothesis however, whisker vibrations directly reflect the spatial properties of a texture and the timing of spikes along the neural pathway would encode these vibrations. In contrast to the resonance hypothesis, in the direct encoding hypothesis the temporal dynamics of neural activity is critical and the importance of the spatial distribution of activity is unclear.

This debate may be resolved by understanding how whisker dynamics reflect texture properties. Key to this resolution is to what degree whisker resonance depends on the spatial properties of a texture. To this end we measured whisker motion in behaving animals under two conditions: during whisking in air, and while animals whisked across sandpapers of varying degrees of roughness. In the whisking onto textures experiment we found that vibrations are filtered by the resonance properties of the whiskers however the degree to which whiskers resonate does not depend on the roughness of the texture, as would be required by the resonance hypothesis. We then proposed an alternative method for texture encoding based on the sticking and slipping of the whisker across the texture.

3.5.1 Evaluation of whisker resonance as a coding mechanism for texture

Previously it was proposed that the resonance properties of the whiskers could be used to convert spatial frequency information into a place code on the whisker pad, analogous to the function of the cochlea in the auditory system (Neimark et al 2003). In order to understand the plausibility of this coding mechanism, we analyzed two aspects of whisker dynamics during active texture palpation. First, we asked whether there is a systematic shift in the spectral content of whiskers of different lengths. In order for the resonance hypothesis to be viable it must be the case that shorter whiskers filter out lower frequency vibrations compared to longer whiskers during active texture palpation. Second, we asked whether the amplitude of whisker resonance is influenced by the spatial properties of the texture.

Interestingly, we found that the shorter whiskers do vibrate at higher frequencies than the longer whiskers during texture palpation. This suggests that resonance does shape whisker vibrations as the whiskers move over a texture. However we did not see a significant change in the amplitude of whisker resonance across surfaces of varying roughness. Because whiskers did not preferentially resonate depending on the spatial properties of the texture we do not consider it likely that whisker resonance is a crucial mechanism for encoding texture properties.

One aspect of whisker motion which we found to be very prevalent was sharp sticking and slipping as the whisker moved over the sandpaper surfaces. These stick-slip events are sharp events which induce a broad range of vibration frequencies in the whisker. Due to its resonance properties the whisker will selectively amplify its resonance frequency from this range of frequencies causing ringing in the whisker.

One explanation to the previous two results is that the stick-slip events during texture palpation induce ringing in the whisker however this ringing does not reflect the spatial properties of the texture. Instead, any frictional interaction between the whisker and a surface may induce a sharp slip event and ringing regardless of the exact nature of the surface's spatial properties. Indeed, the example in figure 3.1A shows this process directly. During whisker protraction on the surface (3.1A, top) there are short segments where the whisker vibrates at a characteristic 180 Hz. Looking at the acceleration trace, it can be seen that these events begin with a relatively large acceleration (a slip) followed by ringing at ~ 180 Hz. From the time-frequency representation it can be seen that it is only during the short ringing events that these higher frequency vibrations occur and that these events give rise to the secondary peak at 180 Hz in the average power spectrum shown on the right of figure 3.1A.

3.5.2 Stick-slip dynamics correlate with texture roughness

From anesthetized experiments we know that high acceleration whisker deflections drive reliable, temporally precise spiking in S1 and that the magnitude of the response is directly related to the acceleration amplitude (Pinto et al 2000, Temereanca and Simons 2003). From this we predict that the magnitude of the observed slip events will be reflected in the neural response. We therefore analyzed the dependence of the slip acceleration on the roughness properties of the texture to

determine if these events can contribute to the coding of texture properties. We found that there was a systematic shift to higher acceleration events as the texture became rougher. Figure 3.4B shows that there are proportionately more low acceleration slips per whisk on the fine textures while there are more high acceleration slips per whisk on the rougher texture. This may be expected from a simplified physical model of a slip event. In order for a slip to occur the force exerted by the muscle on the whisker must be greater than the frictional force exerted by the texture on the whisker. This frictional force must be greater on rough textures compared to smooth textures so that a larger force is required to initiate the slip on the rougher texture. When the slip does occur this greater force should translate into larger slip acceleration. Because larger slip acceleration likely results in a larger neural response the average magnitude of the slip events may contribute to the neural code for texture.

3.5.3 Timing of slips is influenced by muscle activity

While the magnitude of slip acceleration depends on the roughness of the texture we argue that the timing of slip events can depend on the phase of muscle activation. In figure 3.6 we showed that, on average, the whisker slips on the texture at 5.8 +- 1.7 ms following the peak in the EMG. From the physical argument presented above it necessarily requires an interaction between the muscle forces and frictional forces to initiate a slip. Because the frictional properties of the texture are constant in time the timing of slip events must be determined by the changing muscle

activity. Because muscle forces are highly coherent across whiskers we predict that there should be a correlation between the timing of slip events across whiskers. Indeed we show in the cross correlation of slip events between two whisker that there is a peak at 0 ms and this peak is attenuated by almost half by adding temporal jitter with a standard deviation of 20 ms to the timing of these events (fig 3.7). From a neural coding perspective in S1 the correlated occurrence of these events across whiskers may facilitate the neural integration of responses across cortical columns.

3.5.4 Working model for texture encoding

Taking these results together we propose a model in which the sticking and slipping across a texture is important for texture discrimination. On the sensory side of this model the roughness of a texture would determine the average magnitude and frequency of slips on the texture. The proportion of large slip events to small slip events would be higher on rougher textures relative to smooth textures. We predict that the larger slip events on rougher textures would drive robust population responses in S1 (Temereanca and Simons 2003, Pinto et al 2000) and therefore the degree of modulation in the population firing rate would contribute to the neural code for texture.

We also showed that slips are well correlated in time across whiskers and that slips, on average follow the peak in the EMG activity by ~ 5 ms, suggesting that muscle activity may play a role in synchronizing slip events across whiskers. It is well

known that when two whiskers are deflected the relative times of deflection can dramatically alter the neural response to deflection. For near simultaneous deflection, neural integration can have a facilitory affect on the response. However, when the time between deflections of the two whiskers is greater than a few milliseconds neural integration can have a suppressive effect (Boloori and Stanley 2006, Shimegi et al 1999). The well-correlated timing of slips in different whiskers may serve to increase the robustness of the neural response and avoid the suppressive effects that might occur if the slips occurred randomly in time across different whiskers.

The predictions of this model are in good agreement with behavioral observations. First, in contrast to the resonance hypothesis, we would predict that rats could discriminate texture using only one whisker. As shown in figure 3.4 the ratio of the number of large to small slips per whisk in a single whisker is sufficient information to discriminate the four sandpapers measured here. However we would also predict that having multiple whiskers and sampling the texture for longer would increase performance. This prediction is based on the observation that the large slip events occur relatively infrequently (< 1 per whisk) so that having more whiskers and sampling for longer essentially increases the slip sample size. These three predictions are in agreement with previous behavioral studies (Carvell and Simons 1990, Carvell and Simons 1995). Carvell and Simons (1990) also noted that, during texture discrimination, the whisker shaft rather than the whisker tip was generally in contact with the texture. This supports the argument that the frictional interaction between the

whisker and the surface, which determines slip magnitude, is important for texture discrimination.

This model requires neural integration across time because texture roughness is reflected in the average rate of stick slip events. However, we would predict that discrimination ability would greatly increase by integrating neural responses to stick-slip events across whiskers. Therefore, texture information would be encoded in the spatiotemporal neural pattern of activity rather than in just the spatial (as in the resonance hypothesis) or temporal (as in the direct encoding hypothesis) pattern.

3.6 Methods

3.6.1 Training

The data presented in this chapter was taken from measurements done in 3 rats trained to nosepoke and 2 rats trained to whisk while head-fixed. For both whisker measurements in the nosepoke and head-fixed rats the training and handling procedures were the same as described in chapter 2. In order to interleave the presentation of textures to the rats, textures were mounted on a stepper motor (Oriental Motor, PK264B1A-SG10), so that they could be rotated into position next to the nosepoke between trials. The stepper motor and texture control was precisely controlled via computer using custom written Labview (National Instruments) programs. For nosepoke rats, textures were presented in blocks of 3 or 5 and textures

were rotated into place while the animal was drinking from the drinkport. For head-fixed animals, the animal was moved slightly out of the measurement position, the texture was rotated into place and the animal was re-positioned. Because this process of re-positioning appeared to be slightly stressful for the animal, textures were presented in blocks of 20 for the head-fixed animals.

3.6.2 Whisker measurements

Whisker motion was measured using the same methods as described in chapter 2. In order to record whisking onto textures the imaging laser was positioned either 3 mm or 10mm form the texture. For all data presented here the laser was positioned 3 mm from the texture. We also checked however if the results were qualitatively the same when the laser was 10mm from the texture. Our specific concern was that whisker resonance would only be visible when measuring more toward the midpoint of the whisker. We found however that resonance is visible in both locations and these data were qualitatively similar. The advantage of measuring 3 mm from the texture was that we could insure that the whisker was in contact with the surface in all our analyses.

3.6.3 Slip-triggered EMG calculations

Slips were categorized as either positive slips during protraction or negative slips during retraction. This was done because the intrinsic muscles are active during the protraction phase of whisking while the extrinsic muscles are active during retraction. Acceleration events were detected by finding acceleration peaks over a set threshold. These events were then sorted into positive and negative slips using the following criteria. In order for an event to be classified as a positive slip the mean velocity 1ms prior to the event had to be at least .1mm/ms less than the mean velocity during the 1ms following the event and the velocity had to be positive both before and after the event. An example of a positive slip is shown in figure 3.8 (left). The same method was used to find negative slip events however the change in velocity had to be negative and the velocity before and after the slip had to be negative. An example of a negative slip is shown in figure 3.8 (right). For each slip the average EMG trace spanning a 200 ms interval centered on the slip time was found. All slips and EMG traces were then averaged to find the slip-triggered average EMG traces.

3.6.4 EMG Recordings

EMG recordings were performed the same as in chapter 2.

3.6.5 Wigner-Ville time-frequency representation

One drawback to the fourier methods described in chapter 2 is that they assume the time series over which the transform is calculated is stationary. During free whisking in air we assumed that the condition of stationarity was sufficiently met so that the fourier transform would provide meaningful information. During whisking onto textures however we find that there are sharp slip events that occur over short time intervals (less than 10 ms). Because we were interested in these events, we could not assume stationarity during whisking onto texture over the course of an entire trial which could last up to 3 seconds for the head-fixed rats. One solution to this problem is to window the data in short time segments and compute the fourier transforms over those short segments. We found however that the spectral artifacts induced by this windowing, even with the multitaper estimation, made the fourier transform techniques problematic when analyzing the slipping and ringing events.

In order to avoid the problems associated with windowing the data and also achieve good time-frequency resolution, we use the Wigner-Ville Distribution (WVD) to analyze whisker motion onto textures. This distribution is computed by correlating the entire time-series over a trial, s(t), with a time and frequency translated version of itself,

$$WVD(t,\omega) = \int_{-\infty}^{\infty} s\left(t+\frac{\tau}{2}\right) s^*\left(t-\frac{\tau}{2}\right) e^{-j\omega\tau} d\tau \qquad \text{[Eq. 3.6.1]}$$

The WVD is calculated by integrating over the entire time series which avoids the problems with windowing the data. One problem with the WVD however is the presence of cross terms which cause artifacts in the spectra of multiple frequency

component signals. Because these cross terms generally oscillate, one solution to this problem is to smooth the distribution over frequency. We found that by smoothing the whisking power spectra over 10 Hz, the noise in the WVD was sufficiently low while still maintaining good frequency resolution. Figure 1 compares the WVD method to the multitaper method of calculating the spectrogram. For this example a slip event was simulated by adding a small, exponentially decaying oscillation (frequency = .08 $samp^{-1}$), to a larger more slowly oscillating signal (frequency = .001 $samp^{-1}$), to simulate the larger whisking motion (figures 3.9 A,B). Gaussian noise (standard deviation = .01 , mean = .003) was also added to obtain the signal shown in fig. 3.9A. The slip event occurred at t = 800 samples. Data was then bandpassed filtered (low cutoff = .01, high cutoff = .25 $samp^{-1}$), and the WVD and multitaper spectrograms were calculated. Figures 3.9C and 3.9D show the spectrogram calculated with the WVD. In this case the increase in power is almost entirely isolated to the time of ringing, with relatively low spread in frequency. Figures 3.9E and 3.9F, show the spectrogram calculated using the multitaper method. For these figures the power spectra were calculated using overlapping windows of length 150 samples (overlap = 140 samples), the bandwidth parameter NW = 2, and the first 3 tapers were used. With this method, the frequency can be fairly well isolated however the time resolution is considerably worse than the WVD method. The time resolution can be improved by decreasing the window size to 50 samples (figures G,H) however the peak at .08 $samp^{-1}$ becomes more contaminated by the windowing artifacts and the

frequency resolution becomes worse. Overall we found the WVD method provided better time-frequency resolution for looking at the slip ringing events.

Acknowledgement

Parts of chapter 2 are part of a manuscript in preparation for publication, Wolfe JH, Pahlavan S, Hill D, Kleinfeld D, Feldman DE, untitled. The dissertation author was the primary investigator of the paper.

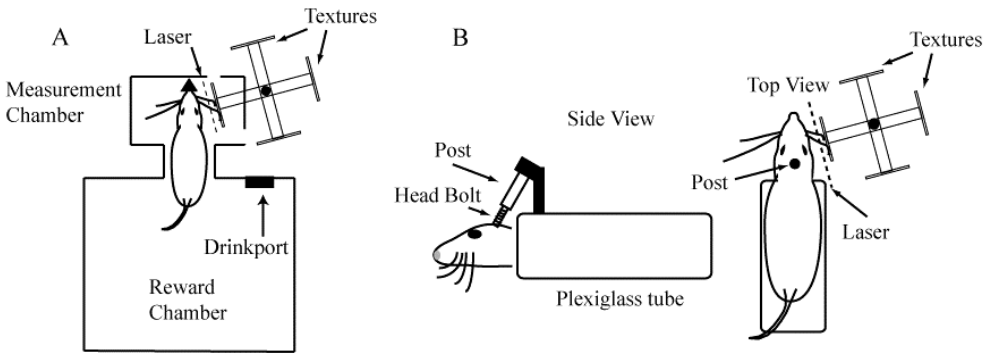

Figure 3.0 **Measurement methods of whisking onto textures** A) Diagram of nosepoke training. Animals were trained to hold their nose in a nosepoke and whisk for water reward. While in the nosepoke the whiskers were imaged using a linear laser that projected across the whiskers and down onto a linear CCD array. While the animal was at the drinkport textures could be rotated in and out of the measurement chamber through two slits in the walls. B) Diagram of whisker measurements in headfixed animals. In order to rotate the textures, animals were briefly slid out of the measurement position while the textures were rotating

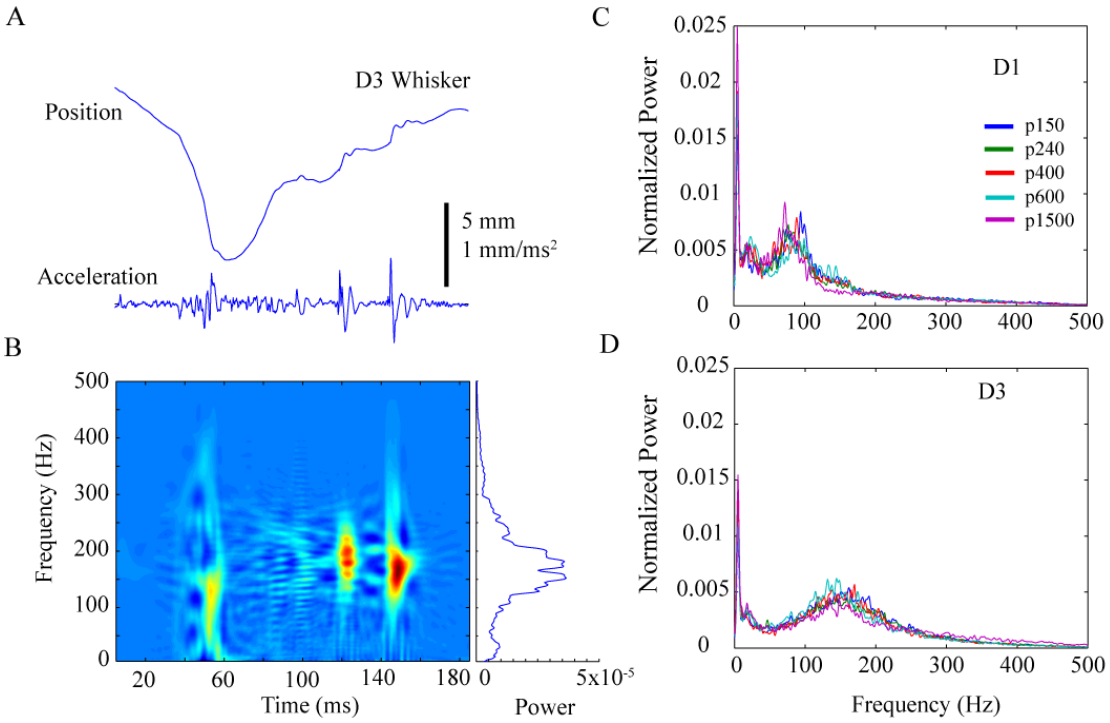

Figure 3.1. **Evaluation of the effect of whisker resonance on texture-induced vibrations**. A) Top trace is an example of D3 whisker motion across p150 sandpaper. Bottom trace shows the acceleration. B) Time-frequency representaion of the whisker motion shown in A. The ringing events seen in the accleration trace show up as peaks in power at ~ 180 Hz. Trace on the side of the time-frequency plot shows the average power spectrum when the time-frequency plot is integrated over time for this trial. Cand D) The average power spectra over all trials shown for five different textures measured in this animal in the D1 and D3 whiskers.

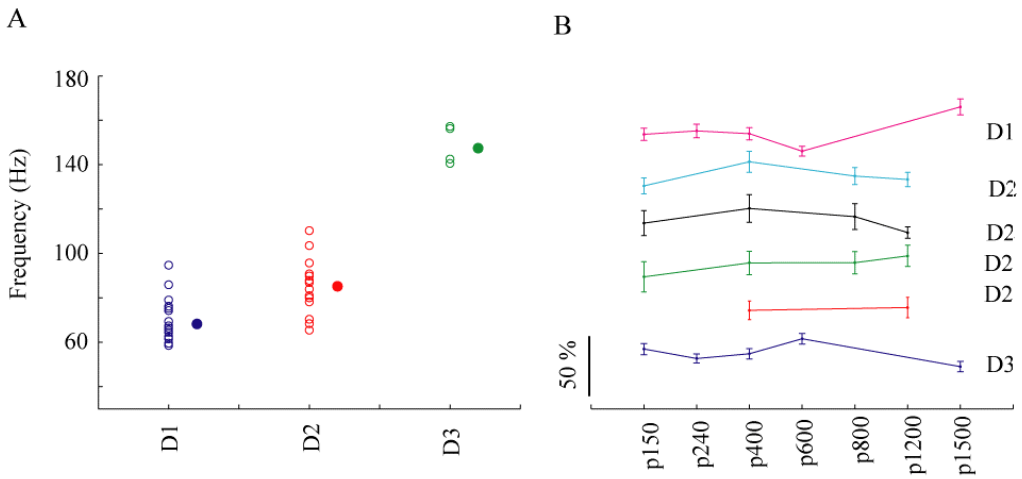

Figure 3.2. **Whisker resonance shapes whisker vibrations but does not differentially encode texture** A) The first peak of the average power spectra shifts toward higher frequency in the shorter whiskers relative to the longer whiskers. Each open circle represents the first peak frequency between 50 amd 250 Hz for the indicated whisker measured on one texture. The filled circles are the averages over all textures and B) Average power at the resonance frequency does not substantially increase on any of the measured textures. Each color is the average normalized power at the resonance frequency of that whisker measured over the indicated range of textures.

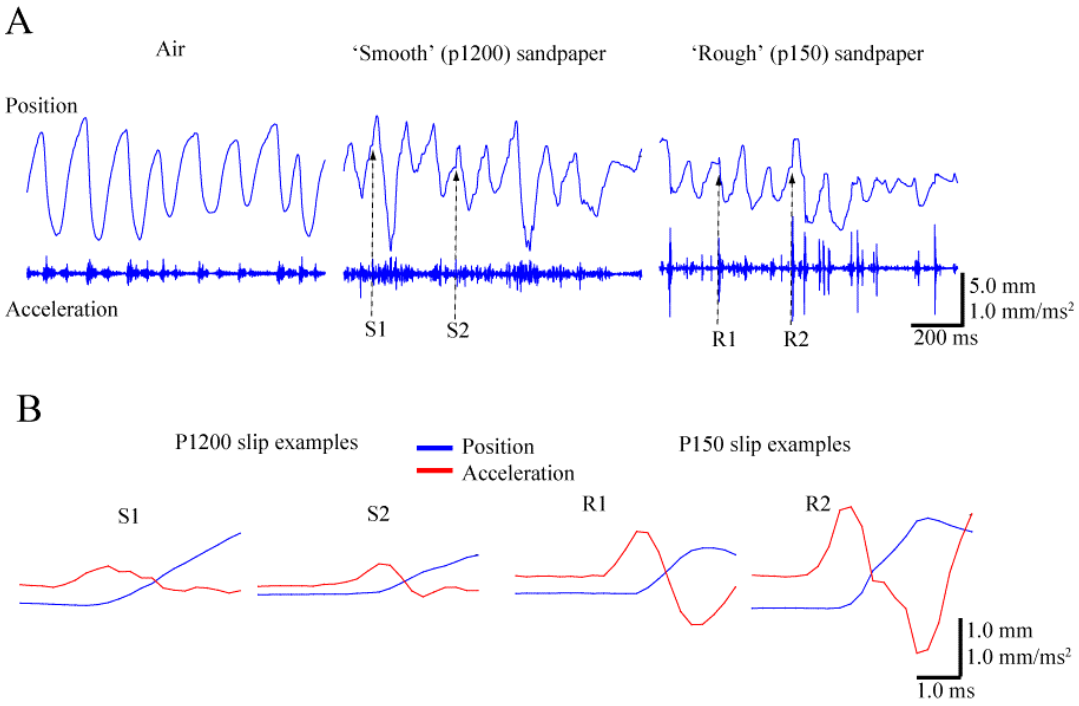

Figure 3.3. **Examples of whisker motion in air and onto sandpaper textures**. A) Examples of whisker motion in air (left) on smooth sandpaper (middle) and on a rough sandpaper (right). B) Expanded view of the slips labeled S1 and S2 on the smooth sandpaper and R1 and R2 on the rough sandpaper.

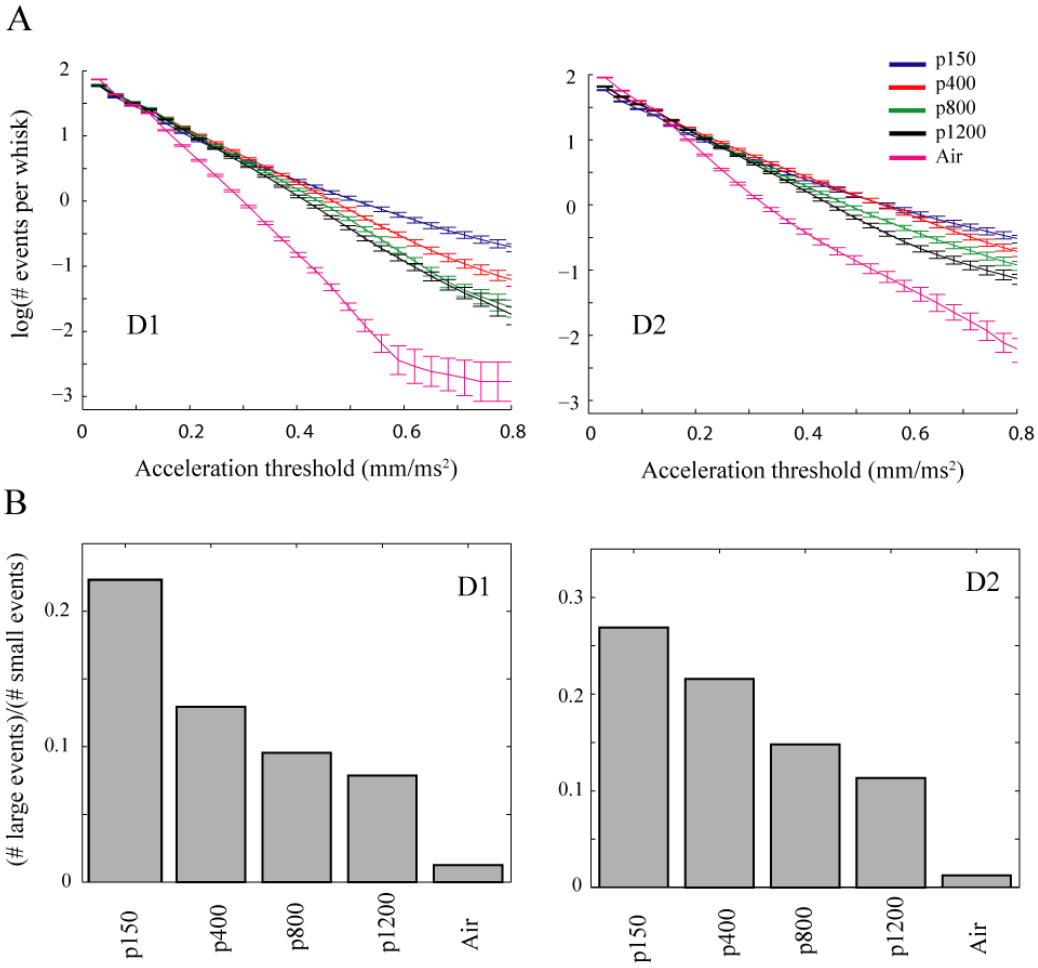

Figure 3.4. **Average slip acceleration increases for rougher surfaces** A) Number of slips versus slip threshold for the D1 (left) and D2 (right) whiskers. Rougher sandpapers have more slips at higher acceleration thresholds than the smoother textures for both whiskers.B) Ratio of the number of 'small' slips to the number of 'large' slips. Small slips were defined as slips with acceleration less than .37 mm/ms2 and large slips were defines as events with acceleration greater than .37 mm/ms2

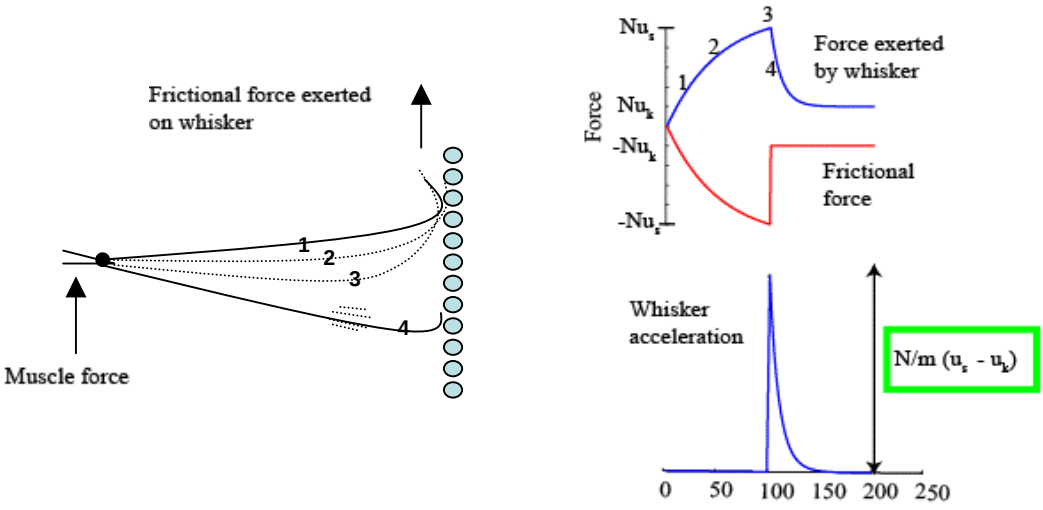

Figure 3.5) **Simpified model of whisker dynamics during a slip event**. A) During texture palpation, friction between the whisker tip and the surface prevents the whisker from moving (position 1). As the muscle force increases the frictional force counteracts the increase so the whisker stays pinned (positions 1-3). At some point the force exerted by the whisker becomes larger than the maximal frictional force and the whisker begins to Slip (position 4). B) Schematic of the forces and acceleration in this slip model. At position 4 the whisker begins to slip. For textures with larger coefficients of static friction, μ_s, the slip begins at larger forces exerted by the whisker (B, top). This will result in larger slip acceleration (B, bottom). Here, N = normal force between whisker tip and surface, μ_s = coefficient of static friction, μ_k = coefficient of kinetic friction, and m = whisker mass.

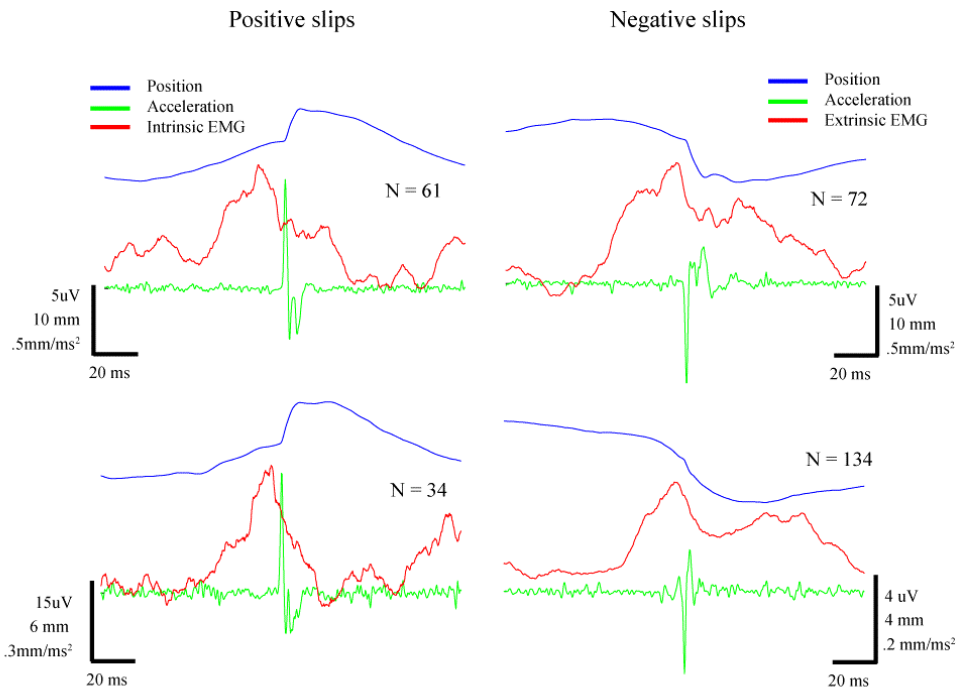

Figure 3.6. **Peaks in both the intrinsic EMG (left) and extrinsic EMG (right) correlate with slips during active texture palpation**. Blue traces on the left are the average whisker motion during positive slip events. Green traces are the average acceleration during the slips. Blue traces on the right are the average whisker motion during negative slip events. On average the peak in the EMG (red traces) occurs 5.8 +- 1.7 ms preceeding the slip event.

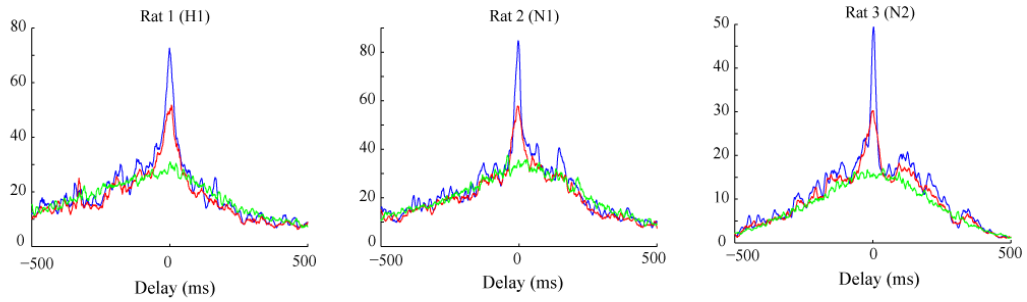

Figure 3.7. **Average cross-correlations between slip events ocurring in two neighboring whiskers in each animal**. Blue trace are the average cross correlations. Red traces are the cross-correlations computed after adding gaussian noise with standard deviation of 10 ms to the slip times in both whiskers. Green traces are the cross-correlations after adding gaussian noise with standar deviation of 100 ms. Slip events were defined as acceleration events greater than 4 standard deviations above zero.

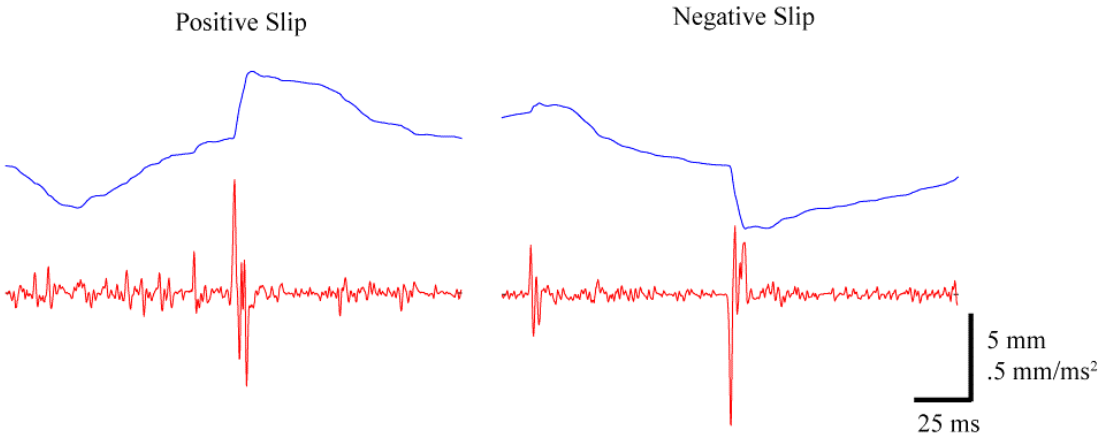

Figure 3.8. **Slip Examples**. Examples of a positive slip (left) and a negative slip (right) used to calculate the slip triggered EMG averages

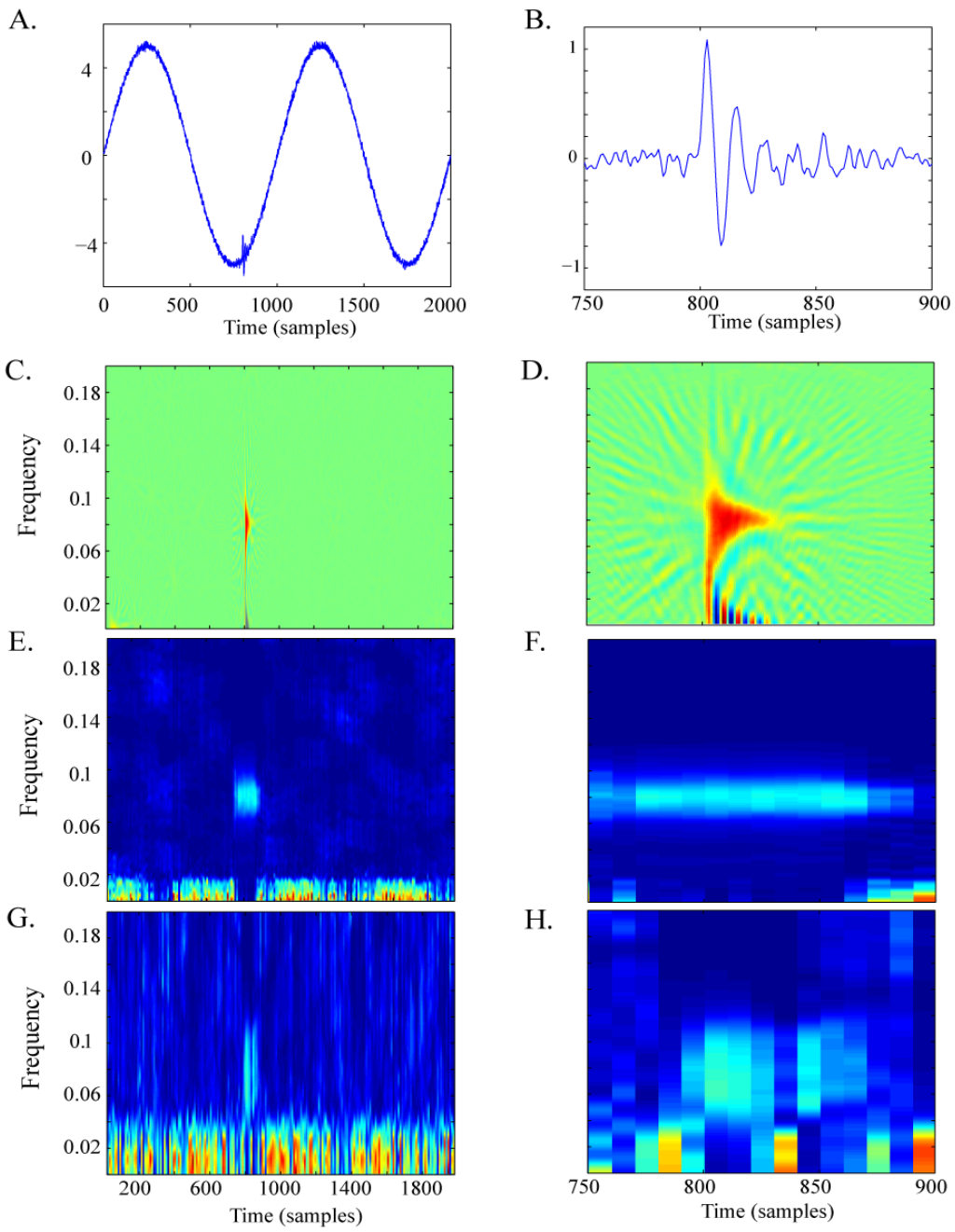

Figure 3.9. **Example of the Wigner-Ville representation**. The Wigner-Ville distribution provides good time-frequency resolution to isolate slip-ring events.A) Simultated ringing occurs at t=800 superimposed on a larger amplitude oscillation. Ringing frequency = .08 Hz B) Zoomed in versionof ringing event after band pass filtering between .01 Hz.and .25 Hz. C) WVD of simulated time series after filtering. D) Zoomed in version of WVD. E,F) Sepctrogram of time series using multitaper method, (The first three tapers were used, with NW =3.) Data windows were 150 points long and translated by 10 points between spectra. Using this time window, the ringing event is not as well isolated in time as in D. G,H) Same as E and F but using a window size of 50 points. Now the ringing is better isolated in time but there is more noise and the frequency resolution is worse.

3.7 References

Andermann ML, Ritt J, Neimark MA, Moore CI. **Neural correlates of vibrissa resonance; band-pass and somatotopic representation of high-frequency stimuli**. Neuron. 2004 May 13;42(3):451-63

Arabzadeh E, Zorzin E, Diamond ME. **Neuronal encoding of texture in the whisker sensory pathway.** PLoS Biol. 2005 Jan;3(1):e17. Epub 2005 Jan 11.

Berg RW, Kleinfeld D. **Rhythmic whisking by rat: retraction as well as protraction of the vibrissae is under active muscular control**. J Neurophysiol. 2003 Jan;89(1):104-17

Boloori AR, Stanley GB. **The dynamics of spatiotemporal response integration in the somatosensory cortex of the vibrissa system**. J Neurosci. 2006 Apr 5;26(14):3767-82

Carvell GE, Simons DJ. **Task- and subject-related differences in sensorimotor behavior during active touch**. Somatosens Mot Res. 1995;12(1):1-9.

Carvell GE, Simons DJ. **Biometric analyses of vibrissal tactile discrimination in the rat.** J Neurosci. 1990 Aug;10(8):2638-48

Fee MS, Mitra PP, Kleinfeld D. **Central versus peripheral determinants of patterned spike activity in rat vibrissa cortex during whisking**. J Neurophysiol. 1997 Aug;78(2):1144-9

Kleinfeld D, Ahissar E, Diamond ME **Active sensation: Insights from the rodent vibrissa sensorimotor system.** Current Opinions in Neurobiology (2006) 16:435-444

Moore, CI. **Frequency-dependent processing in the vibrissa sensory system. J Neurophysiol**. 2004 Jun;91(6):2390-9. Review.

Neimark MA, Andermann ML, Hopfield JJ, Moore CI. **Vibrissa resonance as a transduction mechanism for tactile encoding.** J Neurosci. 2003 23(16):6499-6509

Mehta SB, Kleinfeld D. **Frisking the whiskers: patterned sensory input in the rat vibrissa system.** Neuron. 2004 Jan 22;41(2):181-4. Review.

Pinto DJ, Brumberg JC, Simons DJ. **Circuit dynamics and coding strategies in rodent somatosensory cortex**. J Neurophysiol. 2000 Mar;83(3):1158-66

Shie Qian. **Time-Frequency and Wavelet Transforms**, New Jersey : Prentice Hall, 2002

Shimega S, Ichikawa T, Akasaki T, Sato H. **Temporal characteristics of response integration evoked by multiple whisker stimulations in the barrel cortex of rats**. J Neurosci. 1999 Nov 15;19(22):10164-75

Temereanca S, Simons DJ. **Local field potentials and the encoding of whisker deflections by population firing synchrony in thalamic barreloids**. J Neurophysiol. 2003 Apr;89(4):2137-45.

Towal RB, Hartmann MJ. **Right-left asymmetries in the whisking behavior of rats anticipate head movements.** J Neurosci. 2006 Aug 23;26(34):8838-46.

Weaver SP, Timoshenko DH. **Vibration Problems in Engineering.** New York : Wiley 1990

Chapter 4

Chronic Recordings

4.0 Introduction

In chapter three we made the argument that whisker resonance is not a likely code for texture. We then showed that during active texture palpation whiskers exhibited pronounced sticking and slipping and that the acceleration magnitude of the slips depended on the texture roughness. Based on this we proposed that these slip events are important for texture encoding. As discussed in chapter 3 this hypothesis is compatible with behavioral experiments. While rats can perform some texture discrimination tasks, they are better at performing texture discrimination when they have multiple whiskers and take longer (Carvell and Simons 1995). These behavioral results are consistent with a coding mechanism based on the size and frequency of slip events in the whisker. It was also observed that, during texture discrimination, the whisker shaft is in contact with the surface and not the tip (Carvell and Simons 1990). Because whisker slips on a texture are a result of the frictional interactions between the whisker and the surface, the fact that the shaft is dragged along the surface during texture discrimination is consistent with a slip-based coding mechanism for texture.

It is known that S1 neurons respond very robustly to high velocity transient whisker deflections (Pinto et al 2000). Slip-events are high velocity events that

transiently occur ~ once per whisk. It would thus be predicted from anesthetized experiments that slips would reliably drive spiking in S1, an area which was shown to be necessary for whisker based texture discrimination (Guic-Robles 1992).

In order for slip events to play a role in texture discrimination, both the occurrence and magnitude of these events must be represented by neural responses in S1 during active texture palpation. However it is known that the response properties of neurons in S1 can change depending on the state of the animal (Fanselow and Nicolelis 1999; Ferezou et al 2006). Indeed, it was shown that when an animal is whisking but not attending to a task, neurons in S1 may not respond at all to sharp deflections.

In this chapter we present a method for measuring neural responses to whisker slips in the awake behaving rat and we present preliminary results from one rat showing that slips indeed induce spiking in S1[*].

Detailed methods are given in section 4.4. Briefly, rats were trained on the nosepoke task as described in chapter 2. Once rats were reliably holding their nose in the nosepoke and whisking for ~.5 – 1.0 seconds per trial and completing greater than 50 trials per day the training was complete and they underwent a chronic surgery to implant four tetrodes in the whisker representation of S1. Tetrodes were mounted in a microdrive on the rat's head (Venkatachalam et al 1999). Each tetrode was independently moveable so that single unit responses could be obtained. After the surgery, all but one whisker was trimmed on the right side of the rat's face so that single whisker neural responses could be obtained. Once rats had recovered from the

[*] All Chronic recordings were performed with Shantanu Jadhav.

implantation surgery, they were put back in the training cage and simultaneous whisker and neural data was taken while they held their nose in the nosepoke and actively palpated textures. Data analysis was done offline. Multi-unit spiking data was sorted as described in Fee et al (1996). Slips were identified as described in chapter 3 and peristimulus time histograms of single unit neural responses were constructed based on the slip times.

Results showed that stick-slip events can drive very precise spiking in S1 and that the spiking probability of a neuron increases as the slip magnitude increases. Because we previously showed that the magnitude of slip events also correlated with texture roughness, it is likely that neural responses to slip events contribute to the neural code for texture. Additional experiments are required to confirm and extend these initial observations.

4.1 Slips are precisely represented in spiking probabilities in S1

In order to determine whether stick-slip events are reliably represented by neural activity in S1, animals were trained on the nosepoke task and then chronically implanted with four tetrodes in the whisker representation of S1. Three Long-Evans rats (2 male, 1 female) went through the training procedure as described in the methods section of chapter 2. Animals were determined ready for the chronic implant once they consistently performed greater than 50 trials per day and held their nose in the nosepoke while whisking onto textures for ~ 0.5 – 1.0 seconds per trial. As

described in the methods section animals underwent a chronic surgery during which a small crainiotomy (~ 2mm x 2mm) was opened above the whisker representation in S1. A microdrive with four independently moveable tetrodes (Venkatachalam et al 1999) was secured over the crainiotomy with dental cement. Tetrodes could be lowered by turning four screws (160 μm/turn) which drove shuttles containing the tetrodes. At the final stage of the surgery each tetrode was inserted into the brain by applying a vacuum to the dura and successively lowering each tetrode until a distinct change in neural activity was heard on an audio monitor. This method is described in more detail in the methods section and in Venkatachalam et al (1999). Once all electrodes were in the brain (~ 100 μm deep) the vacuum was removed. The placement of the electrodes was determined by deflecting each whisker on the contralateral side of the face and listening to the neural response on an audio monitor. For this study, we determined which electrode had the most clearly defined principal whisker, with the requirement that that whisker not be located more rostral than arc 3 due to whisker imaging limitations, and trimmed all other whiskers at the skin. After recovery for 3-5 days animals were put back on water restriction and measurement sessions began.

At the beginning of each measurement session the quality of the neural signal was assessed by deflecting the whisker while the animal was in its homecage and listening to the response on an audio monitor. The tetrode was lowered until a sharp response was heard upon whisker deflection and spikes were clearly visible on an oscilloscope monitoring the neural activity. Once neural responses were obtained the

animal was put in the training cage and simultaneous whisker and neural recordings were taken. Whisker and neural data was analyzed offline. Spikes were sorted based on the spike waveforms obtained on each of the four electrodes within the tetrode using the method from Fee et al (1996). For the data from the one animal presented here only the roughest sandpaper (p150) was used.

Figure 4.0 shows an example of a neural recording on one electrode. There is a negative slip marked by the arrow followed by a spike in the neural recording. In this chapter we only ask one question: Do slips affect the probability of a neuron to spike and is the spiking probability greater for higher acceleration slips?

Of the six neurons reported on here, neurons 1-3 (top row of figure 4.1) had sharp increases in their spiking probabilities that were precisely timed to the slip events. The peak in the PSTH occurred on average at 5.3 +/- .3 ms following the slip. This suggests that even though both the muscles and texture are continuously exerting forces on the whisker, the slips are salient events that very precisely drive spiking in S1.

4.2 Spiking probabilities of S1 neurons increase with slip acceleration

The second part of the question stated above asked whether the magnitude of the spiking response increases as the slip acceleration increases. In chapter 3 we showed that the average slip acceleration increases with surface roughness. In order for this to contribute to the neural code for texture, the acceleration magnitude of the

slips has to be reflected in the neural response. For the three neurons that responded to slip events we calculated the PSTH for four different ranges of slip acceleration. Figure 4.3 shows that for these three neurons the slip response increased as slip acceleration increased. The events from the PSTH's in figure 4.2 were divided into four acceleration ranges that increased in value. The average acceleration trace for each range is shown by the red trace in 4.3B. In figure 4.3B, the blue trace is the mean slip motion. For each neuron, figure 4.3A shows that the neural response increased as the slip acceleration increased. Neuron 1 had the most prominent increase in the precisely timed peak, whereas the increase in the responses of neurons 1 and 2 was not as precise.

4.3 Discussion

In a series of papers in anesthetized animals (Kyriazi and Simons 1993; Pinto et al 1996; Pinto et al 2000; Shoykhet and Simons 2000; Bruno and Sakmann 2006), it has been proposed that neurons in layer 4 of the vibrissae cortex are particularly sensitive to the velocity and acceleration of whisker deflection rather than the amplitude of whisker deflection. This set of studies has shown that layer 4 neurons respond strongly to synchronous activity from thalamocortical neurons and that high velocity whisker deflections drive both synchronous spiking in thalamus and large response amplitude in the cortex. The large cortical responses were shown to be driven by a large number of weak thalamocortical synapses (Bruno and Sakmann

2006) rather than a few strong synapses. Integrating the synaptic input from many weak synapses may increase the resolution with which an individual neuron encodes deflection velocity. The results reported here predict that the ability to accurately represent whisker acceleration is functionally important during texture discrimination.

Given that cortical responses can be very different depending on the state of the animal (Fanselow and Nicolelis 1999; Ferezou et al 2006), the dependence of cortical response on whisker acceleration needs to be tested during active whisker use. To this end we have been recording neural activity while precisely measuring whisker motion during active texture palpation. In this chapter we showed preliminary data which indicates that neurons in S1 respond very precisely to whisker slips on textured surfaces. Additionally, for the three neurons that responded to whisker slips, all showed an increased response to larger slip acceleration, as predicted from previous studies. Given that sticking and slipping is prominent during texture palpation, that the acceleration magnitude of slips depends on texture roughness and that slip acceleration is likely well-represented by neurons in S1, it seems likely that stick-slip events contribute to the neural code for texture.

In the current study we have focused on the magnitude and frequency of texture-induced slips. In the introduction to this thesis however we described the direct encoding hypothesis in which texture information is contained in the temporal pattern of whisker motion which is directly reflected in the temporal patterns of spiking in S1. The precise locking of spikes to slip events observed here bolsters the argument that spiking patterns can directly reflect whisker motion during texture

palpation. However a requirement for the direct encoding hypothesis is that whisker motion must be highly reproducible from trial to trial. In our experiments we did not observe precise patterns of whisker motion corresponding to the spatial properties of textures. Furthermore it was previously reported that whisker velocity during texture discrimination can be variable from one trial to the next (Carvell and Simons 1990), making it less likely that patterns of motion are reproducible from trial to trial. Our hypothesis that texture roughness information is contained in the average magnitude and frequency of slips does not require reproducible patterns of motion which is in better agreement with the behavioral observation that whisker motion can be variable between trials.

4.4 Methods

4.4.1 Training

Chronic recordings were performed in 3 adult Long-Evans rats (2 male, 1 female) that had been trained on the nosepoke task. The training procedure was the same as described in chapter 2. Animals were determined fully trained and ready for chronic implants once they consistently performed > 50 trials per day and whisked while in the nosepoke for ~0.5 – 1.0 seconds per trial. While 3 animals have been chronically implanted, data from only one animal was presented here. This chapter presents preliminary results and data from the other two animals has not been fully

analyzed. The methods used here are divided into three sections: electrode and microdrive fabrication, surgery, and recording.

4.4.2 Electrode and microdrive fabrication

Details on the construction of the microdrive are given in Venkatachalam et al (1999). Here we present the basic function of the drive and methods for fabricating the tetrodes used in recording. The microdrive consists of a lower, middle and upper chamber. The lower chamber is secured above the crainiotomy during the surgery using dental cement and the other two chambers are mounted above the crainiotomy by screwing them onto the lower chamber. The upper chamber contains up to six shuttles which hold the electrodes. 0000-160 lead screws pass through threaded holes in the shuttles. By turning the lead screws the shuttles move 160 μm/turn in the vertical direction. The shuttles are arranged in an hexagonal array such that, when placed in the shuttles the electrodes have a tip to tip distance of ~ 450 μm. The middle chamber holds an hexagonal array of guide tubes. The spacing of the guide tube array matched the spacing of the electrode array and served to stabilize the electrodes and maintain their spacing.

Once constructed, the top of the lead screws, which are turned to lower the electrode shuttles, protrude from the top of the upper chamber. An outer casing was built to protect these lead screws and keep the animal from being able to access them with its fore paws. A circuit board was attached to this outer casing. All electrodes

were attached to the circuit board using cactus pins (Neuralynx, small gold pins) and the ground and reference wires were soldered to this board. The circuit board had a 20 pin connector which was connected to the headstage amplifier (Plexon Instruments HST/8o50-G20) during recording sessions. The signal from the headstage amplifier was then transmitted via a set of twisted thin gauge wires to a second amplifier and filter (Plexon Instruments PBX2/16sp-G50). The second amplifier bandpass filtered the signal with high/low cutoff frequencies of 300 Hz and 8 KHz and amplified the signal an additional 50 times. This signal was then passed to the data acquisition card (National Instruments PCI 6259) which was sampled at 32 KHz

Tetrodes used for all neural recordings were constructed from four twisted gold plated Ni/Cr wires. The twisted wires were heated using a hot air gun (Master-mite 475 Watt heat gun) to hold them together. This was never found to short the wires together. After the wires were twisted together, they were inserted into 32 gauge stainless steel tubes (Small Parts) which were mounted in the shuttles. Approximately 2mm of the wire extended past the end of the tube. The tips were sanded at a 45 degree angle using a fine grain sandpaper (p1500) mounted on a home built rotating wheel. After sanding, the electrode tube and shuttles were mounted in the upper chamber and the middle chamber and guide tube array were screwed onto the upper chamber. The tetrodes were then lowered one at a time into a AuCl (Sifco Non-cyanide # 5355) solution in order to plate the tips. The tips were gold plated by passing positive current (~ 10 μA) from the AuCl solution into the Ni/Cr wire. Impedance of the tip was monitored (Bak electronics) and current was passed until the

impedance dropped to 250-500 KΩ. The tips were then rinsed with distilled water and retracted into the guide tube array. Once all electrodes had been plated and raised into the guide tube array the microdrive was ready for implantation.

4.4.3 Surgery*

Surgery was performed over the course of two days. On the first day animals were anesthetized with an initial dose of ketamine/xylazine (100 mg/kg, 10 mg/kg) delivered in the muscle . Supplemental doses of ketamine (10% of the initial dose) and continuous administration of low concentration (2%) isoflourane were administered to maintain an even breathing rate (~60-100 breaths per minute) and a lack of response to pinching the hind paw. Throughout the procedure body temperature was maintained at 37^0 C using a servo controlled heating blanket. The skull was exposed by making an incision ~3cm long above the midline. Connective tissue between the skin and skull was removed and the skull was cleaned. A headbolt was attached to the skull approximately at lambda using dental cement (Teets cold curing A-M systems). For the remainder of the procedure the animal was held using the headbolt. Between four and six holes were drilled and tapped using a 00-90 tap and stainless steel screws were screwed into these holes until they approximately touched the dura. These screws were used to both anchor the microdrive and to serve as a ground for the recording electrodes. The skull was then covered by a thin layer of cyanoacrylic glue. A small (~1mm diameter) craniotomy and duratamy were made

* All Surgeries were performed by Shantanu Jadhav

close to the midline and ~ 3 mm rostral to Lambda to implant a reference wire. A silver reference wire (100 μm diameter) was placed in the brain through this craniotomy. Approximately 1mm of the wire tip had the insulation removed and this was placed 2mm deep in the brain. The crainiotomy was covered with agar gel and dental cement.

A second craniotomy was performed over the barrel cortex 5 mm lateral and 2.5 mm caudal of bregma (Foeller et al 2005). On the first day the skull was thinned but not completely removed. A well of dental cement was formed around this crainiotomy and shaped using a dental drill to fit the lower chamber of the microdrive. A ground wire was soldered to one of the skull screws and wrapped around the remaining screws. Finally, the reference and ground wires were secured under a cap attached to the headbolt. Animals were given an additional dose of ringers (3-5ml) administered sub-cutaneously and analgesic (Buprenex .25ml/kg, i.m.) and allowed to recover.

After a 24 hour recovery period, the second day of surgery was performed. Anesthesia was the same as day one. The thin skull of the crainiotomy was completely removed and the lower chamber of the microdrive was cemented in place above the crainiotomy. The dura was maintained moist by constant application of sterile saline solution. The previously assembled microdrive was screwed onto the lower chamber and cemented in place. The ground and reference wires were soldered to the connector board on the microdrive and all wires were enclosed in dental cement.

All electrodes were pushed into the brain immediately after the microdrive was implanted and the dental cement was almost completely dry. In order to minimize damage to the cortical surface a vacuum (15 in mercury) was applied to the dura (Venkatachalam et al 1999) and the tetrodes were lowered, one at a time, at a rate of approximately 80 μm/min, until a distinct change in the background activity was heard. At this point the animal was given injections of ringers and buprenex as described on the first day and was allowed to recover.

4.4.4 Recording

Simultaneous recordings from up to four tetrodes were performed in 3 rats trained to hold their nose in the nose poke and whisk for water reward. Neural activity from the electrodes was amplified 20 times and impedance buffered on the head using a headstage amplifier (Plexon Instruments HST/8o50-G20). The signal from the headstage amplifier was then transmitted via a set of twisted thin gauge wires to a second amplifier and filter (Plexon Instruments PBX2/16sp-G50). The second amplifier bandpass filtered the signal with high/low cutoff frequencies of 300 Hz and 8 KHz and amplified the signal an additional 50 times. This signal was then passed to the data acquisition card (National Instruments PCI 62659) which was sampled at 32 KHz.

During the recording sessions rats held their nose in the nosepoke for ~ 1 second. Whisker data was acquired during nosepoke trials in 1.5 second blocks as

described above in the whisker measurement section. Neural data however was acquired continuously throughout the recording session. Data from the entire recording session was used for spike sorting however only data taken while the rat had its nose in the nosepoke was used for analyzing neural responses to whisker motion. Neural and whisker data acquisition was synchronized through a series of digital pulses which were acquired on a digital channel synchronously with the neural acquisition. A digital pulse generated by the rat poking its nose in the nosepoke triggered whisker data acquisition. This digital pulse was also sent to the synchronously acquired digital channel. Upon leaving the nosepoke a second digital pulse was acquired. These digital pulses served as precise time stamps that allowed the neural data to be aligned with the whisker data.

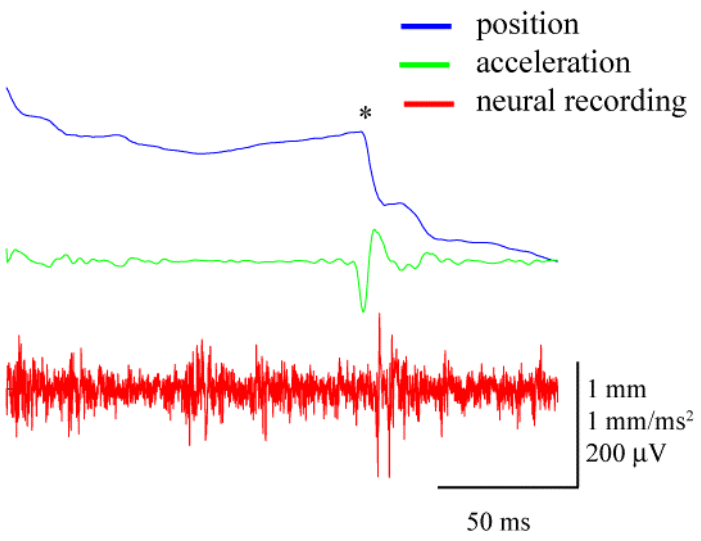

Figure 4.0. **Example slip event and spike**. Example slip event (denoted by *) used to calculate the peristimulus time histogram (PSTH).

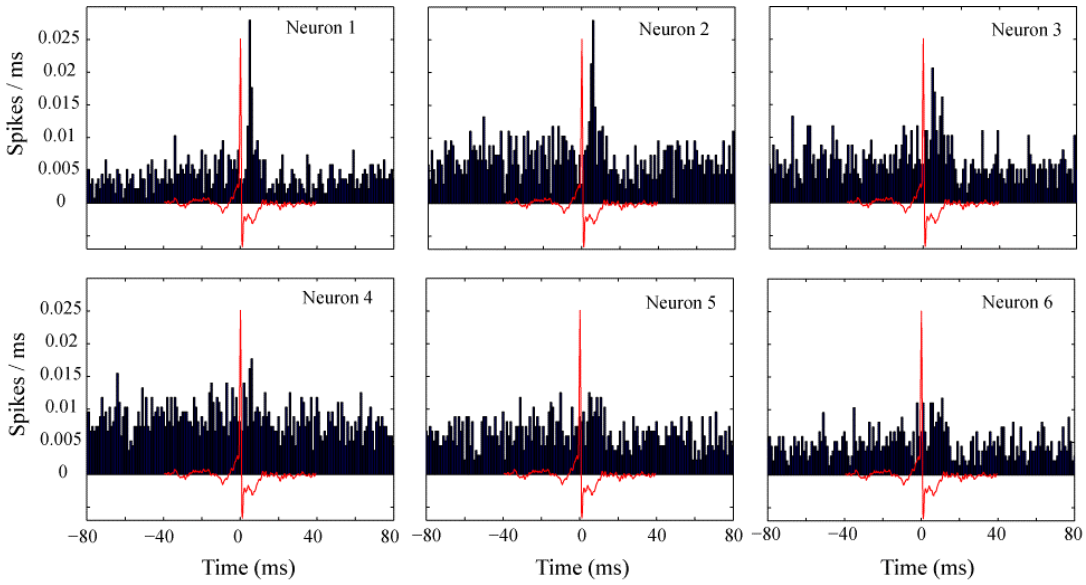

Figure 4.1. **PSTH of neural reponse to texture-induced slips**. 3 out of 6 neurons have sharp increases in firing probability precisely timed to the texture-induced slips.The red trace in each graph is the average slip acceleration for all the events that went into the PSTH calculation.The red trace is the same for all six graphs because the same events were used for each neuron. 2055 slip events were used in the calculation of each PSTH

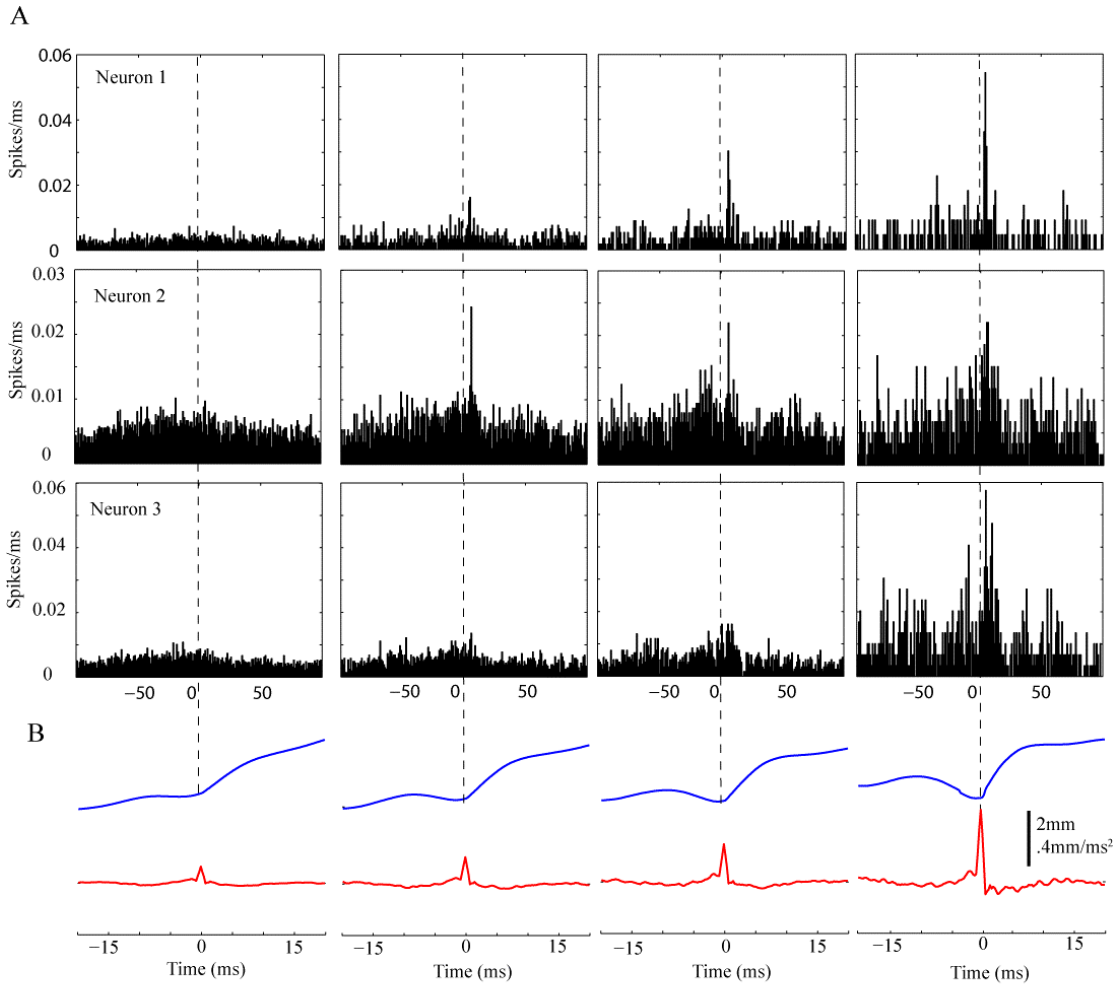

Figure 4.2. **Neurons which responded to slip events also have increased spiking probability for larger slip events**. A) Neurons 1-3 have larger slip-locked responses as slip acceleration increases. Neuron 1's spiking probability is almost linearly dependent on slip acceleration. B) Blue traces are the average motion during the slip events. Red traces are the average slip accelerations. In order to look at the dependence of each neuron's response on slip acceleration, slips were divided into four acceleration groups from small (left) to large (right).

4.5 References

Arabzadeh E, Petersen RS, Diamond ME. **Encoding of whisker vibration by rat barrel cortex neurons: implications for texture discrimination**. J Neurosci. 2003 Oct 8;23(27):9146-54.

Arabzadeh E, Zorzin E, Diamond ME. **Neuronal encoding of texture in the whisker sensory pathway.** PLoS Biol. 2005 Jan;3(1):e17. Epub 2005 Jan 11.

Armstrong-James M. **The functional status and columnar organization of single cells responding to cutaneous stimulation in neonatal rat somatosensory cortex S1** 1975 Apr;246(3):501-38

Bruno RM, Sakmann B. **Cortex is driven by weak but synchronously active thalamocortical synapses**.Science. 2006 Jun 16;312(5780):1622-7

Carvell GE, Simons DJ. **Biometric analyses of vibrissal tactile discrimination in the rat.** J Neurosci. 1990 Aug;10(8):2638-48

Carvell GE, Simons DJ. **Task- and subject-related differences in sensorimotor behavior during active touch**. Somatosens Mot Res. 1995;12(1):1-9.

Chung S, Li X, Nelson SB. **Short-term depression at thalamocortical synapses contributes to rapid adaptation of cortical sensory responses in vivo**. Neuron. 2002 Apr 25;34(3):437-46

Deschenes M, Timofeeva E, Lavallee P. **The relay of high-frequency sensory signals in the Whisker-to-barreloid pathway**. J Neurosci. 2003 Jul 30;23(17):6778-87

Fanselow EE, Nicolelis MA. **Behavioral modulation of tactile responses in the rat somatosensory system**.J Neurosci. 1999 Sep 1;19(17):7603-16

Fee MS, Mitra PP, Kleinfeld D. **Automatic sorting of multiple unit neuronal signals in the presence of anisotropic and non-Gaussian variability**. J Neurosci Methods. 1996 Nov;69(2):175-88. Erratum in: J Neurosci Methods 1997 Feb;71(2):233

Foeller E, Celikel T, Feldman DE. **Inhibitory sharpening of receptive fields contributes to whisker map plasticity in rat somatosensory cortex**. J Neurophysiol. 2005 Dec;94(6):4387-400. Epub 2005 Sep 14.

Guic-Robles E, Valdivieso C, Guajardo G. **Vibrissal roughness discrimination is barrelcortex-dependent**. Behav Brain Res. 1992 Jun 8;48(2):145-52.

Kyriazi HT, Simons DJ. **Thalamocortical response transformations in simulated whisker barrels**. J Neurosci. 1993 Apr;13(4):1601-15.

Ferezou I, Bolea S, Petersen CC. **Visualizing the cortical representation of whisker touch: voltage-sensitive dye imaging in freely moving mice.** Neuron. 2006 May 18;50(4):617-29.

Pinto DJ, Brumberg JC, Simons DJ. **Circuit dynamics and coding strategies in rodent somatosensory cortex**. J Neurophysiol. 2000 Mar;83(3):1158-66

Pinto DJ, Brumberg JC, Simons DJ, Ermentrout GB. **A quantitative population model of whisker barrels: re-examining the Wilson-Cowan equations**.J Comput Neurosci. 1996 Sep;3(3):247-64.

Shoykhet M, Doherty D, Simons DJ. **Coding of deflection velocity and amplitude by whisker primary afferent neurons: implications for higher level processing**. Somatosens Mot Res. 2000;17(2):171-80

Temereanca S, Simons DJ. **Local field potentials and the encoding of whisker deflections by population firing synchrony in thalamic barreloids**. J Neurophysiol. 2003 Apr;89(4):2137-45.

Venkatachalam S, Fee MS, Kleinfeld D. **Ultra-miniature headstage with 6-channel drive and vacuum-assisted micro-wire implantation for chronic recording from the neocortex**. J Neurosci Methods.1999 Aug 1;90(1):37-46

Appendix A

Derivation of the resonance frequencies of a thin conical beam*

For a conical beam with no damping or driving force the equation of motion is:

$$E\frac{\partial^2}{\partial z^2}\left(I(z)\frac{\partial^2 y}{\partial z^2}\right)=-\rho(z)\frac{\partial^2 y}{\partial t^2} \tag{1.1}$$

where:

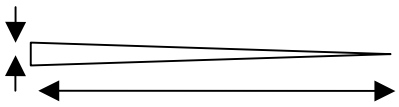

$I(z)=\frac{\pi}{4}\left(\frac{a}{l}\right)^4 z^4$ = the moment of inertia of a cross section of the cone about a diameter

$\rho(z)=\mu\pi\left(\frac{a}{l}\right)^2 z^2$ = density per unit length of the cone

a = radius at base of cone
μ = density
E = Young's modulus
l = length of cone

let $q'=\pi\left(\frac{a}{l}\right)^2$ and $k'=\frac{\pi}{4}\left(\frac{a}{l}\right)^4$

then (1.1) becomes:

* This result was originally derived by Kirchoff in 1882, however the author was not able to find this derivation in a legible format (i.e. it was in German and on microfilm). This derivation is presented here as a reference for anyone interested. Parts of the derivation taken from Kirchoff's original paper are marked by *

$$\frac{k'E}{q'\mu}\frac{1}{z^2}\frac{\partial^2}{\partial z^2}\left[z^4\frac{\partial^2 y}{\partial z^2}\right]=-\frac{\partial^2 y}{\partial t^2}$$

Separate the function y(z,t) = u(z)f(t). Then,

$$-\frac{\partial^2 f}{\partial t^2}=\lambda^2 f(t) \tag{1.2}$$

and,

$$\frac{k'E}{q'\mu}\frac{1}{z^2}\frac{\partial^2}{\partial z^2}\left[z^4\frac{\partial^2 u}{\partial z^2}\right]=\lambda^2 u(z) \tag{1.3}$$

Take the solution to the time-dependent equation be:

$f(t)=\sin(\lambda t)$, λ = angular frequency

Now solve for u(z),

Let $x=z\lambda\sqrt{\frac{q'\mu}{k'E}}$ and, $\gamma^2=\frac{q'\mu\lambda^2}{k'E}$ then, $\frac{dx}{dz}=\gamma$

and eq. 1.3 becomes

$$\frac{1}{x^2}\frac{d^2}{dx^2}\left[x^4\frac{d^2u}{dz^2}\right]=u \tag{1.4}$$

re-write eq. 1.4 as *.

$$\frac{1}{x^2}\frac{d}{dx}x^3\frac{d}{dx}\left[\frac{1}{x^2}\frac{d}{dx}x^3\frac{du}{dx}\right]=u \quad \text{or,}$$

$\frac{1}{x^2}\frac{d}{dx}x^3\frac{du_{\pm}}{dx}=\pm u_{\pm}$, which can be re-written as,

$$\boxed{x\frac{d^2u_{\pm}}{dx^2}+3\frac{du_{\pm}}{dx}\pm u_{\pm}=0} \qquad (1.5)$$

Solving 1.5 will give us the solution to the original equation. In order to solve eq. 1.5 first solve the following equations *:

$$x\frac{d^2\Phi}{dx^2}+\frac{d\Phi}{dx}=\Phi \qquad (1.6a) \qquad \text{and,} \qquad x\frac{d^2\Psi}{dx^2}+\frac{d\Psi}{dx}=-\Psi \qquad (1.6b)$$

Then we can show that $u_{-}=\frac{d^2\Phi}{dx^2}$ (1.7a) and, $u_{+}=\frac{d^2\Psi}{dx^2}$ (1.7b)

In equation 1.6a substitute $s=2x^{1/2}$ then, $x=\frac{s^2}{4}$ and, $\frac{d}{dx}=\frac{2}{s}\frac{d}{ds}$

then equation 1.6a becomes

$$\frac{s^2}{4}\frac{4}{s^2}\left[-\frac{1}{s}\frac{d}{ds}+\frac{d^2}{ds^2}\right]\psi+\frac{2}{s}\frac{d\psi}{ds}+\psi=0 \qquad \text{or,} \qquad \frac{d^2\psi}{ds^2}+\frac{1}{s}\frac{d\psi}{ds}+\psi=0$$

which is Bessel's equation with m=0, and has the solution

$$\psi(x)=J_0\left(2x^{1/2}\right)$$

similarly,

$$\Phi(x)=J_0\left(2ix^{1/2}\right), \qquad \text{where } i=\sqrt{-1}$$

Now show that $u_{+}=\frac{d^2\psi}{dx^2}$ solves $x\frac{d^2u_{+}}{dx^2}+3\frac{du_{+}}{dx}+u_{+}=0$

From 1.6b: $u_{+}=\frac{\partial^2\psi}{\partial x^2}=-\frac{1}{x}\frac{d\psi}{dx}-\frac{1}{x}\psi$

Then differentiating both sides and multiplying by x,

$$x\frac{d^2u_+}{dx^2}=\frac{d}{dx}x\frac{du_+}{dx}-\frac{du_+}{dx}=\frac{d}{dx}\left[x\frac{du}{dx}-u\right]$$

and equation 16b becomes

$$\frac{d}{dx}\left[x\frac{du_+}{dx}+2u_+\right]+u_+=0$$

Substituting equation

$$\frac{d}{dx}\left[\frac{1}{x}\frac{d\psi}{dx}-\frac{\partial^2\psi}{\partial x^2}+\frac{1}{x}\psi-\frac{d\psi}{dx}+2\frac{\partial^2\psi}{\partial x^2}\right]+\frac{\partial^2\psi}{\partial x^2}=0$$

$$=\frac{d}{dx}\left[-\frac{d\psi}{dx}\right]+\frac{\partial^2\psi}{\partial x^2}=0$$

So, $u_+=C_1\frac{\partial^2\psi}{\partial x^2}$ and, $u_-=C_2\frac{\partial^2\Phi}{\partial x^2}$

Then, $\frac{d\psi}{dx}=\frac{ds}{dx}\frac{d\psi}{ds}=\frac{2}{s}\frac{d\psi}{ds}=\frac{2}{s}\frac{d}{ds}J_0(s)=-\frac{2}{s}\frac{d}{ds}J_1(s)$

And using the property of Bessel functions that: $\frac{d}{dx}\left[x^{-\upsilon}\right]J_\upsilon(x)=-x^{-\upsilon}J_{\upsilon+1}(x)$

Then, $\frac{\partial^2\psi}{\partial x^2}=-2x^{-1/2}\frac{d}{ds}\left[s^{-1}J_1(s)\right]=\frac{J_2(2x^{1/2})}{x}$

And, $u_+=C_1\frac{J_2(2x^{1/2})}{x}$, $u_-=C_2\frac{J_2(2ix^{1/2})}{x}$

$$\boxed{u=C_1\frac{J_1(2x^{1/2})}{x}+C_2\frac{J_2(2ix^{1/2})}{x}}$$

Now switch back to the z variable using $x = z\lambda\sqrt{4\frac{l^2\mu}{a^2E}}$ and apply the boundary conditions

$u(l) = 0;$ and $\left.\frac{du}{dz}\right|_{z=l} = 0$ in order to obtain the eigenfrequencies of the system

The condition for nontrivial *C1*,*C2* is:

$$\begin{vmatrix} \frac{J_2(2\gamma^{1/2}l^{1/2})}{\gamma l} & \frac{J_2(2i\gamma^{1/2}l^{1/2})}{\gamma l} \\ \left.\frac{d}{dz}\frac{J_2(2\gamma^{1/2}z^{1/2})}{\gamma z}\right|_{z=l} & \left.\frac{d}{dz}\frac{J_2(2i\gamma^{1/2}l^{1/2})}{\gamma l}\right|_{z=l} \end{vmatrix} = 0$$

Now let,

$s_1 = 2\gamma^{1/2}z^{1/2}$ and $s_2 = 2i\gamma^{1/2}z^{1/2}$

Then,

$$\frac{d}{dz}\left(\frac{J_2(2\gamma^{1/2}z^{1/2})}{\gamma z}\right) = 4\gamma^{1/2}z^{-1/2}\left(-s_1^{-2}J_3(s_1)\right) \quad \text{and}$$

$$\frac{d}{dz}\left(\frac{J_2(2i\gamma^{1/2}z^{1/2})}{\gamma z}\right) = 4i\gamma^{1/2}z^{-1/2}\left(s_2^{-2}J_3(s_2)\right)$$

And let $w = 2\gamma^{1/2}l^{1/2}$, and using the Bessel function property,

$$J_3(w) = \frac{4}{t}J_2(w) - J_1(w) \quad \text{and} \quad J_3(iw) = \frac{4}{iw}J_2(iw) - J_1(iw)$$

The equation for nontrivial *C1*, *C2* becomes,

$$iJ_2(w)J_1(iw) - J_2(iw)J_1(w) = 0$$

or,

$$\boxed{J_2(w)I_1(w) - I_2(w)J_1(w) = 0}$$ where, $I_{1,2}$ are the modified Bessel functions

The zeros of this equation occur at (figure A1), $w = 5.9, 9.2, 12.4.....$

And the eigenfrequencies of equation 1.1 are $\lambda_i = \frac{w_i^2}{8}\frac{a}{l^2}\sqrt{\frac{E}{\mu}}$, or

$$\lambda_i = t_i \frac{a}{l^2}\sqrt{\frac{E}{\mu}} \qquad \text{with} \qquad t_i = 4.4, 10.6, 19.2.....$$

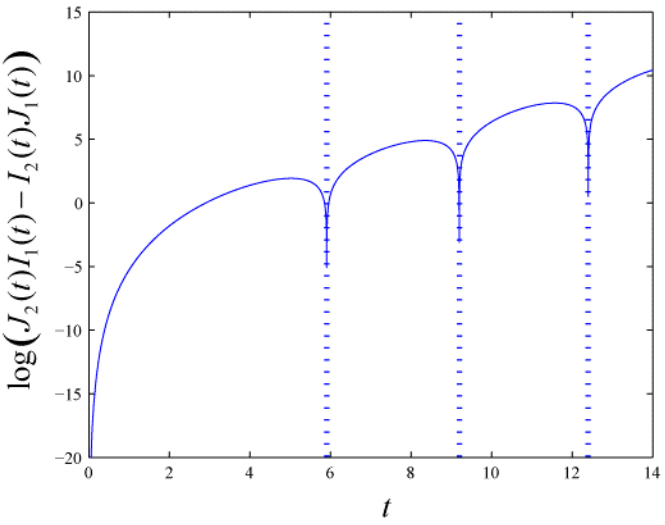

Figure A1. **Zeros of the equationfor nontrivial C1,C2**.
Nontrivial solutions for C1,C2 exist for t = 5.9, 9.2, 12.4...

A1. References

Erwin Kreyszig. **Advanced Engineering Mathematics**. New York : John Wiley and Sons 8th ed. 2001

Kirchoff GR. **Gesammelte Abhandlungen**, Leipzig 1882